5-2016

Transparent Solar Panel Antenna Array

Taha Shahvirdi Dizaj Yekan
Utah State University

TRANSPARENT SOLAR PANEL ANTENNA ARRAY

by

Taha Shahvirdi Dizaj Yekan

A dissertation submitted in partial fulfillment
of the requirements for the degree

of

DOCTOR OF PHILOSOPHY

in

Electrical Engineering

Approved:

Reyhan Baktur Major Professor	Jake Gunther Committee Member
Charles M. Swenson Committee Member	Regan Zane Committee Member
T. C. Shen Committee Member	Mark R. McLellan Vice President for Research and Dean of the School of Graduate Studies

UTAH STATE UNIVERSITY
Logan, Utah

2016

ABSTRACT

Transparent Solar Panel Antenna Array

by

Taha Shahvirdi Dizaj Yekan, Doctor of Philosophy

Utah State University, 2016

Major Professor: Reyhan Baktur
Department: Electrical and Computer Engineering

This dissertation research presents a comprehensive study to answer the question of "Can it be possible to integrate a high gain optically transparent antenna array directly on top of solar cells?". The answer to such question is extremely important in space exploration where very small satellites have been extensively employed. Due to their small mass and size, those small satellites create challenges for one to mount the antennas, and the challenge is further increased when a high gain antenna is need for more communication capacity. Based on feasibility studies, the dissertation concludes that it is possible to do such an integration, and then proceeds to present the approaches for design and integration.

On the element level, the thesis presents research in assessing the effects between a planar antenna integrated on the solar cell and the photovoltaic cell. A series of experiments were designed to perform assessments for antennas operating from C to X bands. It is concluded that a commercial triple junction space–certified solar cell normally would decrease the gain of the antenna to 2–3 dB and is not affected by the working states of solar cells. The shadow of the antenna casts on solar cells, however, is not significant (less than 2%). The thesis also provides a model of a common space solar cell that helps to explain the gain loss. The model was validated by experimental data, and it was utilized to predict

a possible custom design of solar cell where with a minimal design modification, it would facilitate less gain loss of the antenna integrated on top.

On the array level, the research surveys different high gain antenna array design and then focus on an optimal sub–wavelength reflectarray design. The final antenna array design is a 30 cm by 20 cm, X band (8.475 GHz) reflectarray that shows 94% transparency, 24 dB gain, and higher than 40% aperture efficiency. The design is then prototyped and tested on actual solar panel. The measurement of the reflectarray placed on the solar panel showed a gain of 22.46 dB and an aperture efficiency of 29.3%. While those results are considered excellent, the thesis continues to address the reasons for reduction of the antenna's performance due to the solar panel, through both theoretical analysis and experiments.

(103 pages)

PUBLIC ABSTRACT

Transparent Solar Panel Antenna Array

Taha Shahvirdi Dizaj Yekan

A CubeSat is a very small satellite that has been achieving growing interests in space exploration. The base unit of CubeSats 1U, which is a cube with 10 cm on each side. In applications, CubeSats can be deployed as just 1U, or multiple unites can be stacked together to form a larger CubeSat for extended functionality. Due to their small sizes, it is challenging to fit antennas onto CubeSats because the antenna always fights for surface real estate with solar cells. The challenge is further aggravated when an antenna is required to have high gain such as more than 20 dB because the size of the antenna grows in accordance to the gain.

This doctoral dissertation presents a comprehensive study to answer the question of "Can it be possible to integrate a high gain optically transparent antenna array directly on top of solar cells?". The answer to such question is extremely important because it solves the issue of allocating the antenna and solar cells on a CubeSat. After asserting the feasibility of such an integration of antenna with solar cells, the thesis shows detailed guideline on how to integrate a single transparent antenna element and antenna array on solar panels.

On the element level, the thesis presents research in assessing the effects between a planar antenna integrated on the solar cell and the photovoltaic cell. A series of experiments were designed to perform assessments for antennas operating from 5 to 10 GHz. It is concluded that a commercial triple junction space–certified solar cell normally would decrease the gain of the antenna to 2–3 dB and is not affected by the working states of solar cells. The shadow of the antenna casts on solar cells, however, is not significant (less than 2%). The thesis also provides a model of a common space solar cell that helps to explain

the gain loss. The model was validated by experimental data, and it was utilized to predict a possible custom design of solar cell where with a minimal design modification, it would facilitate less gain loss of the antenna integrated on top.

On the array level, the research surveys different high gain antenna array design and then focus on an optimal sub–wavelength reflectarray design. The final antenna array design is a 30 cm by 20 cm, X band (8.475 GHz) reflectarray that shows 94% transparency, 24 dB gain, and higher than 40% aperture efficiency. The design is then prototyped and tested on actual solar panel. The measurement of the reflectarray placed on the solar panel showed a gain of 22.46 dB and an aperture efficiency of 29.3%. While those results are considered excellent, the thesis continues to address the reasons for reduction of the antenna's performance due to the solar panel, through both theoretical analysis and experiments.

To my lovely wife, Shadi
and my sweet son, Araz!
whose love, encouragement, and support made this work possible.

ACKNOWLEDGMENTS

I would like to express my sincere gratitude to all who made this work possible. I would like to acknowledge my major advisor, Dr. Reyhan Baktur. She taught me many invaluable things not only Electromagnetics and Antenna, but also being a professional engineer and researcher. I am grateful to her as she has provided me the opportunities so that I could develop my engineering skills and creativity. I appreciate her hospitality, constant support, and guidance through my PhD study. She has been a great supervisor and friend.

I would like to thank my committee members: Dr. Charles Swenson, Dr. Jake Gunther, Dr. Regan Zane, and Dr. T. C. Shen for their helpful and insightful comments and kindness.

I would like to thank my loving parents Mohammad and Zibandeh, who have always supported me and taught me to be strong in difficult times and to achieve my goals. I also would like to thank my brothers Yasin and Hannan, and my cousins Ehsan and Iman, who have always been a great source of energy to me and believed in me.

Finally, my special and greatest thanks go to Shadi, my beloved wife, whose unconditional love, caring, support, and positivity have always motivated and inspired me to progress during hard times. Also, I would like to thank my lovely son Araz who has given me more energy to work. Having him was a great motivation to me when I faced a problem. Shadi and Araz, your love and encouragement are what carried me through this works and made it attainable.

Taha Shahvirdi Dizaj Yekan

CONTENTS

LIST OF TABLES

LIST OF FIGURES

CHAPTER 1

INTRODUCTION

A CubeSat is a very small satellite designed with modular components to have a minimum payload [1]. In general, a 1U (meaning one unit) CubeSat is a standard CubeSat module, with a size of 10 cm x 10 cm x 10 cm and a weight of no more than 1.33 kg. A 1U CubeSat can be launched alone or multiple units can be stacked together to form nU (n =2, 3,) CubeSats (Fig. 1.a). For example, Fig. 1.b shows two 1.5U CubeSats, DICE satellites launched by Utah State University (USU) [2], and Fig. 1.c is a structural illustration of USU's RUNNER (Research Utility Nanosatellite for Near Earth object Rendezvous) mission project, where a 6U CubeSat with deployed panels is constructed to study near earth objects (comets, asteroids and other small bodies in the interior of the Solar System which are 1.3 AU away from the Sun). Larger CubeSats extended mission capacity, but have higher payload than 1U ones.

Antenna design for small satellite has its own challenge and has been an important topic in CubeSat industry [3]. Integration of conformal antennas with solar cells has tremendous value in CubeSat communication, as the antennas, when strategically integrated with the solar cells, do not compete for the limited surface real estate and do not require mechanical deployment. Thus, an effective conformal integration yields a low CubeSat payload and a reliable communication. There have been four main types of conformal integrations reported: (1) antennas integrated under solar cells [4–8]; (2) antennas integrated on the same plane with or on the side wall perpendicular to solar cells [9–12]; (3) antennas integrated on top of solar cells [13–18], and (4) parts of the solar cells function as antenna [19–22]. As the first and forth types of integrations require custom–designed solar cells so that the antennas can function properly, the focus of this doctoral thesis research is only on the third type of antenna where all components can be off–the–shelf, which is favored in a CubeSat payload. Accordingly, the objective of this dissertation is to present optically transparent antennas

(a)

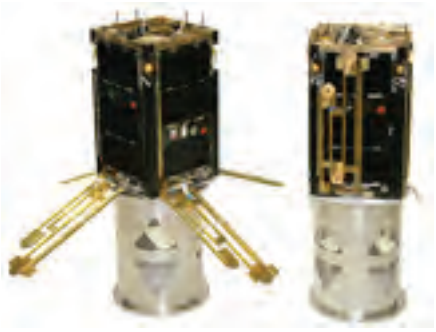

(b)

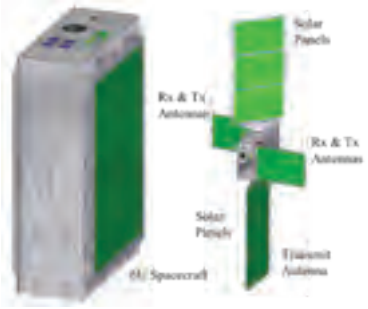

(c)

Fig. 1.1: CubeSat: (a) 1U (Right) and 3U (Left) . (b) USU's 1.5U DICE. (c) USU's 6U RUNNER.

that can be placed on top of solar cells. The design has a fair degree of independence from the solar cell and can be designed in modular fashion. This type of antenna can be applied either as the individual radiating element for 1U Cubesats, or designed into arrays for larger CubeSats, where there is more solar panel area to host antennas.

This dissertation is organized following a multiple–journal–publication–format, which means each chapter is composed of a journal or conference papers. Chapter 2 to 4 focus on element level integration. Chapter 2 and chapter 3 are experimental assessments on how the integrated antenna and solar cell affect each other at 5 GHz and 10 GHz range, respectively. Chapter 4 is an analytical model of a typical space solar cell. The model helps to explain the gain reduction of the antenna due to the solar cell underneath, and has been shown to be validated through experimental data. The model also predicts a possible future co–design of solar cell and integrated antenna.

Compared to a single element antenna, high gain array antennas offer many advantages in expanding communication capacity. But the integration with solar panels has been limited by the surface area of CubeSats to host those larger antennas. With larger CubeSats (such as 6U and 9U CubeSats) and deployed solar panels are becoming more common, it is feasible to integrate antenna arrays with CubeSat solar panels. NASA's ISARA is one of such successful integrations, where a Ka band antenna array was integrated with the backside of the solar panel [23]. The challenge is, this technology cannot be applied to cases where both sides of a solar panel have solar cells. Such a solar panel is becoming popular and is important for various missions. Chapter 5 presents an alternative design to ISARA, where a low profile, optically transparent reflectarray is integrated directly on top of solar cells. The transparency of the antenna is higher than 90%, which is the highest to date, and the reflectarray design promises more than 22 dB gain and 29% aperture efficiency. The chapter presents the reflectarray design, initial prototyping using circuit board material, measurements, and measurements of the array when integrated on a functional solar panel. The results are good and the reasons for minor gain reduction for the measurement results are analyzed and explained. The targeted application of such an integrated reflectarray is for is for Near Earth Network (NEN), however, the design can be conveniently scaled to other space networks.

Chapter 6 is an additional study, where the objective is achieving polarization reconfigurability of an integrated solar cell antenna. Although the study is for an element, the method can be extended to array level.

References

[1] Small satellites: A revolution in space science, keck institute for space studies report. [Online]. Available: http://www.kiss.caltech.edu/study/smallsat/KISS-SmallSat-FinalReport.pdf

[2] [Online]. Available: https://directory.eoportal.org/web/eoportal/satellite-missions/d/dice

[3] S. Gao, K. Clark, M. Uniwin, J. Zackrisson, W. A. Shiroma, J. M. Akagi, K. Maynard, P. Garner, L. Boccia, G. Massa, C. Underwood, M. Brenchley, M. Pointer, and

M. N. Sweeting, "Antennas for modern small satellites," *IEEE Antennas Propag. Mag.*, vol. 51, no. 4, pp. 21–30, 2009.

[4] M. Tanaka, Y. Suzuki, and K. Araki, "Microstrip antenna with solar cells for microsatellites," *Electron. Lett.*, vol. 31, no. 1, pp. 5–6, 1995.

[5] S. Vaccaro, P. Torres, J. R. Mosig, A. Shah, J. F. Zurcher, A. K. Skrivervik, F. Gardiol, P. de Maagt, and L. Gerlach, "Integrated solar panel antennas," *Electron. Lett.*, vol. 36, no. 5, pp. 390–391, 2000.

[6] ——, "Stainless steel slot antenna with integrated solar cells," *Electron. Lett.*, vol. 36, no. 25, pp. 2059–2060, 2000.

[7] ——, "Combination of antennas and solar cells for satellite applications," *Microw. Opt. Tech. Lett.*, vol. 29, no. 1, pp. 11–16, 2001.

[8] S. Vaccaro, J. R. Mosig, and P. de Maagt, "Two advanced solar antenna "SOLANT" designs for satellite and terrestrial communications," *IEEE Trans. Antennas Propag.*, vol. 51, no. 8, pp. 2028–2034, 2003.

[9] T. Wu, R. L. Li, and M. M. Tentzeris, "A mechanically stable, low profile, omnidirectional solar-cell integrated antenna for outdoor wireless sensor nodes," in *Antennas and Propagation Society International Symposium (APS 2009)*, Charleston, SC, 2009, pp. 1–4.

[10] M. Mahmoud, R. Baktur, and R. Burt, "Fully integrated solar panel slot antennas for small satellites," in *Proc. 15th Annual AIAA/USU Conf. on Small Satellites*, Logan, UT, Aug. 2010.

[11] T. Wu, R. L. Li, and M. M. Tentzeris, "A scalable solar antenna for autonomous integrated wireless sensor nodes," *IEEE Antennas Wireless Propag. Lett.*, vol. 10, pp. 510–513, 2011.

[12] R. Caso, A. D'Alessandro, A. Michel, and P. Nepa, "Integration of slot antennas in commercial photovoltaic panels for stand-alone communication systems," *IEEE Trans. Antennas Propag.*, vol. 61, no. 1, pp. 62–69, 2013.

[13] T. W. Turpin and R. Baktur, "Meshed patch antennas integrated on solar cells," *IEEE Antennas Wireless Propag. Lett.*, vol. 52, pp. 693–696, 2009.

[14] S. V. Shynu, M. J. Roo-Ons, P. McEvoy, M. J. Ammann, S. J. McCormack, and B. Norton, "Integration of microstrip patch antenna with polycrystalline silicon solar cell," *IEEE Trans. Antennas Propag.*, vol. 57, no. 12, pp. 3969–3972, 2009.

[15] E. H. Lim and K. W. Leung, "Transparent dielectric resonator antennas for optical applications," *IEEE Trans. Antennas Propag.*, vol. 58, no. 4, pp. 1054–1059, 2010.

[16] M. J. Roo-Ons, S. V. Shynu, M. J. Ammann, S. J. McCormack, and B. Norton, "Transparent patch antenna on a-Si thinfilm glass solar module," *Electron. Lett*, vol. 47, no. 2, pp. 85–86, 2011.

[17] O. Yurduseven, D. Smith, and M. Elsdon, "UWB meshed solar monopole antenna," *Electron. Lett.*, vol. 49, no. 9, pp. 58–584, 2013.

[18] P. Dreyer, M. Morales-Masis, S. Nicolay, C. Ballif, and J. Perruisseau-Carrier, "Copper and transparent-conductor reflectarray elements on thin-film solar cell panels," *IEEE Trans. Antennas Propag.*, vol. 62, no. 7, pp. 3813–3818, 2014.

[19] N. Henze, C. Bendel, J. Kirchhof, and H. Fruchting, "Application of photovoltaic solar cells in planar antenna structures," in *Proc. 12th Int. Conf. on Antennas and Propagation*, Exeter, U.K., Mar. 2003, pp. 731–734.

[20] N. Henze, M. Weitz, P. Hofmann, C. Bendel, J. Kirchoff, and H. Fruchting, "Investigations on planar antennas with photovoltaic solar cells for mobile communications," in *Proc. IEEE Int. Symp. on Personal, Indoor and Mobile Radio Commun*, Sep. 2004, pp. 622–626.

[21] O. Yurduseven, D. Smith, and M. Elsdon, "A solar cell stacked multi-slot quad-band PIFA for GSM, WLAN and WiMAX networks," *IEEE Antennas Wireless Propag. Lett.*, vol. 23, pp. 285–287, 2013.

[22] J. Oh, K. Lee, T. W. Hughes, S. Forrest, and K. Sarabandi, "Flexible antenna integrated with an epitaxial lift-off solar cell array for flapping-wing robots," *IEEE Trans. Antennas Propag.*, vol. 62, no. 8, pp. 4356–4361, 2014.

[23] Integrated solar array and reflectarray antenna (ISARA) for high bandwidth cubesats, NASA document. [Online]. Available: https://www.nasa.gov/sites/default/files/files/ISARA_Fact_Sheet-15Oct14.pdf

CHAPTER 2
AN EXPERIMENTAL STUDY ON THE EFFECT OF COMMERCIAL TRIPLE JUNCTION SOLAR CELLS ON PATCH ANTENNAS INTEGRATED ON THEIR COVER GLASS

Abstract

A patch antenna integrated on the cover glass of a commercial space–certified solar cell is examined. Test fixtures were fabricated to study the antenna designed at 4.9 GHz when there is an active solar cell under the antenna. It is found that the solar cell affects the input impedance of the antenna and causes a 2-3 dB gain reduction. Repetitive tests were performed to confirm that the effect from solar cells on the antenna remained the same regardless of the working states of the solar cell, type of cover glass, or the assembly of the solar panel.

2.1 Introduction

Integration of antennas with solar cells has important applications for small satellites [1], deep space exploration [2], and self-powered ground sensors [3]. Such an integration can be particularly valuable for a CubeSat (a very small satellite designed with modular components to have a minimum payload) [4] as the antennas, when effectively integrated with the solar cells, do not compete with solar cells for the limited surface real estate. There have been four main types of integrations reported: (1) antennas integrated under solar cells [1, 5–7]; (2) antennas integrated on the same plane with or on the side wall perpendicular to solar cells [8–10]; (3) antennas integrated on top of solar cells [11–18], and (4) parts of the solar cells function as antenna [19–21] (the antenna in [7] also belongs to this category as the solar cell above the antenna acts as a parasitic elements of the antenna). The third type of integration is of particular interest and promise to a CubeSat system

as the antenna topology, especially when it is small or optically transparent, facilitates a possible modular design. Accordingly, it is important to understand the interaction between the solar cell and the antenna. The impact of the antenna on the solar cell can be estimated with relative ease. One may evaluate the shadow or blockage caused by the antenna on the solar cell to determine the reduction in the solar cell's efficiency. The experimental set-up for such a study is also straightforward. For the effect of the solar cell on the antenna integrated on top, the reported results are limited. The objective of the research in [14, 15] was on the transparency or bandwidth of the antenna, and hence, there is no report on the effect of the solar cell. The dielectric resonator antenna in [13] was reported to have little effect on the solar cell, however, there was not sufficient information given on the specific solar cell, and hence the conclusion from [13] may not be applicable to satellite solar cells. In addition, the form factor of the antenna may present pressure on the solar cells if they were to fly in space. A more comprehensive research by Shynu et al. [12] presented a solar cell model, simulated and measured antenna's parameters with and without solar cell. Because the study was performed on one single relatively large (larger than one side of a CubeSat) bare (i.e. without cover glass) solar cell, the results may not be applied to antennas integrated with other types of solar cells with different cover glass. In addition, commonly, the conductive layer of a solar cell is its electric positive plate [7]. Therefore, the designs where the integrated antenna uses the solar cell as ground may induce unknown compatibility issues.

Quantifying and presenting a reliable estimation of how commonly used CubeSat solar cells effect the antenna design not only impact communication link budget and payload, but also provide design guidelines for integrated solar cell antenna arrays. In addition, it is a common practice to bond solar cells with their cover glass using transparent adhesive. The effect of such adhesive has not been studied yet. The objective of this study is to provide a consistent assessment on the performance of the integrated antenna due to the solar cell beneath it while the two are electrically separated. This includes repetitive tests, experiments with different cover glass and solar panel assembly, and examining the antenna

against different states of active solar cells.

2.2 Method

A commercial space solar cell always has a cover glass on top of the photovoltaic layer as protection. The existence of the cover glass is the design basis of the integrated patch antenna, where the cover glass acts as the dielectric substrate of the antenna.

2.2.1 Test Fixtures

To assess the effect of the solar cell on the antenna's performance, we prototyped a two-cell solar panel composed entirely of all space certified off–the–shelf components. The size and the material of the solar panel is compatible with a standard 1U CubeSat (i.e. it is a cube of 10 cm on each edge.). Two fixtures to study the effect of the solar cell on the antenna integrated on top, are shown in Fig. 2.1 and Fig. 2.2, where one fixture has a functional solar cell (Fig. 2.1) and the other one does not have (Fig. 2.2). The cross section view of the fixture with solar cell and antenna is illustrated in Fig. 2.3. From bottom to top, the layer information is as follows. The first layer is a copper plate that serves as the base of the solar panel and the ground for electronics. A thin Kapton sheet (orange colored sheet in Fig. 2.1) with a thickness of $t_k = 0.0508$ mm is placed on top of the ground, and then two triple-junction space-certified solar cells from EmCore [22], are connected together and mounted on top of the Kapton sheet. The Kapton sheet is to electrically isolate the bottom of the solar cell, which is a metal coating and is the electrical positive of solar cells, from the RF ground. The height of solar cells is $h_s = 0.15$ mm. On top of each solar cell is a AF32 cover glass [23], which is a standard space-certified material for solar cells in a deep space environment because of its very high optical transparency and high temperature tolerance. The height of the AF32 glass is $h = 1$ mm, the glass is pre-cut by the manufacture to cover the solar cell seamlessly. The dielectric constant (ϵ_r) and loss tangent ($tan\delta$) of the AF32 glass are 4.5 and 0.015, both being measured at X band [17]. Finally, a patch antenna is screen printed on the AF32 cover glass with silver based conductive ink (124-46 by Creative Material). It is obvious that the antenna uses the cover glass as its substrate,

and the copper plate as the ground. It should be noted that, although there is only one solar cell with an antenna printed on its cover glass in the illustration (Fig. 2.3), the antenna integration is not limited to such a specific configuration. One may integrate antennas on each solar cell when needed.

For the fixture without solar cells (Fig. 2.2), the assembly is, from bottom to top, the copper plate, AF32 glass, and antenna. Because the Kapton sheet is very thin and casts negligible impact on the antenna's performance, we did not include the sheet in this fixture. One may include the sheet in the fixture without solar cells as long as it is carefully handled so that there are no air bubbles between the sheet and copper plate. In the fixture with solar cells (Fig. 2.1), the solar cells help to squeeze the air out. Both fixtures are then fastened on with four nylon clips machined in house.

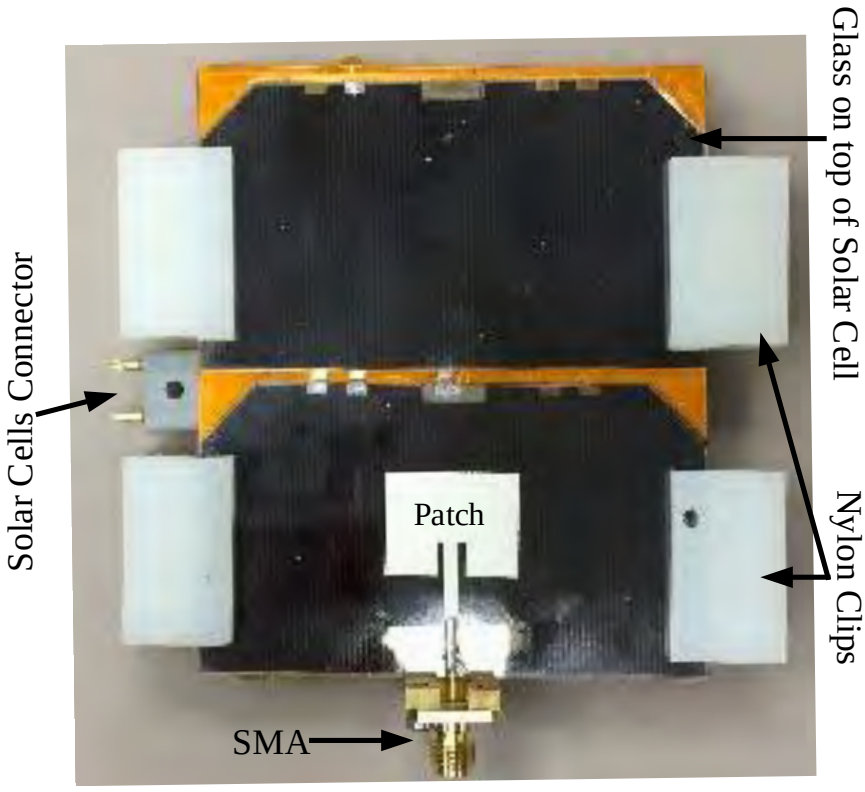

Fig. 2.1: Patch antenna printed on AF32 cover glass with functional solar cells under it.

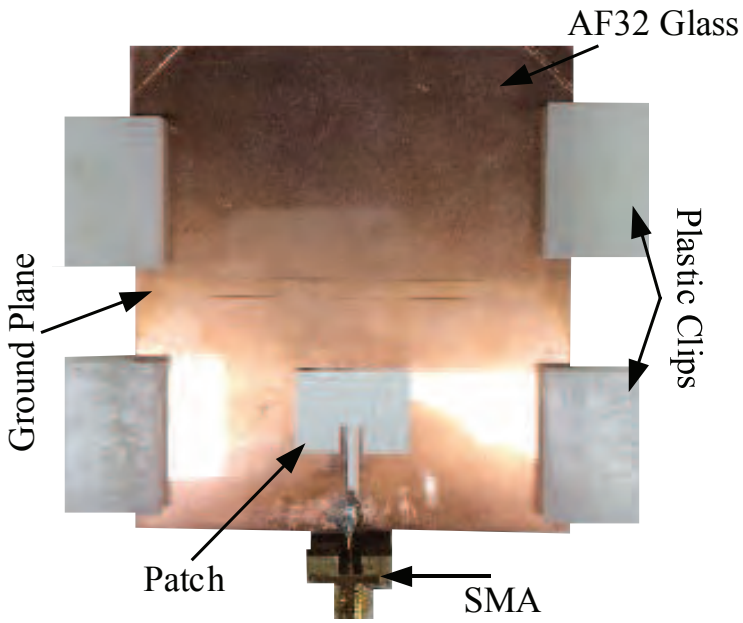

Fig. 2.2: Patch antenna printed on AF32 glass without solar cells.

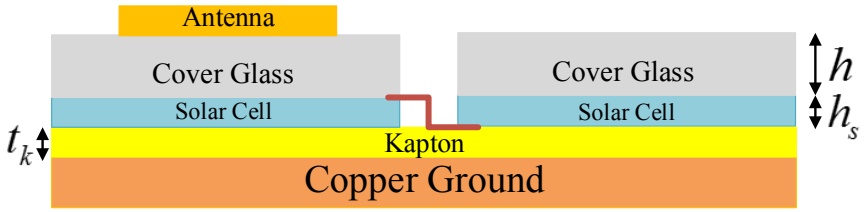

Fig. 2.3: Cross section view of the fixture with solar cell and integrated antenna.

2.2.2 Antenna Geometry

Fig. 2.4 is an illustration of the geometry of the antenna integrated on a cover glass of the two-cell solar panel. The size of the solar panel, which is also the ground plane, is defined by W_G and L_G. The parameters L_S and L_C, together with W_G demonstrate the geometry of the cover glass, which is the same as the solar cells examined in this project. The spacing between the two solar cells can be easily determined from $L_G - 2L_S$. The design parameters for the patch antenna fed by a 50 Ω inset microstrip line are W, L, S_g, S_i, W_f and L_f. The antenna and microstrip line, operating at 4.9 GHz, were designed with Ansys' HFSS by considering the cover glass as the antenna's only substrate (i.e. the antenna integrated on the assembly shown in Fig. 2.2). The values of these design parameters are

presented in Table 2.1. While printing the antenna on the cover glass with conductive ink, we repeated the printing process multiple times to ensure the thickness of the conductor is sufficiently higher than the microwave skin depth (i.e. 0.91 μm for the silver ink at 4.9 GHz).

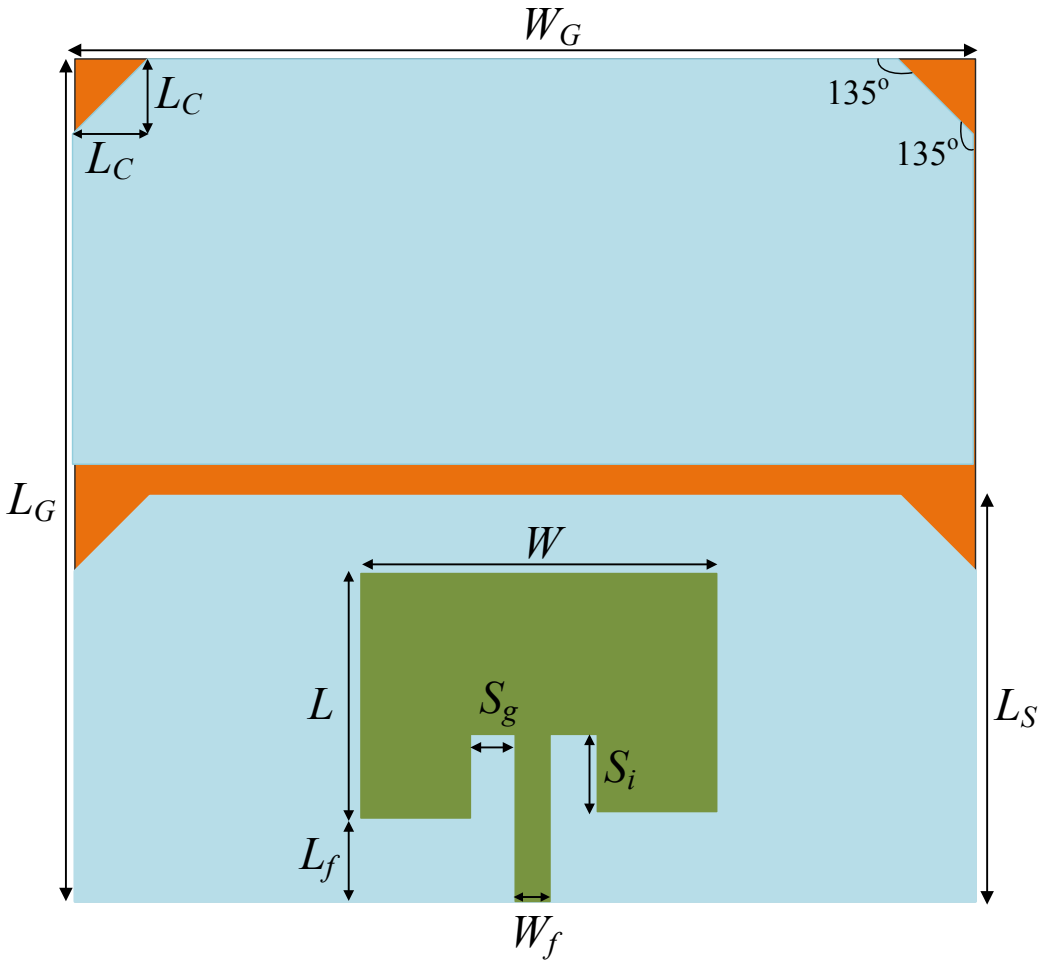

Fig. 2.4: Geometry of the antenna integrated on a cover glass of the two–cell solar panel.

2.2.3 Measurement Setup

Performance of the antenna integrated on the AF32 glass with and without solar cells was examined using standard tests in an anechoic chamber. When the antenna is integrated on solar cells (Fig. 2.1), it is measured at different status of the solar panels such as without

Table 2.1: Geometrical parameters of the antenna on AF32 cover glass.

Parameter	Value (mm)	Parameter	Value (mm)
L_G	83	W	18
W_G	69	S_g	0.9
L_S	39.5	S_i	4.6
L_C	7.5	W_f	1.9
L	14	L_f	13.4

illumination or being illuminated by an artificial light. The two solar cells on the fixture in Fig. 2.1 were connected in series and have an output connector as shown. The connector not only allows us to measure the solar cells' output under illuminations, but also enables tests where we connect different resistive loads to the panel and then measure the antenna's performance.

2.3 Results and Discussions

2.3.1 Effect of the Solar Cell on the Microstrip Feed Line

As the patch antenna under study is excited using an inset feed microstrip line, it is important to first examine whether or not the solar cell affects the feed line. In order to do so, a 50 Ω microstrip line is designed and printed on a cover glass using the same assembly as the test fixture in Fig. 2.2. After being measured without solar cells (Fig. 2.5), the cover glass with printed microstrip line was measured on solar cell (Fig. 2.6), using the same assembly as in Fig. 2.1. The measured scattering parameters of the microstrip line are plotted in Fig. 2.7. From the measured S_{11} with and without solar cells, it is seen that the microstrip line is matched to the 50 Ω coax terminal at both cases, although matching is better when there is no solar cell. The S_{21} measurements indicate that there is loss when solar cell is present. This is understandable as the solar cell is a lossy substrate at RF frequency [12]. Overall, at the frequency of interest (4.9 GHz), the impedance of the microstrip line can be regarded as not being affected by the solar cell.

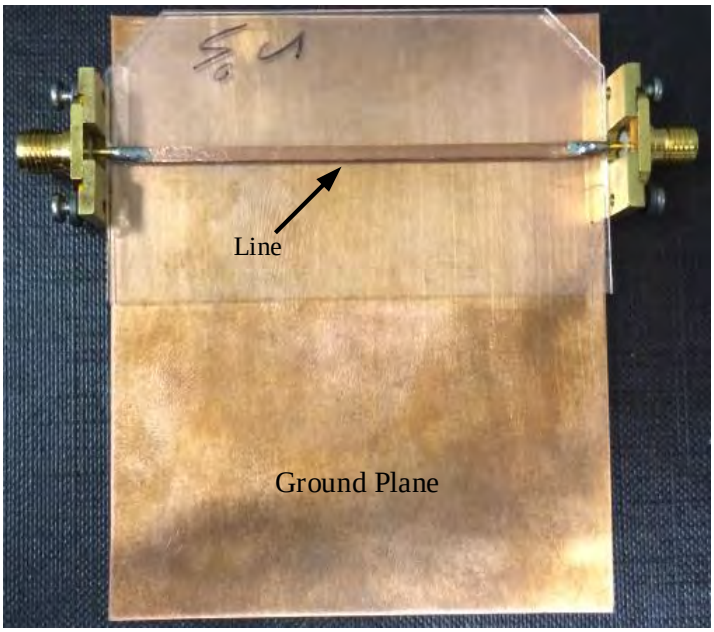

Fig. 2.5: Examination of the microstrip feed line on AF32 glass.

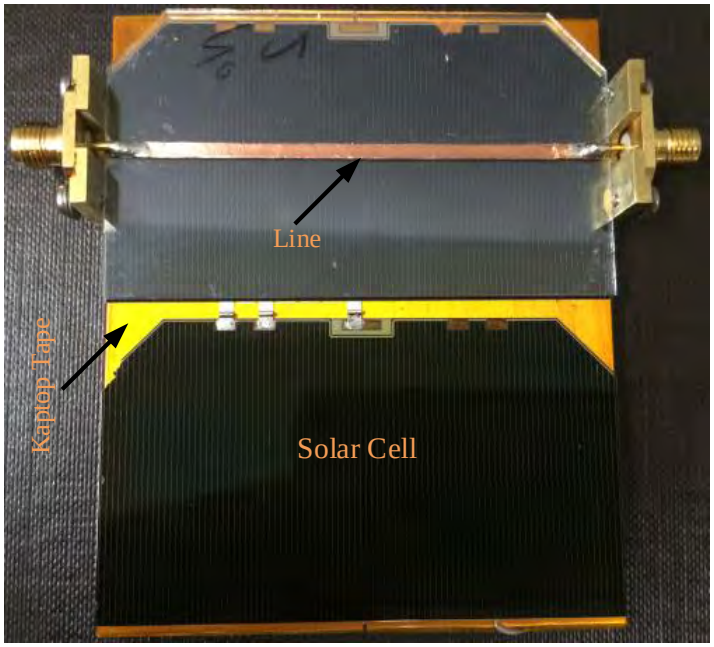

Fig. 2.6: Examination of the microstrip feed line on AF32 glass with solar cells under it.

2.3.2 Effect of the Solar Cell on the Antenna

The antenna described in section 2.2.2 was tested with and without solar cells using the fixtures in Fig. 2.1 and Fig. 2.2. The measured reflection coefficient is presented in

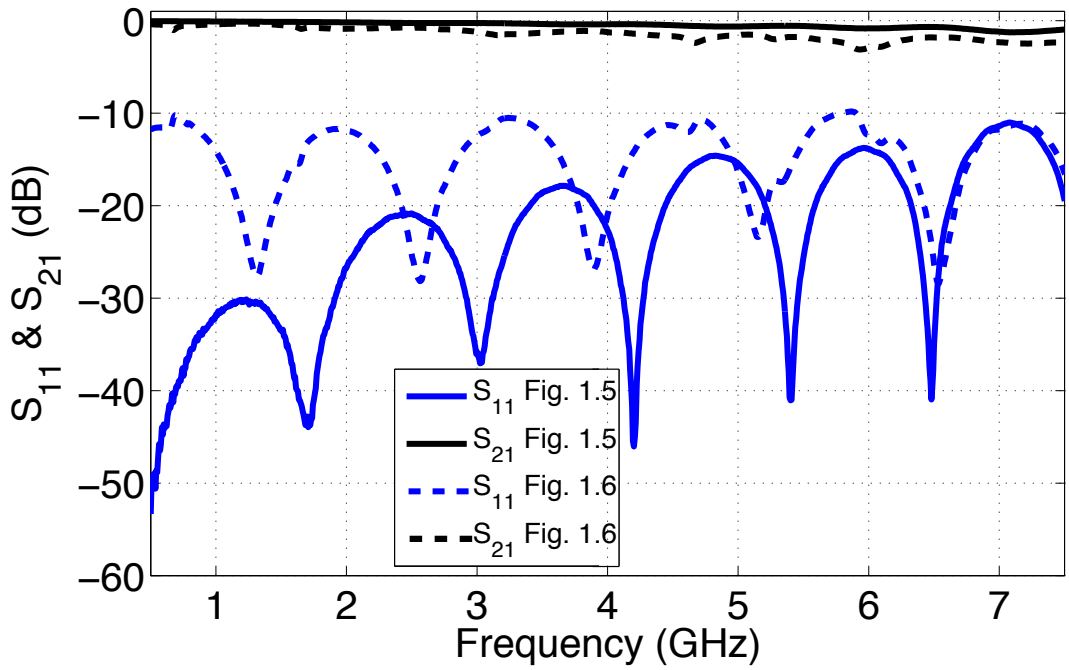

Fig. 2.7: Measured scattering parameters of the microstrip feed line on AF32 glass with and without solar cells under it.

Fig. 2.8. It is seen that the solar cell affected the input impedance of the antenna and its resonant frequency, shifting it from 4.89 GHz to 5.15 GHz. The reasons for the shift of frequency is studied in more detail in section 2.3.6, and the conclusion on the change of input impedance is obtained because of the test results on the feed line in section 2.3.1 where the impedance of the feed line was not affected by the solar cell. As a result, the antenna was tuned to achieve better impedance matching. The tuned antenna was then measured for its radiation pattern using a spherical scanner in an anechoic chamber. Fig. 2.9 presents the measured radiation pattern of the antenna with and without solar cells. Each radiation pattern is normalized to its co-polar maximum to see whether the solar cell affects the shape of the radiation pattern. It is seen that the shape and the cross-polar level of the antenna is not affected by the solar cells. The solar cell, as a lossy substrate beneath the cover glass for the antenna, has caused a decrease on the antenna's gain. In order to assess the gain loss of the antenna in a more reliable manner, we performed repetitive tests, where five identical antenna designs were printed on five AF32 cover glass with the same

dimension and then the gain of these antennas were measured with and without the solar cells (the same two fixtures as described previously). The measured values of the antenna's gain are listed in Table 2.2. It is seen that, other than the No. 2 antenna, the gain difference between antenna with and without solar cells is consistent, and is somewhere between 2 and 3 dB. The data from the antenna No. 2 could be due to the printing procedure.

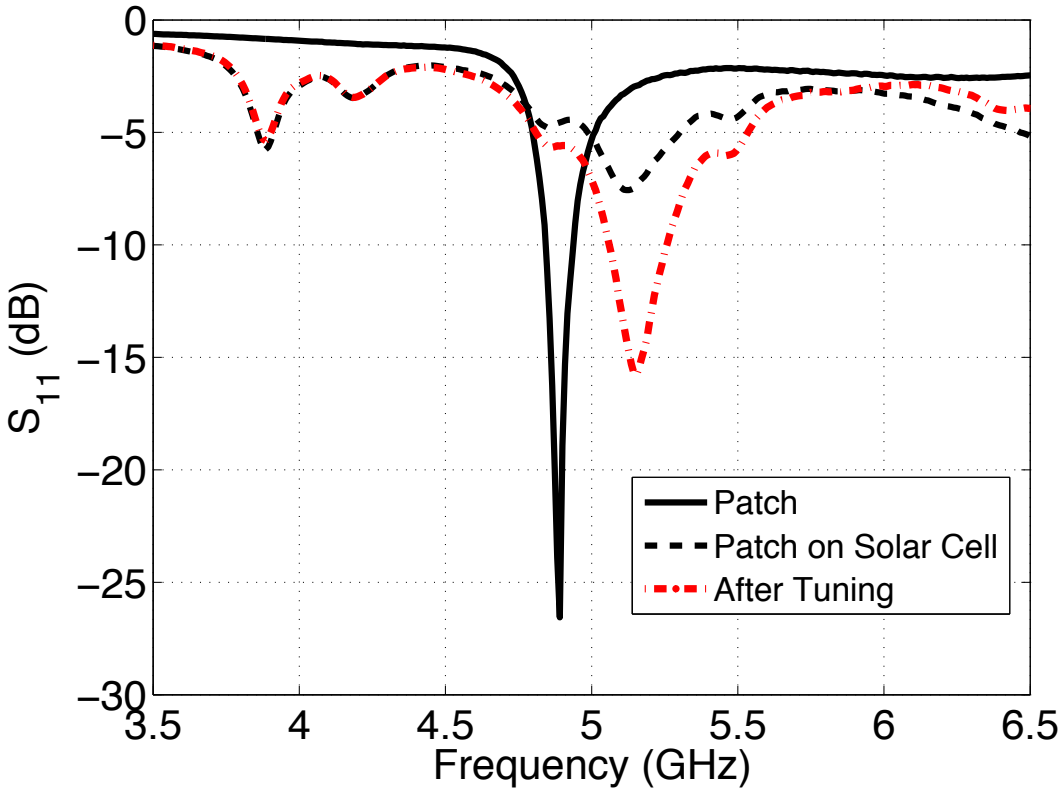

Fig. 2.8: Effect of solar cells on the S_{11} parameter of the patch antenna.

Table 2.2: Repetitive tests: effect of the solar cell on the antenna's gain.

Antenna Number	1	2	3	4	5
Patch w/o Solar Cell Gain (dB)	6.1	4.9	6.5	5.84	6.1
Patch with Solar Cell Gain (dB)	3.12	3.32	3.37	3.37	3.32
Gain Difference (dB)	2.98	1.58	3.1	2.47	2.78

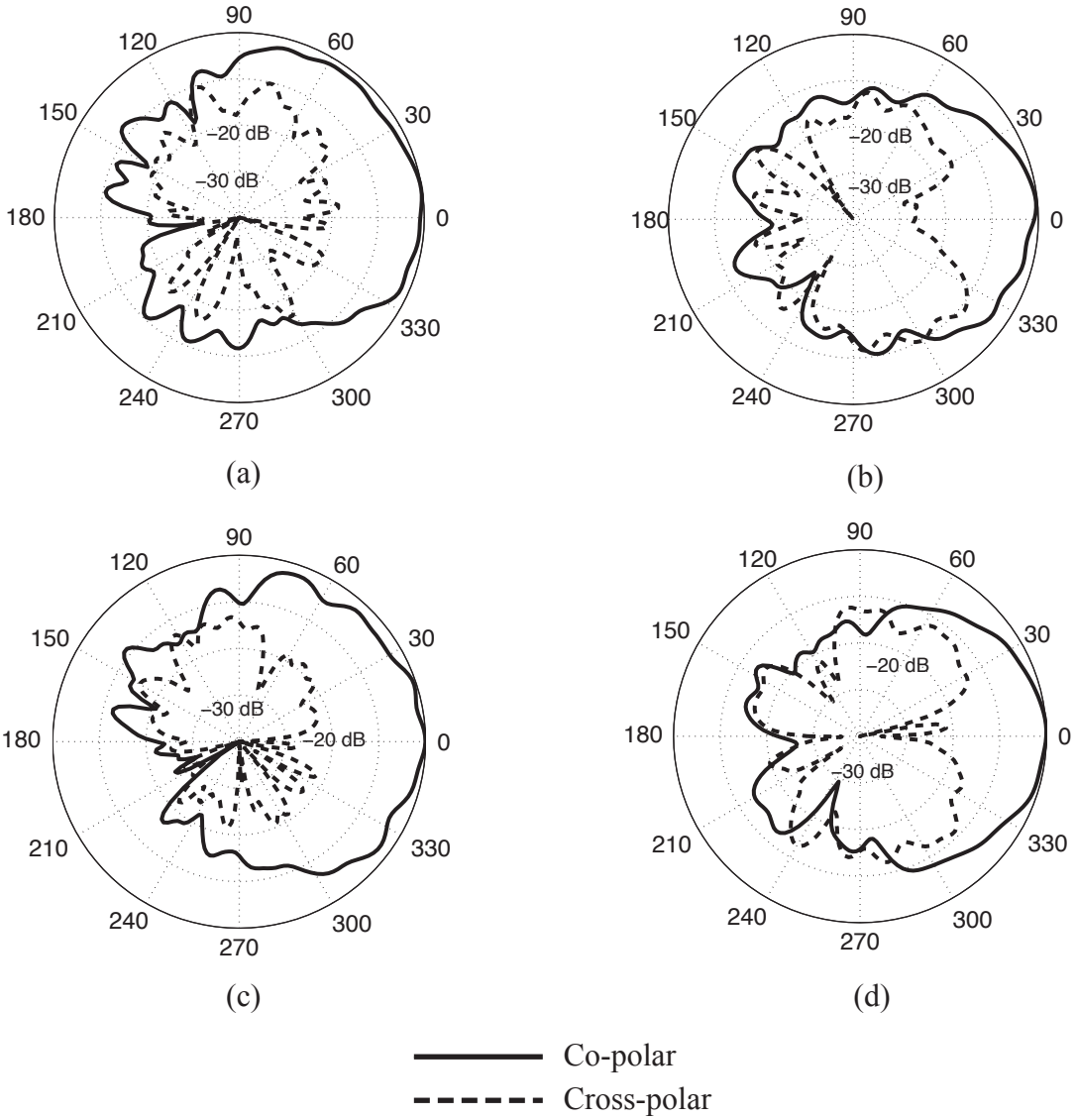

Fig. 2.9: Radiation pattern of patch antenna with and without solar cells under it. (a) E-plane pattern for the patch with solar cells. (b) H-plane pattern for the patch with solar cells. (c) E-plane pattern for the patch without solar cell. (d) H-plane pattern for the patch without solar cell.

2.3.3 Repetitive Tests on Plexiglass as the Cover Glass

The examinations presented in the previous two sections were repeated by replacing the AF32 with off-the-shelf Plexiglass ($\epsilon_r = 2.6$, $tan\delta = 0.0057$ at 1 MHz) that is easy to handle. This test is to ensure that the results from the previous two studies are not specific to a certain cover glass material. We kept the text fixtures the same as ones in Fig. 2.1 and

Fig. 2.2, but changed the cover glass to Plexiglass. Accordingly, we modified the antenna geometry and the feed line. The geometrical and design parameters corresponding to Fig. 2.3 and 2.4 are listed in Table 2.3. It is again seen that impedance of the antenna with solar cell under it has been affected by the solar cell, and we have to tune the antenna to achieve a better matching. The measured S_{11} data for the antenna with (after being tuned for the impedance matching) and without solar cells are plotted in Fig. 2.10. It is seen that in the two cases, the antenna resonated at 5 and 4.83 GHz respectively. The normalized radiation pattern is plotted in Fig. 2.11, and the same conclusion drawn in 2.3.2 stands for this study. The gains of the antenna with and without solar cells were measured to be 2.4 and 5 dB, yielding a difference of 2.6 dB, which is consistent with the results in 2.3.2.

Table 2.3: Geometrical parameters of the antenna on Plexiglass.

Parameter	Value (mm)	Parameter	Value (mm)
L	19.1	S_i	5.9
W	23.5	W_f	3.8
S_g	1.9	L_f	12.1
h	1.3		

2.3.4 Effect of the Working Status of the Solar Cells

One of the questions frequently being asked for antennas integrated with solar panels is whether or not the working status of the solar cells affects the antenna. In other words, whether the current in the electrodes of working solar cells affects the antenna. To address this question, we measured S_{11}, radiation pattern, and the gain of the antenna on a solar cell (Fig. 2.1), when the solar panel was illuminated by an artificial light with varying intensity. We have also measured these parameters by opening, shorting, and connecting different resistive loads to the connector of the solar panel. The tests were repeated for both cases where the AF32 and Plexiglass were used as cover glass. From the test results, there was no significant difference observed for the antenna's performance (S_{11}, radiation

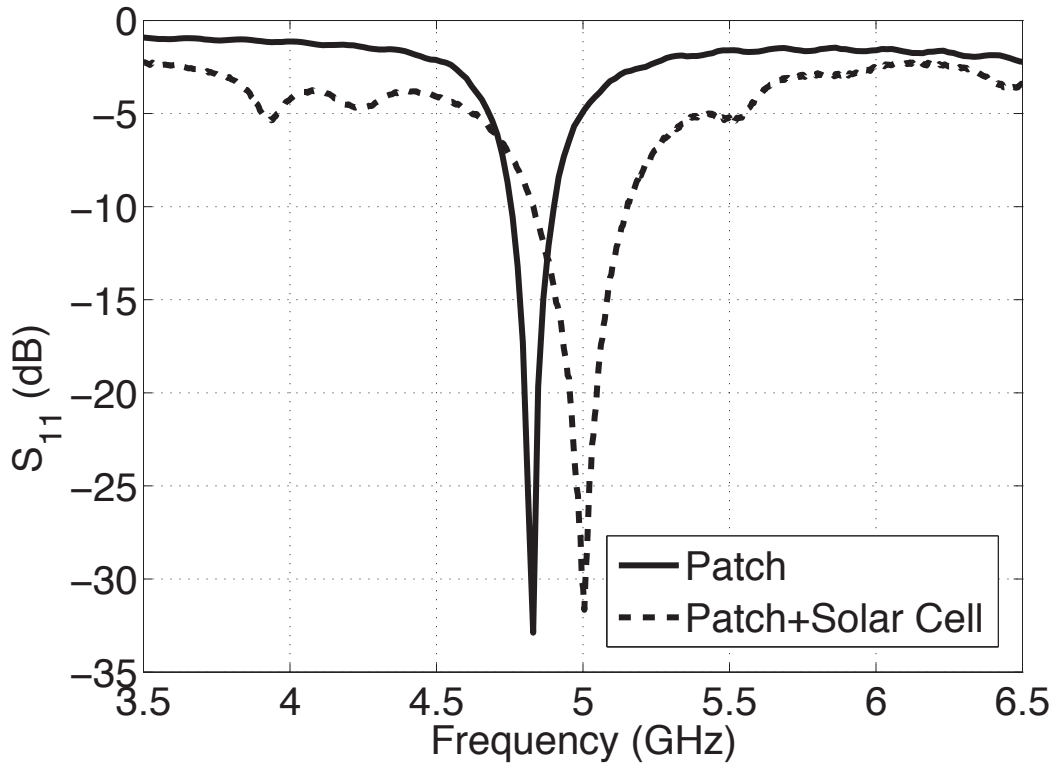

Fig. 2.10: Repetitive test: Effect of solar cells on the S_{11} parameter of the patch antenna.

pattern, gain) at different status of the solar cells. In particular, the decrease due to the solar cell on the antenna's gain remained the same (2-3 dB) regardless of the working status of the solar cells.

2.3.5 Effect of Solar Panel Geometry

To understand whether the assessment on the gain loss of the antenna due to the solar cell is dependent on the solar panel geometry (i.e. number of solar cells, orientation of solar cells), the following simulative studies have been performed. From the experimental results, we entered the fixtures in Fig. 2.1 into HFSS by modeling the solar cell as a Ge substrate with added conductivity (σ). Then we adjusted σ until achieving 2.5 dB gain loss of the antenna from the case where there is no solar cell (Fig. 2.2). After that, the structure is altered into a one-cell solar panel as in Fig. 2.12 while keeping all the parameters the same except the size of the panel and number of solar cells. It is found that the gain loss on

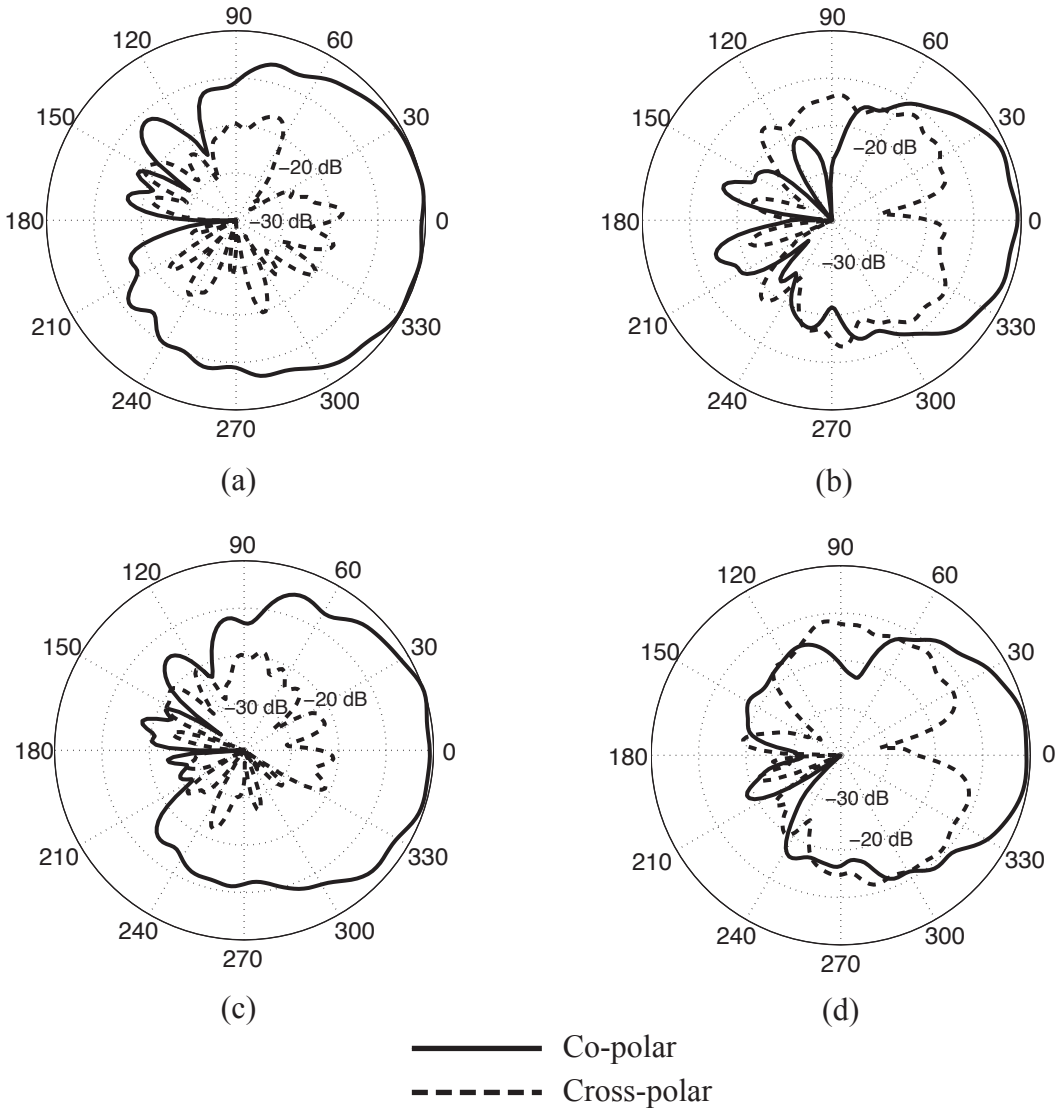

Fig. 2.11: Repetitive Test: Radiation pattern of patch antenna with and without solar cells under it. (a) E-plane pattern for the patch with solar cells. (b) H-plane pattern for the patch with solar cells. (c) E-plane pattern for the patch without solar cell. (d) H-plane pattern for the patch without solar cell.

the antenna due to the solar cell is still within 2-3 dB range for an antenna that operates around 4.9 GHz.

In addition, from experiments, the orientation of the solar cells (or the orientation of the antenna relative to the solar cell, such as in Fig. 2.12.a and Fig. 2.12.b) has shown very small or little effect on the antenna.

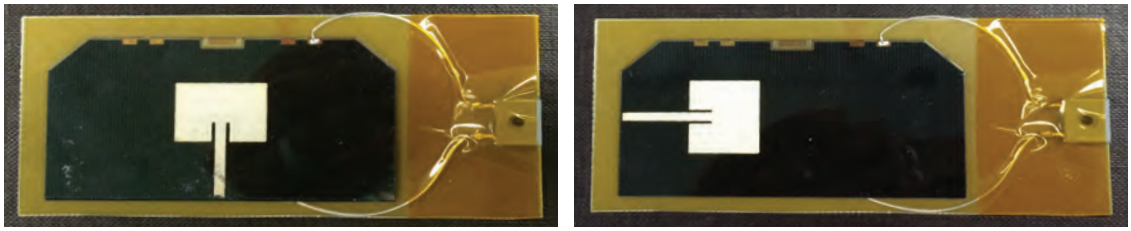

(a) (b)

Fig. 2.12: Antenna integrated on a single solar cell. (a) Orientation 1. (b) Orientation 2.

2.3.6 Effect of Air Gap or Adhesive Layer

The results in 2.3.2 showed that the solar cell shifted the resonant frequency of the antenna upwards, contradictory to the previous results [12]. This is mostly due to the possible air gaps between solar cell and the AF32 cover glass. In Shynu's study [12], the solar cell is a bare cell without cover glass. Therefore, the solar cell may increase the overall effective permittivity of the substrate for the antenna, and accordingly lower the resonant frequency. To verify the effect of the air gap, which is possible in our assembly as solar cell and glass were clipped together, we entered the fixture in Fig. 2.1 into HFSS, and added an air layer between the solar cell and the glass. The antenna geometry is kept the same as in Table 2.1 and it resonates at 4.87 GHz when there is no solar cell (Fig. 2.2). The effect of the air layer is summarized in Table 2.4, where h_{air} is the thickness of this layer and f_r is the resonant frequency. It is seen that when there is no air gap, the solar cell shifts the f_r downward. When an air layer is present, even if it is very thin such as 50 μm, f_r is shifted to be higher than the case when there is no solar cell.

In space solar cell manufacturing, it is a common practice to use a highly transparent

Table 2.4: Effect of air gap and adhesive layer.

$h_{air}(mm)$	$f_r(GHz)$	$h_{adhesive}(mm)$	$f_r(GHz)$
0	4.68	0	4.68
0.05	5.02	0.05	4.78
0.1	5.22	0.1	4.83
0.15	5.4	0.15	4.89

adhesive layer to bond a solar cell with its cover glass. An example of such adhesive is Dow Corning 93-500 Space Grade Encapsulant 115 Gram (g) Kit [24], which has a dielectric constant of 2.59 at 100 kHz. While recognizing that this ϵ_r may be different at 5 GHz, we used it for study purposes and the results are summarized in Table 2.4, with $h_{adhesive}$ being the thickness of the adhesive layer. It is seen again that the inclusion of an adhesive material, which is necessary in space application, between cover glass may affect the resonant frequency of the antenna. Most adhesive has lower ϵ_r than the cover glass, and therefore, the solar cell and the adhesive shift the resonant frequency to opposite directions. Depending on the material and thickness of the adhesive, the final resonant frequency of the antenna may not be affected (e.g. when adhesive is between 0.1 mm and 0.15 mm according to Table 2.4) or shifted slightly up or down from the case when there is no solar cell.

2.4 Conclusion

The paper presents a series of detailed experimental studies to quantify the effect of a real–world active space solar cell on a solid patch antenna integrated on it. Test fixtures, with RF ground electrically isolated from the solar cells, were fabricated to study the frequency response, input impedance, radiation pattern, and gain of a patch antenna designed at 4.9 GHz when there is an active solar cell under the antenna. It is found that the solar cell affects the input impedance of the antenna, and more importantly, reduces the gain of the antenna for 2-3 dB. The shape of the radiation pattern and cross-polarization level are not affected by the solar cells. Solar cell alone may shift the resonant frequency of the antenna downward, however, such conclusion claimed by previous study may not be applicable in space applications as it is a common practice that solar cells are bonded with cover glass with an adhesive layer, which normally has a smaller dielectric constant than cover glass. Therefore, the combined effect on the resonant frequency from the solar cell and adhesive may not be dramatically different from when the antenna is designed on the cover glass only. In addition, it is found that the effect of the solar cells on the antenna does not vary for the different working states of the solar cells. In other words, the DC current in the electrodes of the solar cells has little effect on the antenna performance. On

the reliability side, three types of repetitive tests were performed. First, five repetitive tests were performed on AF32 cover glass. Next, a Plexiglass substrate was used as the cover glass, and we saw the gain decrease of the antenna due to solar cell was consistent. Finally, the antenna was studied on a single solar cell, and the effect of the solar cell on the antenna remained the same as the prior tests. Although the experiments were performed at 4.9 GHz, it is reasonable to expect a similar result for frequencies around 5.0 GHz, which may be the next frequency of interest for CubeSat community. In summary, it has been shown consistently that one needs to expect a 2-3 dB gain reduction of a patch antenna operating at the vicinity of 5.0 GHz when being integrated on top of a common commercial triple junction solar cell. This will provide an important design consideration and entry to the link-budget for CubeSat missions.

References

[1] S. Vaccaro, P. Torres, J. R. Mosig, A. Shah, J. F. Zurcher, A. K. Skrivervik, F. Gardiol, P. de Maagt, and L. Gerlach, "Integrated solar panel antennas," *Electron. Lett.*, vol. 36, no. 5, pp. 390–391, 2000.

[2] M. Zawadzki and J. Huang, "Integrated RF antenna and solar array for spacecraft application," in *IEEE International Conference on Phased Array Systems and Technology*, Dana Point, CA, 2000, pp. 239–242.

[3] T. Wu, R. L. Li, and M. M. Tentzeris, "A mechanically stable, low profile, omnidirectional solar-cell integrated antenna for outdoor wireless sensor nodes," in *Antennas and Propagation Society International Symposium (APS 2009)*, Charleston, SC, 2009, pp. 1–4.

[4] T. Shahvirdi and R. Baktur, "A study on the effect of space solar cells on the antennas integrated on top of their cover glass," in *Antennas and Propagation Society International Symposium (APSURSI 2014)*, Memphis, TN, 2014, pp. 215–216.

[5] M. Tanaka, Y. Suzuki, and K. Araki, "Microstrip antenna with solar cells for microsatellites," *Electron. Lett.*, vol. 31, no. 1, pp. 5–6, 1995.

[6] S. Vaccaro, J. R. Mosig, and P. de Maagt, "Two advanced solar antenna "SOLANT" designs for satellite and terrestrial communications," *IEEE Trans. Antennas Propag.*, vol. 51, no. 8, pp. 2028–2034, 2003.

[7] O. Yurduseven, D. Smith, and M. Elsdon, "A solar cell stacked multi-slot quad-band PIFA for GSM, WLAN and WiMAX networks," *IEEE Antennas Wireless Propag. Lett.*, vol. 23, pp. 285–287, 2013.

[8] M. Mahmoud, R. Baktur, and R. Burt, "Fully integrated solar panel slot antennas for small satellites," in *Proc. 15th Annual AIAA/USU Conf. on Small Satellites*, Logan, UT, Aug. 2010.

[9] T. Wu, R. L. Li, and M. M. Tentzeris, "A scalable solar antenna for autonomous integrated wireless sensor nodes," *IEEE Antennas Wireless Propag. Lett.*, vol. 10, pp. 510–513, 2011.

[10] R. Caso, A. D'Alessandro, A. Michel, and P. Nepa, "Integration of slot antennas in commercial photovoltaic panels for stand-alone communication systems," *IEEE Trans. Antennas Propag.*, vol. 61, no. 1, pp. 62–69, 2013.

[11] T. W. Turpin and R. Baktur, "Meshed patch antennas integrated on solar cells," *IEEE Antennas Wireless Propag. Lett.*, vol. 52, pp. 693–696, 2009.

[12] S. V. Shynu, M. J. Roo-Ons, P. McEvoy, M. J. Ammann, S. J. McCormack, and B. Norton, "Integration of microstrip patch antenna with polycrystalline silicon solar cell," *IEEE Trans. Antennas Propag.*, vol. 57, no. 12, pp. 3969–3972, 2009.

[13] E. H. Lim and K. W. Leung, "Transparent dielectric resonator antennas for optical applications," *IEEE Trans. Antennas Propag.*, vol. 58, no. 4, pp. 1054–1059, 2010.

[14] M. J. Roo-Ons, S. V. Shynu, M. J. Ammann, S. J. McCormack, and B. Norton, "Transparent patch antenna on a-Si thinfilm glass solar module," *Electron. Lett*, vol. 47, no. 2, pp. 85–86, 2011.

[15] O. Yurduseven, D. Smith, and M. Elsdon, "UWB meshed solar monopole antenna," *Electron. Lett.*, vol. 49, no. 9, pp. 58–584, 2013.

[16] T. Yasin and R. Baktur, "Circularly polarized meshed patch antenna for small satellite application," *IEEE Antennas Wireless Propag. Lett.*, vol. 12, pp. 1057–1060, 2013.

[17] P. Dreyer, M. Morales-Masis, S. Nicolay, C. Ballif, and J. Perruisseau-Carrier, "Copper and transparent-conductor reflectarray elements on thin-film solar cell panels," *IEEE Trans. Antennas Propag.*, vol. 62, no. 7, pp. 3813–3818, 2014.

[18] T. Shahvirdi and R. Baktur, "Analysis of the effect of solar cells on the antenna integrated on top of their cover glass," in *Antennas and Propagation Society International Symposium*, Vancouver, 2015, pp. 2429–2430.

[19] N. Henze, C. Bendel, J. Kirchhof, and H. Fruchting, "Application of photovoltaic solar cells in planar antenna structures," in *Proc. 12th Int. Conf. on Antennas and Propagation*, Exeter, U.K., Mar. 2003, pp. 731–734.

[20] N. Henze, M. Weitz, P. Hofmann, C. Bendel, J. Kirchoff, and H. Fruchting, "Investigations on planar antennas with photovoltaic solar cells for mobile communications," in *Proc. IEEE Int. Symp. on Personal, Indoor and Mobile Radio Commun*, Sep. 2004, pp. 622–626.

[21] J. Oh, K. Lee, T. W. Hughes, S. Forrest, and K. Sarabandi, "Flexible antenna integrated with an epitaxial lift-off solar cell array for flapping-wing robots," *IEEE Trans. Antennas Propag.*, vol. 62, no. 8, pp. 4356–4361, 2014.

[22] [Online]. Available: http://www.emcore.com

[23] [Online]. Available: http://www.schott.com

[24] [Online]. Available: http://www.ellsworth.com

CHAPTER 3
AN X BAND PATCH ANTENNA INTEGRATED WITH COMMERCIAL TRIPLE–JUNCTION SOLAR CELLS

Abstract

An X band patch antenna was integrated on top of the cover glass of commercial space–certified solar cell and was studied for understanding the interaction between the solar cell and the antenna. It was found that the solar cell acts as a lossy substrate for the antenna and reduces the gain of the antenna by about 2 dB, and such a reduction remains consistent for different working states of the solar cell. The patch antenna reduces the efficiency of the solar cells because it blocks light, however, at 10 GHz, the impact of a patch antenna alone to the solar cell's efficiency is less than 1%.

3.1 Introduction

CubeSats, due to their modular design, low cost, and versatility, are receiving increased interest in space missions [1], and consequently, designing a reliable and effective antenna system compatible with CubeSat specifications is in demand. Considering disadvantages such as being mechanically expensive of deployed wire antennas, and limited surface real estate of a CubeSat (Fig. 3.1), it is favorable to integrate planar antennas with CubeSats solar cells. Integrations of antennas under or around solar cells have been reported [2–6]. This paper is to present our study in printing a 10 GHz antenna directly on top of the solar cell and examination of how solar cells and the antenna affect each other. Due to the high operational frequency, the size of the antenna is small and the effect on the solar cell's efficiency is manageable. The study also provides a baseline for extending the printed antenna to optically transparent meshed antenna [7] as well as a completion for previously reported integration [8], where a patch antenna with its own substrate was placed on solar

cells. While the study in [8] has its own merit, this paper examines a modular printing of the antenna on all off–the–shelf space–certified components that are convenient for a flight mission.

3.2 Antenna Geometry and Test Fixtures

The assembly of the integrated solar cell antenna is as shown in Fig. 3.2. The geometry information is as follows. From bottom to top, there are a copper layer as the ground followed by a Kapton layer, solar cell, and cover glass with antenna printed on top. The Kapton layer is very thin ($\sim$ 0.06 mm) and it is used to isolate the metal coating on the bottom of the solar cell from the ground because the metal layer is the electric positive of the photovoltaic cell. The cover glass is common for space solar cells to protect them from complex environment, and can be conveniently utilized as the dielectric substrate for the antenna.

In order to assess how solar cells affect the printed patch antenna, we prototyped two fixtures as shown in Fig. 3.3, where the fixture in Fig. 3.3.a has two functional solar cells

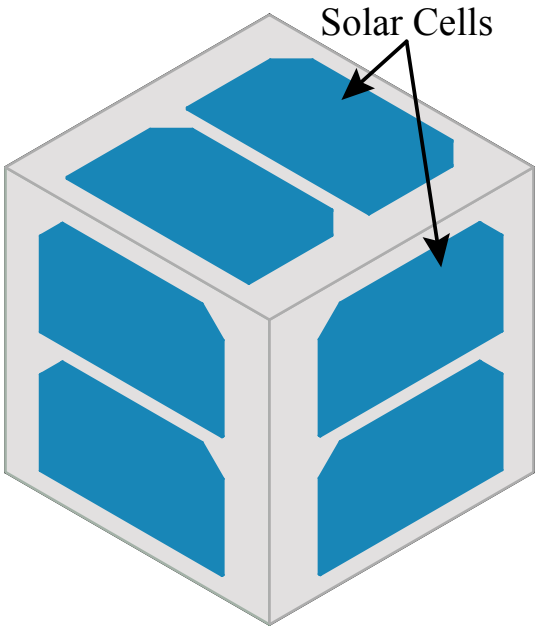

Fig. 3.1: 1U CubeSat schematic ($10\times10\times10$ cm^3).

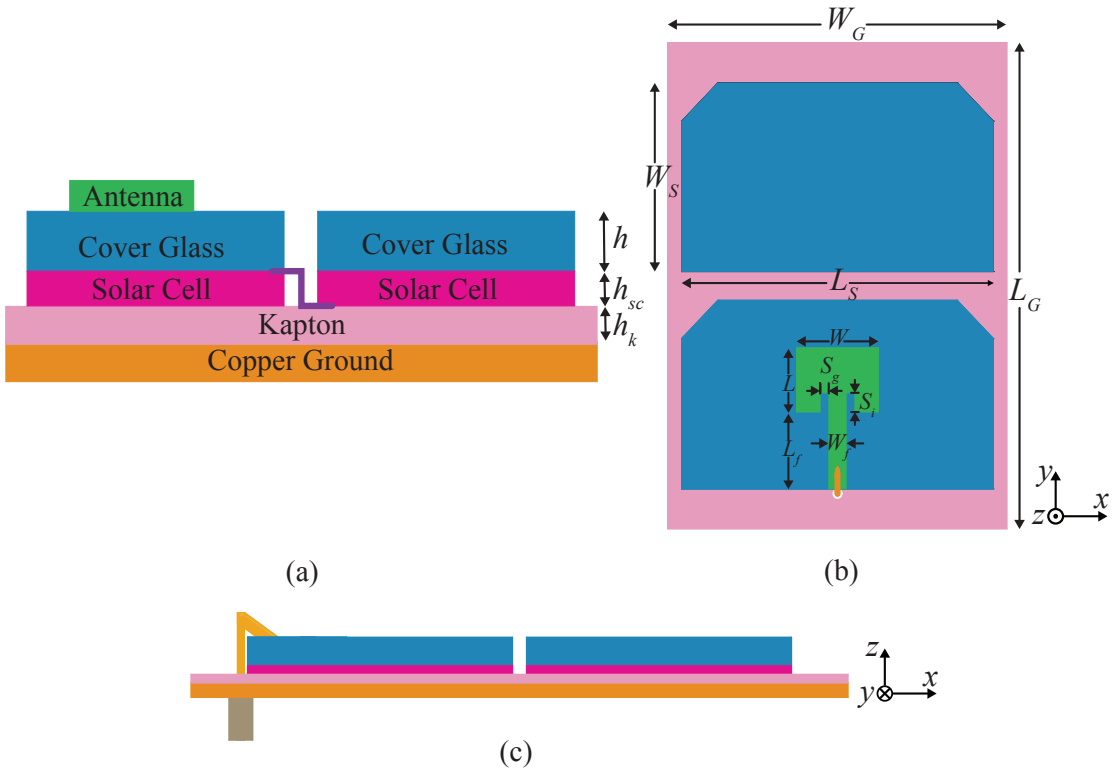

Fig. 3.2: Proposed fixture geometry: (a) Fixture layers. (b) Top view. (c) Side view.

connected in serial, and the one in Fig. 3.3.b does not have solar cells. A cover glass with a printed antenna is then tested on the two fixtures for comparisons. The size and material information of the fixture are as follows. Emcore's triple junction bare cells [9] and a glass (AF32 [10]) with high optical transparency (93%) and high temperature resistance are used. The dielectric constant and loss tangent of the AF32 glass are 4.5 and 0.015 at X band. The design frequency is 10 GHz and the values for parameters marked on Fig. 3.2 are listed in Table 3.1. The antenna was designed using HFSS and screen printed multiple times using silver conductive ink [11] on the glass to ensure that the thickness of the antenna is significantly higher than the microwave skin depth.

In order to eliminate the interaction between the SMA connector with the antenna, the fixture is such that the connector is under the ground plane (Fig. 3.3.c). We have also printed antennas with two orientations: parallel and perpendicular. In the parallel

orientation (Fig. 3.3.a), the length (L in Fig. 3.2) side of the patch antenna is parallel to the width of the solar cell. In this case, the direction of the surface current on the patch is parallel to the copper electrode lines of the solar cell [12]. The other orientation is denoted as perpendicular (Fig. 3.3.d). After printing an antenna on an AF32 glass, the glass is then assembled on the test fixture and fastened with nylon clips.

3.3 Results

The antenna with an orientation as explained in section 3.2 was put on the fixture without solar cells for measurements and then the procedure was repeated on the fixture with solar cells. The measurements were performed using Agilent's PNA network analyzer and NSI's spherical scanner in a near–field anechoic chamber. Frequency response, normal-

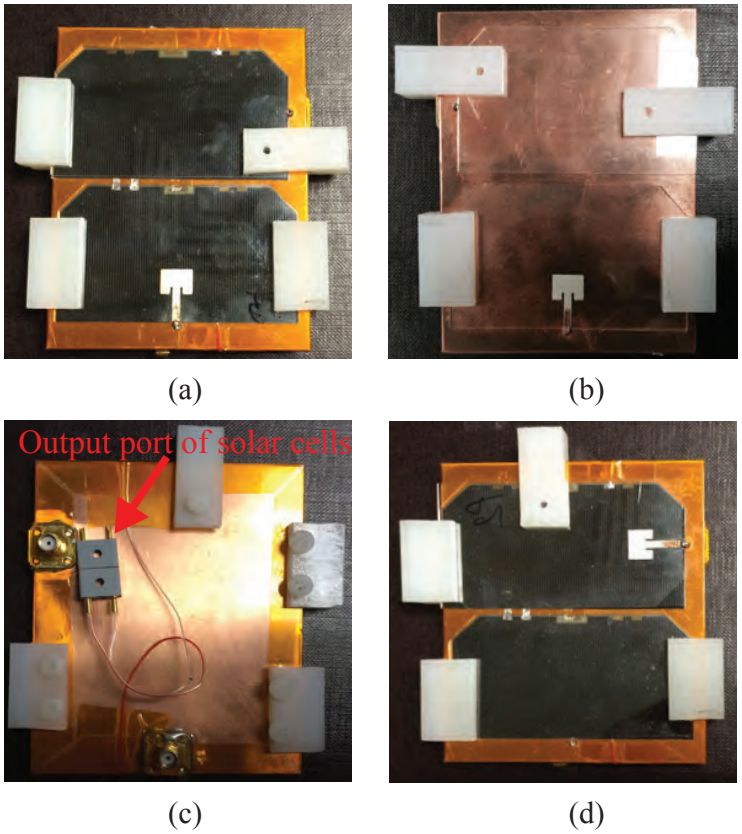

Fig. 3.3: Prototyped fixture: (a) Fixture with solar cells. (b) Fixture without solar cell. (c) Backside of the fixture. (d) Perpendicular orientation of the printed patch antenna.

Table 3.1: Geometrical parameters of the antenna and the fixture.

Parameter	Value (mm)	Parameter	Value (mm)
h	1	W	9
h_{sc}	0.15	L	6.7
h_k	0.058	W_f	1.9
W_G	75	L_f	10
L_G	97	S_i	0.95
W_S	39.5	S_g	2
L_S	69		

ized radiation pattern of the antenna were measured for both orientations and presented in Figs. 3.4–3.7. Table 3.2 lists the absolute gain of the antenna with and without solar cells underneath.

3.3.1 Effect of Solar Cells on the Antenna

From Fig. 3.4 and Fig. 3.5, it is seen that the solar cell acts as a lossy substrate. As the dielectric constant of the solar cell is normally higher than the cover glass, one expects a resonant frequency shifts downward whereas Fig. 3.4 and Fig. 3.5 show an upward shift. This is because of the air bubbles between the solar cell and cover glass that is inevitable when using nylon clips as discussed in [13]. The solar cells show little effect on the shape of the radiation pattern and the cross polarization level (Fig. 3.6 and Fig. 3.7). The gain reduction of the antenna due to the lossy solar cells can be read from Table 3.2 and is slightly higher than 2 dB. The results in the Table 3.2 were obtained through repeated tests that showed consistent data. This gain loss also remained consistent for different cover glass material or thickness, as long as it is thick enough to support an effective antenna radiation and thin enough not to excite higher modes.

3.3.2 Effect of Working States of Solar Cells

To verify the antenna's performance under different working states of the solar cells, the antenna with solar cells under it was measured while the solar cells were terminated

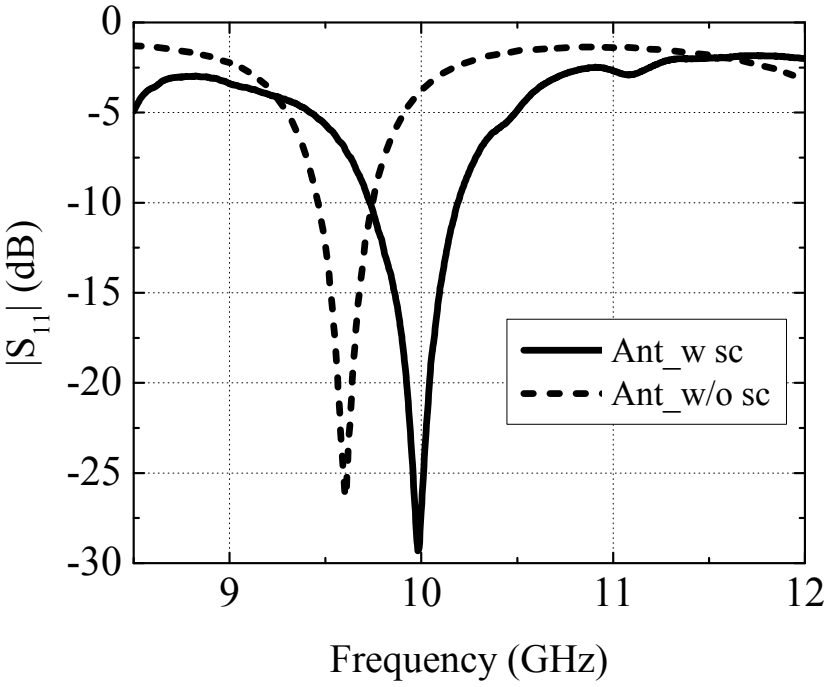

Fig. 3.4: Reflection coefficient of parallel orientation.

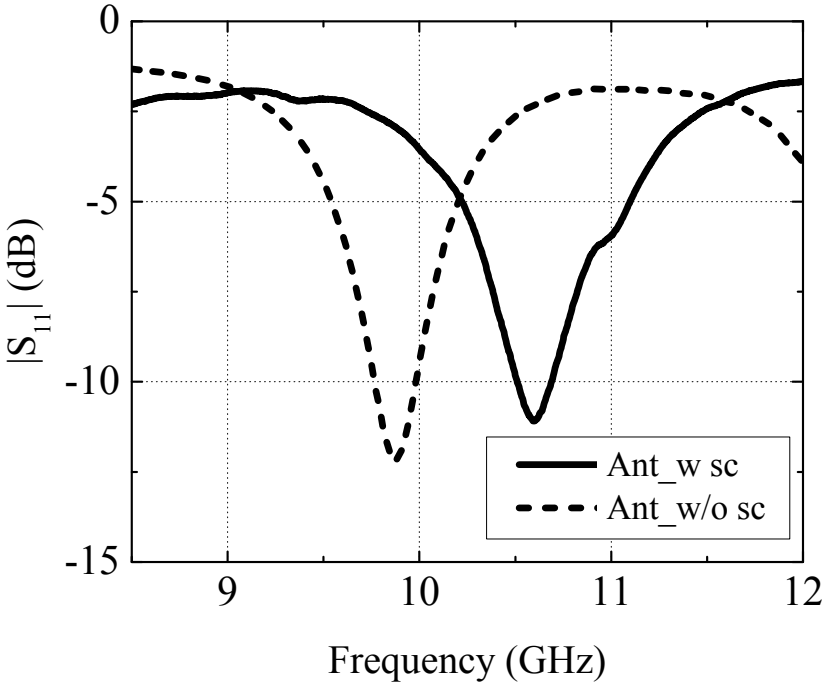

Fig. 3.5: Reflection coefficient of perpendicular orientation.

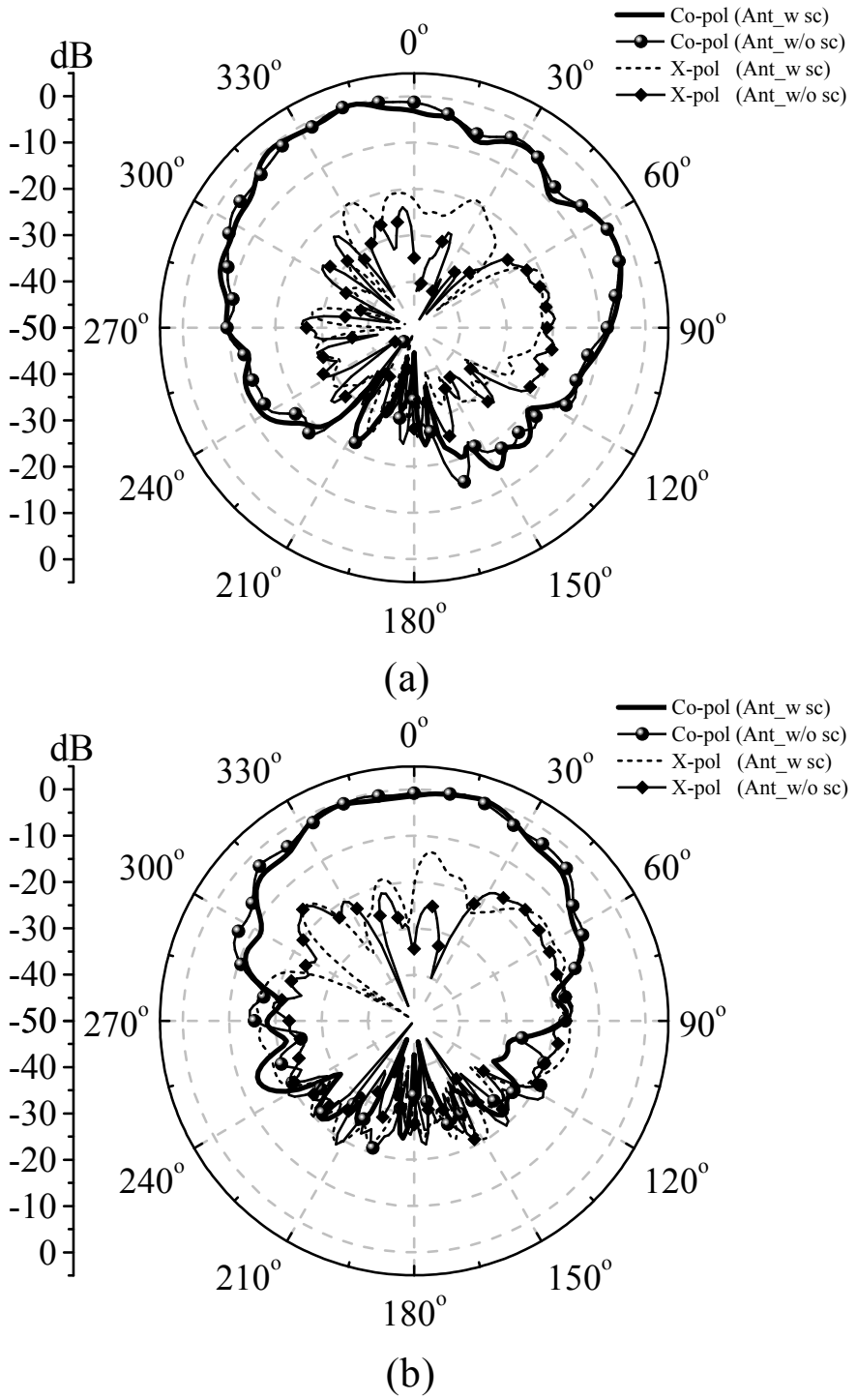

Fig. 3.6: Normalized radiation pattern of parallel orientation: (a) y–z plane. (b) x–z plane.

Table 3.2: Measured antennas' gain.

Orientation	Parallel	Perpendicular
Ant_w sc Gain(dB)	4.1	3.9
Ant_w/o sc Gain(dB)	6.4	6.1
Gain Difference (dB)	-2.3	-2.2

with different loads at the output port (Fig. 3.3.c) and under different illumination. No visible effect was noted on the antenna's resonant frequency (Fig. 3.8), radiation pattern (Fig. 3.9), or gain for different status of solar cells.

3.3.3 Effect of the Antenna on Solar Cells

To assess the effect of the patch or the blockage of the patch on the solar cells, a series of tests were performed in a controlled environment to measure solar cell's output voltage, power, and I–V curve. Before each test, the solar cells were cleaned with alcohol and an ionizer was turned on near the test bench for air purifying. The measurement setup consists of artificial light, pyrometer, computer–controlled variable resistor, and multimeter. The test procedure is that first a bare solar cell was measured, then a clear cover glass was placed on the solar cell to repeat the tests, and finally a cover glass with printed antenna on top was placed on the solar cell for measurements. The results are summarized in Fig. 3.10 only for the antenna with parallel orientation because the other orientation was found to have the same effect. The efficiency of the bare solar cell is calculated accordingly and summarized in Table 3.3. The efficiency of the bare cell is lower than factory data [9] because it has stayed on shelf for more than seven years. From Fig. 3.10 and Table 3.3, it is seen that the antenna together with the cover glass reduces the output power and efficiency of the solar cell, however, as a 10 GHz patch antenna has a small size, the efficiency reduction due to the antenna alone on a solar cell with cover glass is only 0.6%. This provides an important entry in the link and power budget consideration for a CubeSat mission.

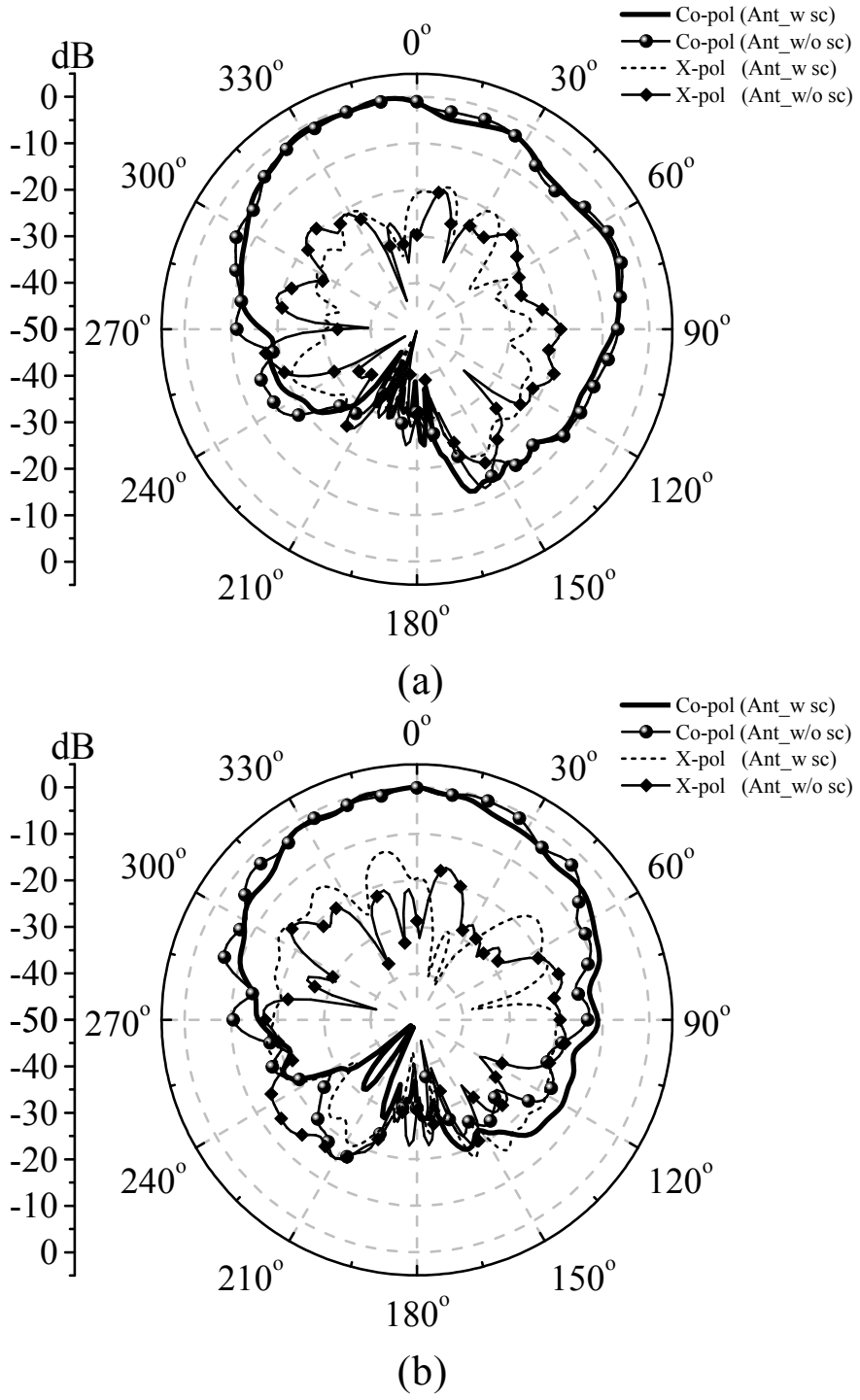

Fig. 3.7: Normalized radiation pattern of perpendicular orientation: (a) x–z plane. (b) y–z plane.

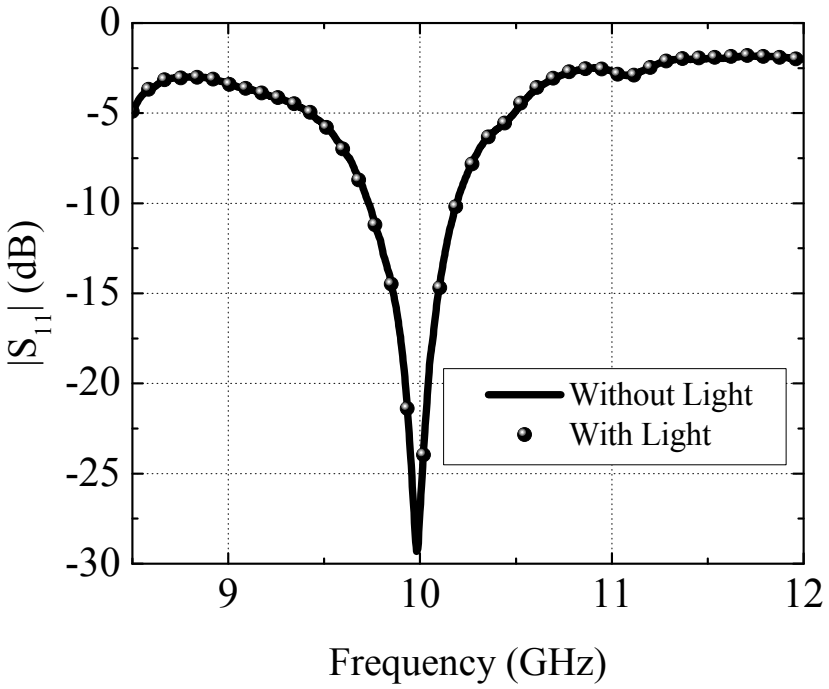

Fig. 3.8: Reflection coefficient of integrated structure under illumination.

Table 3.3: Measured solar cell efficiency.

Name	Bare Cell	+ Glass	+ Patch
Efficiency (%)	21	18	17.4

3.4 Conclusion

This paper examines the interaction between a commercial space solar cell and the patch antenna printed on top of the cover glass of the solar cell. The operational frequency is 10 GHz, and therefore, the size of the antenna is small enough not to cast significant shadow on the solar cell. It was found that the solar cell reduced the antenna's gain to about 2 dB and did not affect the shape of the radiation pattern. The working states of the solar cell was also found to have little effect on the antenna. In other words, the DC current in the electrodes of the solar cells does not affect the antenna's performance. The same conclusion holds for the different orientation of the antenna on the solar cell. When the solar cell's performance was explained, it was found that the antenna together with the

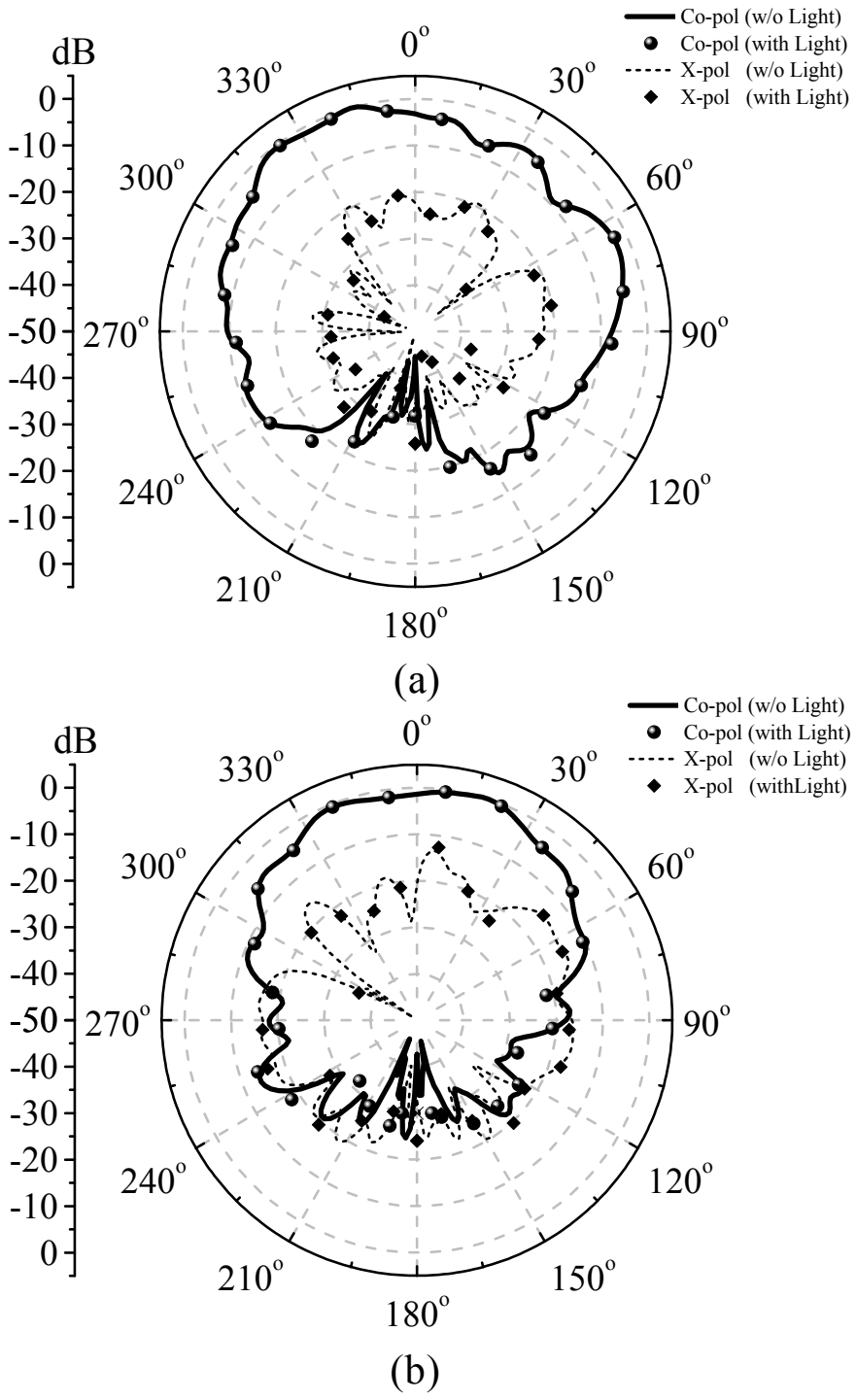

Fig. 3.9: Normalized radiation pattern under illumination: (a) y–z plane. (b) x–z plane.

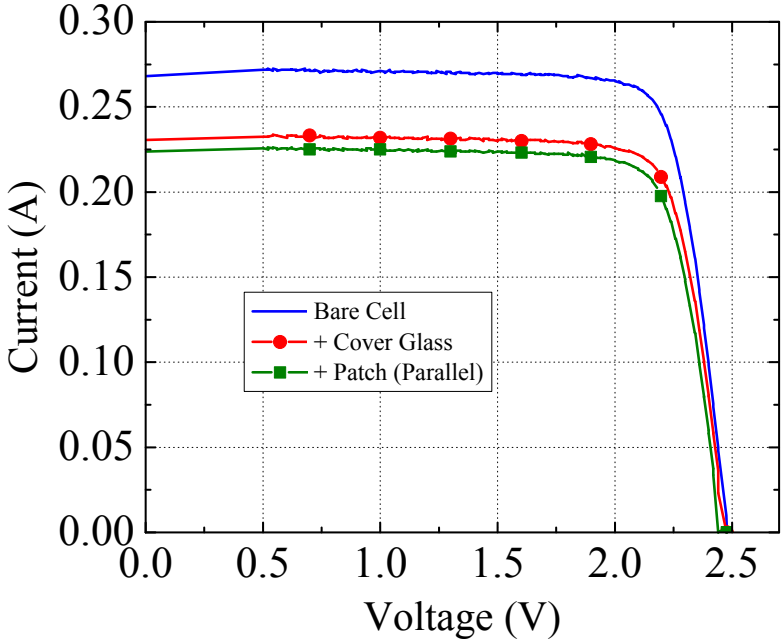

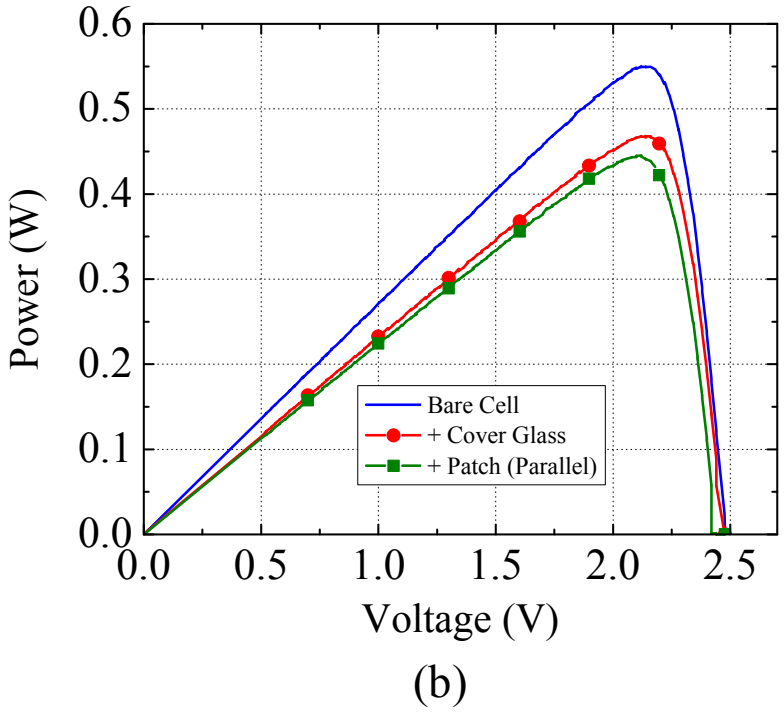

Fig. 3.10: (a) Measured I–V curve. (b) Measured output power.

cover glass reduced the efficiency of the solar cell. But, the antenna alone has only 0.6% effect on the solar cell, and therefore, providing support in integrating antenna directly on solar panels of CubeSats to save surface real estate.

References

[1] M. Swartwout, "The first one hundred CubeSats: a statistical look," *JoSS*, vol. 2, pp. 213–223, 2014.

[2] M. Tanaka, Y. Suzuki, and K. Araki, "Microstrip antenna with solar cells for microsatellites," *Electron. Lett.*, vol. 31, no. 1, pp. 5–6, 1995.

[3] S. Vaccaro, J. R. Mosig, and P. de Magat, "Making planar antennas out of solar cells," *Electron. Lett.*, vol. 38, no. 17, pp. 945–947, 2002.

[4] O. Yurduseven and D. Smith, "A solar cell stacked multi-slot quad-band PIFA for GSM, WLAN and WiMAX networks," *IEEE Antennas Wireless Propag. Lett.*, vol. 23, no. 6, pp. 285–287, 2013.

[5] R. Caso, A. DAlessandro, A. Michel, and P. Nepa, "Integration of slot antennas in commercial photovoltaic panels for stand-alone communication systems," *IEEE Trans. Antennas Propag.*, vol. 61, no. 1, pp. 62–69, 2013.

[6] M. Mahmoud, R. Baktur, and R. Burt, "Fully integrated solar panel slot antennas for small satellites," in *Proc. 15th Annual AIAA/USU Conf. on Small Satellites*, Logan, UT, Aug. 2010.

[7] T. W. Turpin and R. Baktur, "Meshed patch antennas integrated on solar cells," *IEEE Antennas Wireless Propag. Lett.*, vol. 52, pp. 693–696, 2009.

[8] S. V. Shynu, M. J. Roo-Ons, , M. J. Ammann, S. J. McCormack, and B. Norton, "Integration of microstrip patch antenna with polycrystalline silicon solar cell," *IEEE Trans. Antennas Propag.*, vol. 57, no. 12, pp. 3969–3972, 2009.

[9] [Online]. Available: http://www.emcore.com

[10] [Online]. Available: http://www.schott.com

[11] [Online]. Available: http://www.creativematerials.com

[12] T. Shahvirdi and R. Baktur, "Analysis of the effect of solar cells on the antenna integrated on top of their cover glass," in *IEEE Antennas and Propagation Society International Symposium (APS 2015)*, Vancouver, BC, 2015, pp. 1522–3965.

[13] T. Yekan and R. Baktur, "An experimental study on the effect of commercial triple junction solar cells on patch antennas integrated on their cover glass," *Progress In Electromagnetics Research C*, vol. 63, pp. 131–142, 2016.

CHAPTER 4

ANALYSIS OF SOLAR CELLS' EFFECT ON THE INTEGRATED ANTENNA

4.1 Effect of Ag Electrode Lattice in a Commercial Space Solar Cell on a Patch Antenna Integrated on Top of It

Abstract

A solar cell normally has a conductive electrode lattice embedded with its semiconductor layer. In space solar cells, in particular, those lattices are commonly made from Ag and are between the layer of solar cell junctions and cover glass. This paper examines the effect of those Ag lattice in space solar cells on the patch antenna integrated on the cover glass. It is found that as solar cell is a lossy material at GHz frequency range, the lattice helps to shield the antenna from the lossy layer and hence minimize its gain reduction due to the solar cells underneath.

4.1.1 Introduction

Integrating planar antennas on top of solar cells has enormous potentials in space explorations [1, 2]. Two questions rise directly from an attempt of such an integration: (1) what is the effect of the antenna on the solar cell's efficiency? and (2) how much is the impact of the solar cell on the antenna's properties. The first question can be addressed easily by measuring a solar cell's efficiency with and without an antenna placed on top of it. The second question depends heavily on the material and geometrical characteristics of the solar cells. There are many vendors that supply solar cells, and many research groups fabricate their custom designed solar cells. But, most of those solar cells have one thing in common, i.e. they all have a metal electrode lattice to conduct current. Therefore, it is important to study how these lattices affect the antenna design.

In our study EMcore's (www.emcore.com) space certified triple junction solar cells are of main interest for a simple reason that these solar cells are among the most commonly used ones in space industry. The geometry of a typical triple junction solar cell of EMcore is as follows (Fig. 4.1). From bottom to top are a metal backing layer, Ge based photovoltaic layer, a layer of metal (Ag is the most commonly used material) electrode lattice, and a cover glass. AF32 ($\epsilon_r = 4.5$) is a commonly used cover glass manufactured by Shott (www.schott.com). When integrating a patch antenna on top of such a solar cell, the cover glass acts as the substrate and the bottom metal layer as ground plane for the antenna. Although many studies presented measured dielectric constant of the photovoltaic layer [3], we found that the effect of the lattice casts more impact on the antenna design. This motivated an examination of these lattices as presented in this paper.

4.1.2 Effect of the Ag Lattice

In order to understand the nature of the lattice layer in terms of its effect on the antenna design, three structures were studied. The first is as shown in Fig. 4.1 and as explained in the introduction. The second geometry is an imaginary solar cell without the lattice (Fig. 4.2), and the third one, which serves as a reference, is a patch antenna on the cover glass backed by a ground plane (Fig. 4.3). Also, Fig. 4.4 shows the patch antenna geometry and Table 4.1 lists the geometrical parameters used in this study. In addition, initial experiments did not show much difference in the effect working status of the solar cell on the antenna design, which means whether the junctions are active or not does not

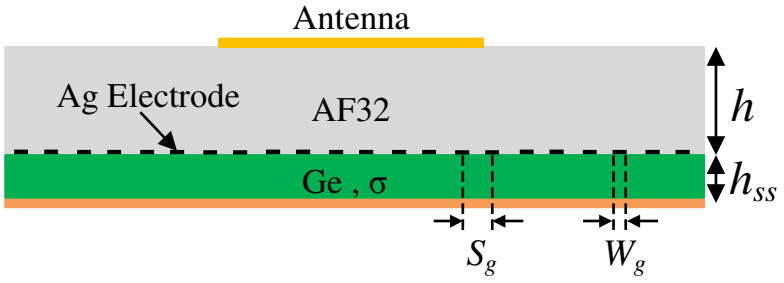

Fig. 4.1: Geometry of a triple junction solar cell with an antenna integrated on top of it.

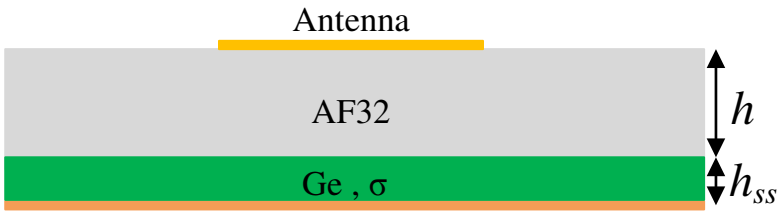

Fig. 4.2: Antenna on a fictitious solar cell without electrodes.

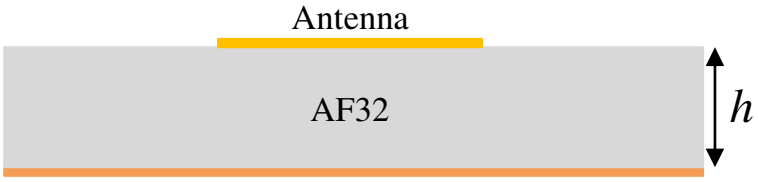

Fig. 4.3: Reference antenna.

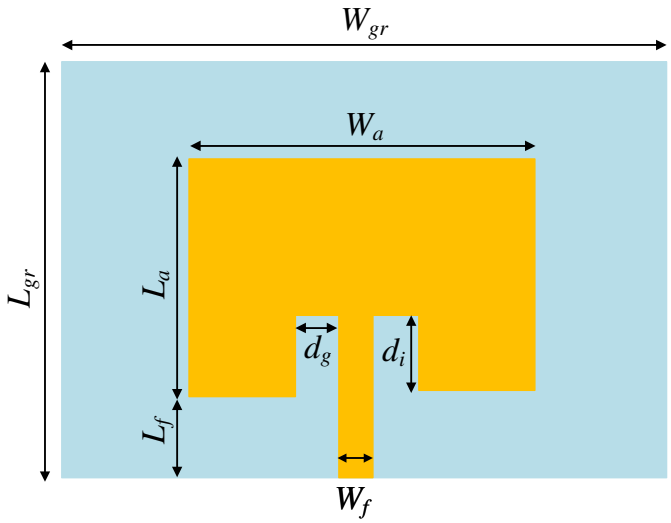

Fig. 4.4: Antenna geometry.

Table 4.1: Geometrical parameters of the antenna.

h	h_{ss}	W_g	S_g
1 mm	0.15 mm	13.8 μm	754 μm
L_a	W_a	L_f	W_f
14.18 mm	18.46 mm	15 mm	1.9 mm
d_g	d_i	L_{gr}	W_{gr}
0.94 mm	4.72 mm	44 mm	44 mm

affect the antenna severely [4]. The solar cell layer in this study is treated simply as a layer with the permittivity of Ge ($\epsilon_r = 16$) and some conductivity (σ). The conductivity is due to the conductivity of Ge and doping.

When the conductivity is zero ($\sigma = 0$), the S_{11} curve and gain of the antennas in Figs. 4.1–4.3 are in Fig. 4.5 and Table 4.2. This result is as expected because in this case the fictitious solar cell layer is just a dielectric substrate added under the glass layer, and therefore yields higher antenna gain. The lattice, on the other hand, raises the ground for the antenna, leaving only the glass as the substrate. When the conductivity of the solar cell layer is as high as copper (σ_{cu}), the S_{11} and gain of the antenna in Figs. 4.1–4.3 overlap. This is also understandable because now the solar cell layer is simply a metal layer that is attached to the lattice.

A more interesting observation was made when the conductivity is between zero and as high as a normal conductor. As soon as the conductivity is raised higher than 1, the structure in Fig. 4.2 exhibits loss and the gain of the antenna reduces. The gain of the antenna reduces for the configuration in Fig. 4.1 too, however, not as high as for the case without the lattice. There is a point where the gain loss due to the solar cell layer reaches its maximum. In our study, such a point occurs at $\sigma = 10^4$ S/m. At this point, when the gain of the antenna without the lattice (Fig. 4.2) is 0 dB, the one with lattice (Fig. 4.1) shows a gain of 1.81 dB as shown in Table 4.2, which is acceptable in many communication link budget. This result can be explained as that the metal lattice layer has acted as a shielding mechanism for the antenna from the lossy solar cell substrate. It does not fully shield the antenna from the solar cell because it is not a solid metal, hence there is still a gain reduction, but less than the case without a lattice layer. It should be noted that

Table 4.2: Effect of the lattice on the antenna's gain.

σ (S/m)	0	10^4	σ_{cu}
Gain (w/o-lattice)	4.65 dB	0 dB	5.2 dB
Gain (w-lattice)	3.81 dB	1.81 dB	5.2 dB

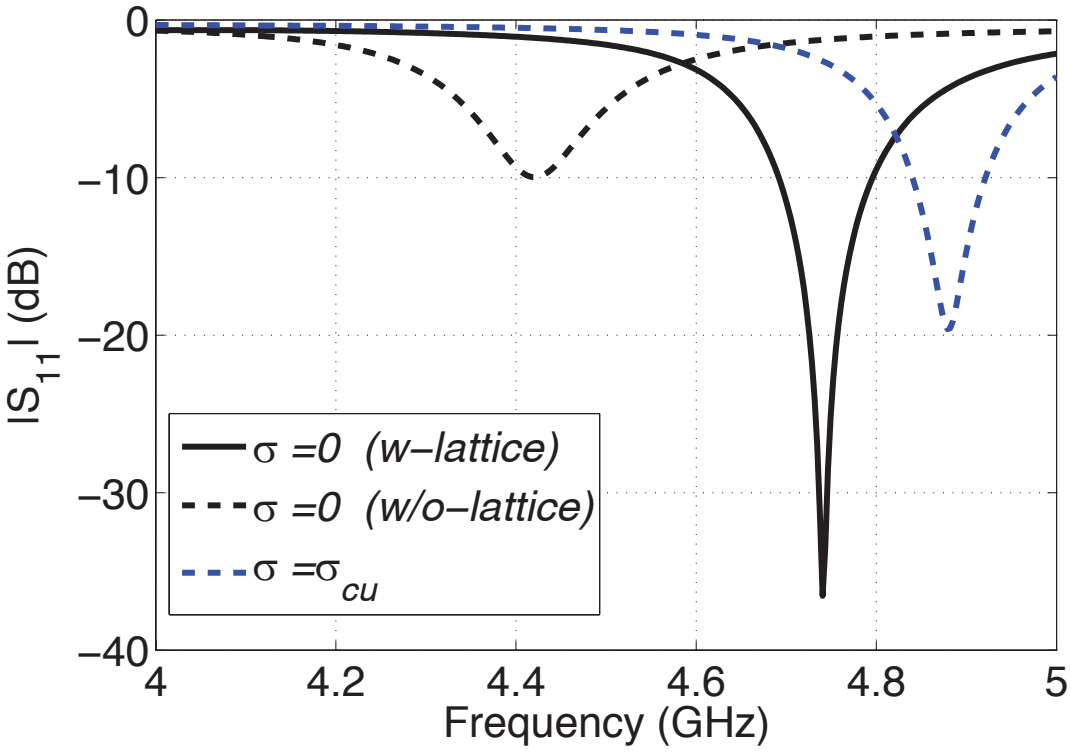

Fig. 4.5: Effect of the lattice on the frequency response.

although the presented results are only in C band, we did examine S and X bands, and the results are similar to the ones at 5 GHz range.

4.1.3 Conclusion

The Ag electrode lattices in space solar cells may have been thought to be a disadvantageous factor for the antenna designs integrated on top. Such an assumption is understandable because often time one may wonder if the DC current on the lattice may affect the antenna's performance. Our study shows that the lattice actually shields the antenna from the gain loss due to the conductivity of the solar cells. This gives rise to a possible design modification for solar cells because if it is feasible to have solar cell's lattice to be denser, then the gain reduction for the antennas can be reduced.

4.2 Analysis of the Effect of Solar Cells on the Antenna Integrated on Top of Their Cover Glass

Abstract

A patch antenna integrated on the cover glass of a commercial space solar cell is examined. The effect of the solar cell on the gain of the antenna is analyzed and validated. It is found that the solar cell casts 2-3 dB gain loss of the antenna when standard cover glass is considered. This value provides an important design consideration when integrating optically transparent antennas on solar cells to save surface real estate of small space vehicles.

4.2.1 Introduction

Integrating planar antennas, whether they are optically transparent or have a small profile, directly on top of solar cells has been actively sought-after in the past decade [1]. The advantage of such an integration is clear–to reuse the surface space occupied in space vehicles, especially small ones. Although a handful of research groups have reported different integrations and results, the effect of solar cells on the antenna's performance was never addressed clearly and convincingly. The reason for that is perhaps due to the complexity of different types of solar cells. In addition, we have not found a clear model or complete geometrical information of solar cells. Quantifying and presenting reliable estimation of such effect impact not only communication link budget, payload, but also provides design guidelines for integrated solar cell antenna arrays. Consequently, the objective of this study is to provide a solar cell model with detailed layer information, and an analysis that yields a reliable estimation on the performance of the integrated antenna due to the solar cell.

As the composition of solar cells from different suppliers often varies, we have chosen EMcore's (www.emcore.com) triple junction space certified solar cells to be examined. The results can be easily adapted to other types of solar cells.

The geometry of an EMcore's typical triple junction solar cell is as follows. From the bottom to top are a metal backing layer, photovoltaic layer, a layer of metal (Ag is

the most commonly used material) electrode lattice, and a cover glass. AF32 ($\epsilon_r = 4.5$) is a commonly used cover glass manufactured by Shott (www.schott.com). To get more information on the photovoltaic layer and details on the geometry, we examined such a solar cell under a high-resolution electron microscope. The extracted information is as in Fig. 4.6.a, where the active junctions are sandwiched between the Ag metal backing and the electrode lattice, details of which is as seen in Fig. 4.6.b.

4.2.2 Analysis

It is clear from Fig. 4.6.a that Ge occupies more than 90% in a solar cell's composition.

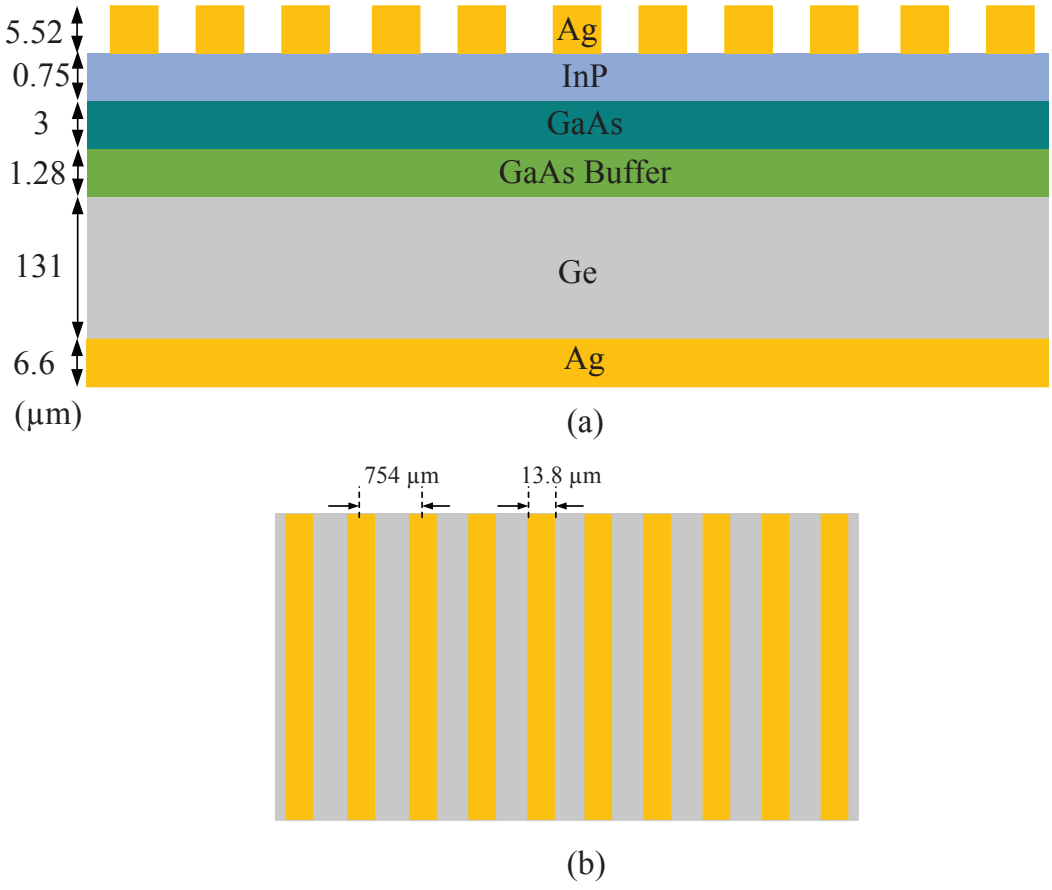

Fig. 4.6: Illustration of the solar cell model: (a) Layer information. (b) Top view.

Also, previously reported experiments did not show much difference in the effect of the working status of the solar cell on the antenna design, which means whether the junctions are active or not does not affect the antenna severely [4]. Therefore, in this study, the solar cell layer is treated simply as a layer with the permittivity of Ge ($\epsilon_r = 16$) with a conductivity (σ) that is due to the intrinsic conductivity of Ge plus doping. The patch antenna under study is then integrated on top of the AF32 cover glass and uses the Ag backing of the solar cell as its ground plane (Fig. 4.6). The electrode lattice is not studied at this time because the main goal is to determine the effect of the solar cell layer. The geometrical parameters of the antenna are presented in Fig. 4.7 and Table 4.3.

As the first step, whether a complex surface wave due to the solar cell layer may be present is examined. For a single layer dielectric slab backed by a ground plane, as long as the thickness of the slab (h) satisfies (4.1), where λ_0 is the free space wavelength, the power coupled into the surface wave can be neglected [5]. For the case of solar cell, taking ϵ_r as 16 and frequency to be 5 GHz, it is clear that the thickness of the solar cell is thin enough not to consider surface waves. Therefore, we conclude that the Ge layer is simply a lossy substrate for the antenna that dissipate some power into heat.

$$\frac{h}{\lambda_0} \leq \frac{0.3}{2\pi\sqrt{\epsilon_r}} \tag{4.1}$$

It is easy to study the two extreme cases of the Ge layer when σ is 0 and as high as

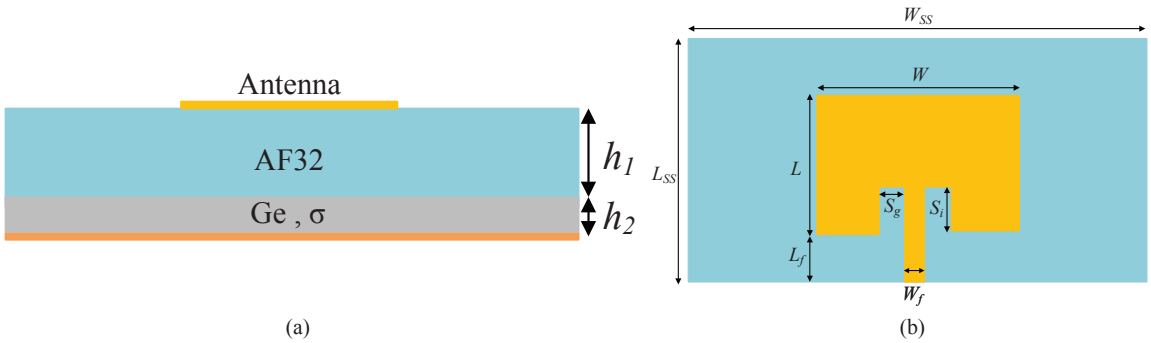

Fig. 4.7: Antenna geometry: (a) Side view. (b) Top view.

Table 4.3: Geometrical parameters of the antenna.

Parameter	Value (mm)	Parameter	Value (mm)
h_1	1	L_f	15
h_2	0.15	S_g	0.94
L	14.18	S_i	4.72
W	18.46	L_{SS}	39.5
W_f	1.9	W_{SS}	68.9

copper (σ_{cu}). In the first case, the solar cell acts as a lossless substrate, and in the second case, a perfect ground. There will not be gain reduction of the antenna due to the solar cell. The antenna's gain reduces to its minimum when the sigma is somewhere in between.

When the thickness of the solar cell (h_2) is in the order of 10 times of the skin depth (δ), the solar cell layer can be considered as a good conductor. In this case, calculating the conductivity from (4.2) at 5 GHz by setting n as 10 yields σ = 225,158 (S/m), which is in the order of 10^5. When h_2 is in the order of δ, which means the solar cell layer is fairly lossy, σ is calculated to be 2,251 (order of 10^3) by setting n as 1. The highest loss should occur when h_2 is somewhere less than one skin depth.

$$\delta = \frac{1}{\sqrt{\pi f \mu \sigma}} = \frac{h_2}{n} \Rightarrow \sigma = \frac{n^2}{\pi f \mu h_2^2} \tag{4.2}$$

4.2.3 Validations

The dimensions of the antenna (Fig. 4.7.b) and material constants of the solar cell model (Fig. 4.6) are simulated in Ansys' HFSS. The gain of the antenna with respect to different σ is as presented in Fig. 4.8. This result confirms the analysis that the antenna suffers from severe gain reductions peaking at when $\sigma = 10^4$.

We now consider the electrode lattice. The lattice acts as a shielding mechanism that decouples the antenna from the solar cell to certain degrees. Therefore, when σ is between 10^3 and 10^4, the gain of the antenna is the lowest, but the lattice keeps the reduction to be between 2-3 dB. This is consistent with the σ measured by [3], and Fig. 4.9 shows our measured antenna gain patterns with and without a solar cell under the AF32 cover glass.

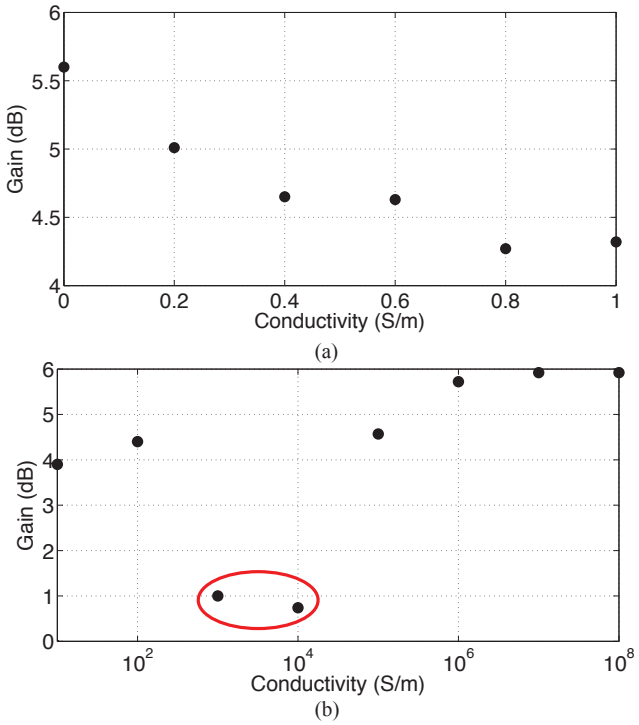

Fig. 4.8: Effect of the solar cell conductivity on the antenna's gain: (a) $0 \leq \sigma \leq 1$. (b) $10 \leq \sigma \leq 10^8$.

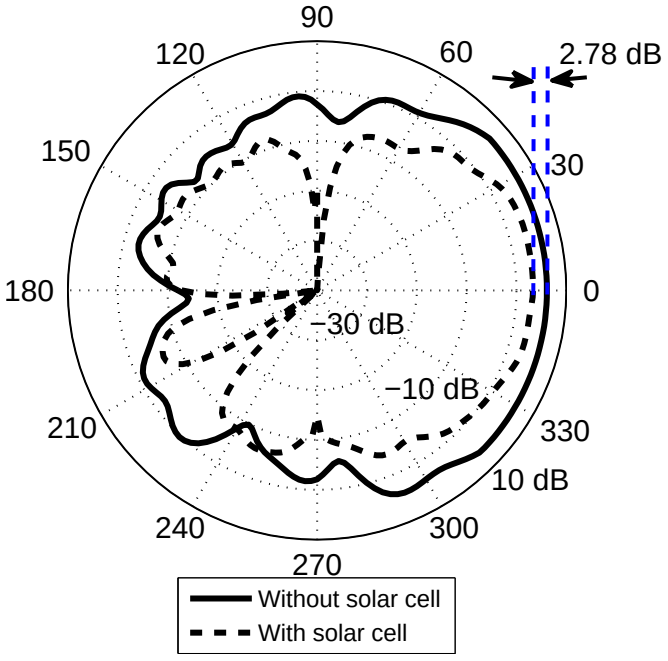

Fig. 4.9: Measured H-plane gain patterns of the antenna with and without a solar cell at 5 GHz.

4.2.4 Conclusion

When integrating a patch antenna on the cover glass of a solar cell, the antenna suffers from a gain reduction due to the solar cell. Most practical solar cells have a conductivity at the order of 10^3 (S/m). Together with the electrode lattice in the cell, the gain reduction of the antenna can be estimated to be 2-3 dB. This result is valid for 1–10 GHz for the thickness of the standard solar cell cover glass.

References

[1] M. Zawadzki and J. Huang, "Integrated RF antenna and solar array for spacecraft application," in *IEEE International Conference on Phased Array Systems and Technology*, Dana Point, CA, 2000, pp. 239–242.

[2] T. W. Turpin and R. Baktur, "Meshed patch antennas integrated on solar cells," *IEEE Antennas Wireless Propag. Lett.*, vol. 52, pp. 693–696, 2009.

[3] W. An, S. Xu, F. Yang, , and J. Gao, "A Ka-Band reflectarray antenna integrated with solar cells," *IEEE Trans. Antennas Propag.*, vol. 62, no. 11, pp. 5539–5546, 2014.

[4] T. Shahvirdi and R. Baktur, "A study on the effect of space solar cells on the antennas integrated on top of their cover glass," in *Antennas and Propagation Society International Symposium*, Memphis, TN, 2014, pp. 215–216.

[5] B. Bhartia, I. Bahl, R. Garg, and A. Ittipiboon, *Microstrip Antenna Design Handbook*. Artech House, 2001.

CHAPTER 5

REFLECTARRAY ANTENNA INTEGRATED ON TOP OF A SOLAR PANEL

Compared to a single element antenna, high gain array antennas offer many advantages in expanding communication capacity. But the integration with solar panels has been limited by the surface area of CubeSats to host those larger antennas. With larger CubeSats (such as 6U and 9U CubeSats) and deployed solar panels are becoming more common, it is feasible to integrate antenna arrays with CubeSat solar panels. NASA's ISARA is one of such successful integrations, where a Ka band antenna array was integrated with the backside of the solar panel [1]. The challenge is, this technology cannot be applied to cases where both sides of a solar panel have solar cells. Such a solar panel is becoming popular and is important for various missions. The goal of this section is to present an alternative design to ISARA, where a low profile, optically transparent reflectarray is integrated directly on top of solar cells. The transparency of the antenna is higher than 90%, which is the highest to date, and the reflectarray design promises more than 40% aperture efficiency. The targeted application is for Near Earth Network (NEN), however, the design can be conveniently scaled to other space networks.

The reflectarray of our interest consists of a ground plane, substrate (i.e. cover glass of solar cells), and antenna elements printed on the substrate. It has elements with different sizes, and is fed by a horn antenna (Fig. 5.1). The horn antenna can be easily replaced by planar array feed. The element size (i.e. geometrical dimension) is carefully determined to supply sufficient required phase to compensate the phase of the incoming wave from the feed, and to provide the dedicated phase to have desired beam pointing angle. Equation (5.1) calculates the required reflection phase φ_r by i^{th} element on xy plane (Fig. 5.1) to point the array beam to (ϕ_0, θ_0). In this equation, k_0 is free space propagation constant, (x_i, y_i) is the position of array element, d_i is the distance from the phase center of the horn to the center of i^{th} element, and N is an integer [2].

$$\varphi_r = k_0(d_i - (x_i cos\phi_0 + y_i sin\phi_0)sin\theta_0) \pm 2N\pi \tag{5.1}$$

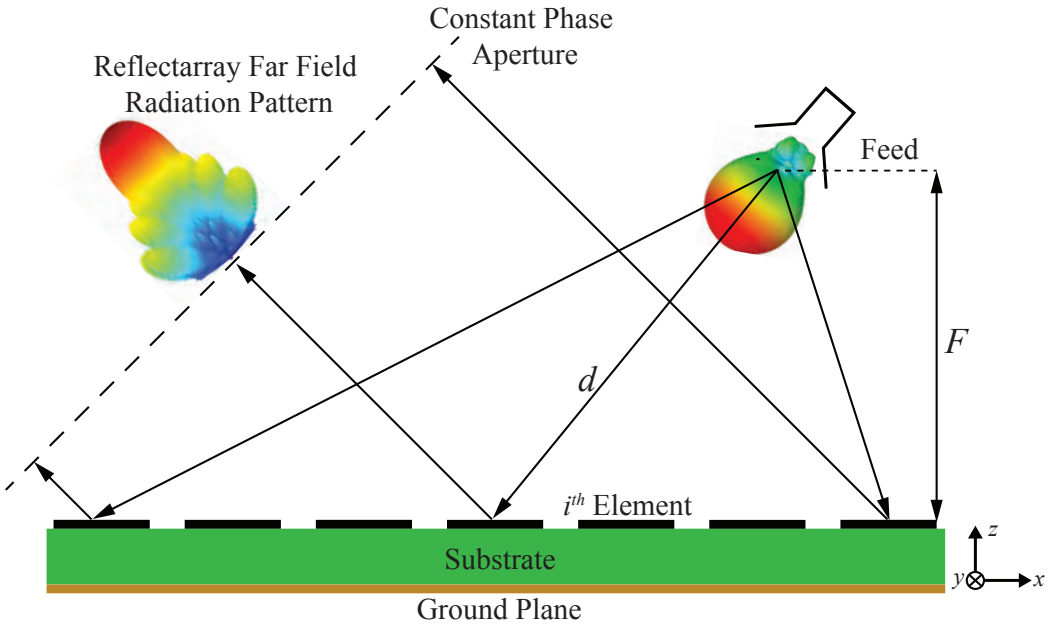

Fig. 5.1: Illustration of reflectarray antenna.

5.1 Examination of Two Types of Quasi Transparent Reflectarray Elements

Abstract

The paper examines two types of antenna elements suitable for a reflectarray design that can be integrated on top of solar cells. The study presents the performance of the two element designs for different substrate thickness and lattice sizes.

5.1.1 Introduction

The importance of integrating antennas with solar cells for small satellite application is clear and a few results in element level integration has been presented [3, 4]. On the array level, NASA has shown an integration of a high gain array antenna on the opposite side

of a deployed solar panel [1]. The goal of this paper is to present an alternative design to ISARA, where a low profile, quasi-transparent reflectarray is integrated directly on top of solar cells. The targeted application is for Near Earth Network (NEN), however, the design can be conveniently scaled to other space networks.

5.1.2 Transparent Elements

Two types of antenna elements can be considered as best candidates for integration on solar cells: (a) cross dipole, and (b) loop. Both are low profile and near transparent. Fig. 5.2 depicts the geometry of the unit cell for the reflectarray, where an antenna element (cross or loop) is printed on top of a cover glass and then backed by a copper ground plane. The cover glass is chosen to be commercial AF32 glass that has high transmittance and high temperature tolerance, making it desirable for space applications. The AF32 glass has dielectric constant (ϵ_r) of 4.5 and loss tangent ($tan\delta$) of 0.015 at X band [5]. The height (h) of the AF32 substrate is critical in affecting the performance of the reflectarray, and will be discussed in the next section of the paper. It is seen that both of the proposed array elements (Fig. 5.2.b) are symmetric, and can easily excite both linear and circular polarizations. As seen, the solar cells are not included in this stage of the design. In the final implementation of this project, the solar cell is sandwiched between the cover glass and ground. The effect of the solar cell in the reflectarray design can be extracted by entering the solar cell model from the previous study [5] to the design simulation. The reflectarray is simulated using Ansys' HFSS by adapting periodic boundary conditions and Floquets excitation with normal incident fields to extract element phase response for different lattice sizes at 8.475 GHz.

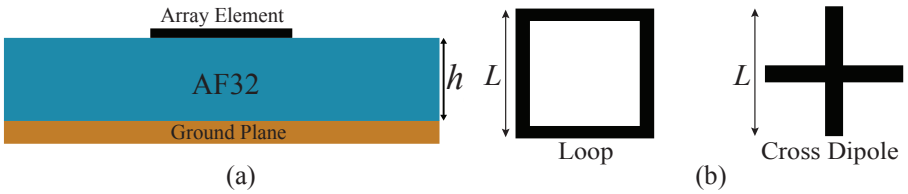

Fig. 5.2: Reflectarray element: (a) Layer information. (b) Antenna elements.

Cross Dipole

A cross dipole is composed of two orthogonal dipole elements with length of L (Fig. 5.2.b). The width of cross dipole was chosen to be 0.25 mm. The reflection phase of the element can be changed by adjusting its length. Fig. 5.3.a shows the reflection phase of the cross dipole element with lattice size of half wavelength ($\lambda/2$) for different values of h. Also, the symmetric shape of element results in having same electromagnetic response under normal incident wave for TE and TM modes. Fig. 5.3.b is the reflection magnitude of the unit cell. As seen in Fig. 5.3.a, when h is small, the provided phase is almost constant, making it unsuitable for reflectarray design. This condition happens when radiation Q is greater than element Q (under coupled) [6]. The value of h=1.5 mm is found to be the critically coupled condition that happens when radiation Q is equal to element Q [6]. In this case, the phase response is too sharp and there is nothing reflected back as seen from Fig. 5.3.b, (near zero reflection). When h is greater than 1.5 mm, radiation Q is less than element Q (over coupled) [6]. Then, the phase response is applicable for reflectarray deign. Increasing h shows reduction of phase range but smoother phase variations. Considering all of these, h= 2.5 mm was chosen in this study as a more optimal substrate thickness that provides good trade–off between phase range and feasible phase curve.

Reducing cell periodicity to sub–wavelength can provide special features like reducing loss and broadening the gain bandwidth and can be an effective method to design reflectarray on lossy substrates [7]. As we already know that the solar cells are lossy [5, 8], we studied the cross dipole unit cell for different sub–wavelenth lattice sizes as shown in Fig. 5.4. It is confirmed that working at the sub–wavelength shrinks the phase range and reduces the loss at the same time.

Loop

The same study performed for the cross dipole, was carried out for a loop geometry (Fig. 5.2.b). The reflection phase of the loop element is obtained by adjusting the loop length while fixing its width as 0.25 mm. The same observation for the cross dipole was seen, where h =1.5 mm being critically coupled condition and h = 2.5 mm being a reasonable

substrate thickness to work with (Fig.5.5). Reflection phase and magnitude of the loop unit cell with different lattice sizes are summarized in Fig. 5.6.

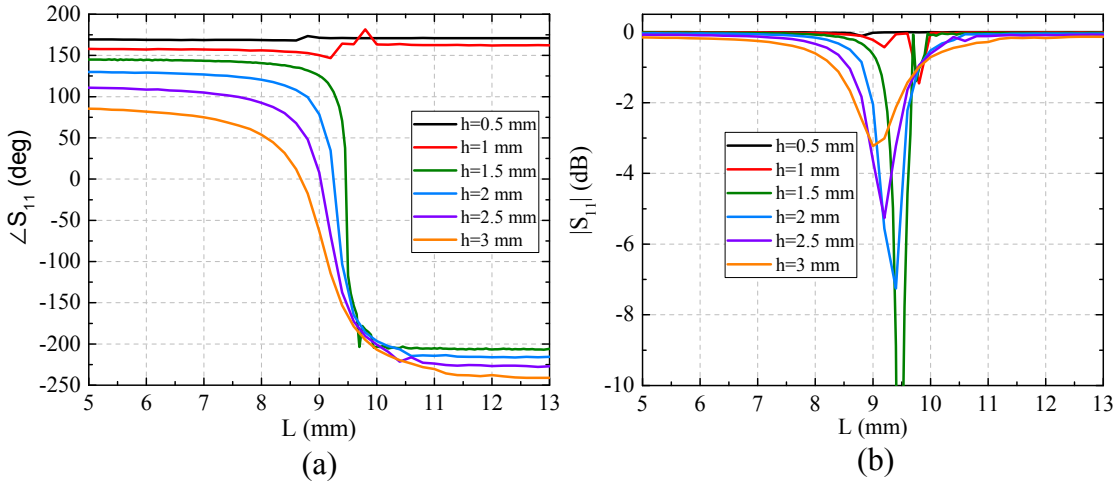

Fig. 5.3: Cross dipole element: (a) Reflection phase. (b) $|S_{11}|$ response.

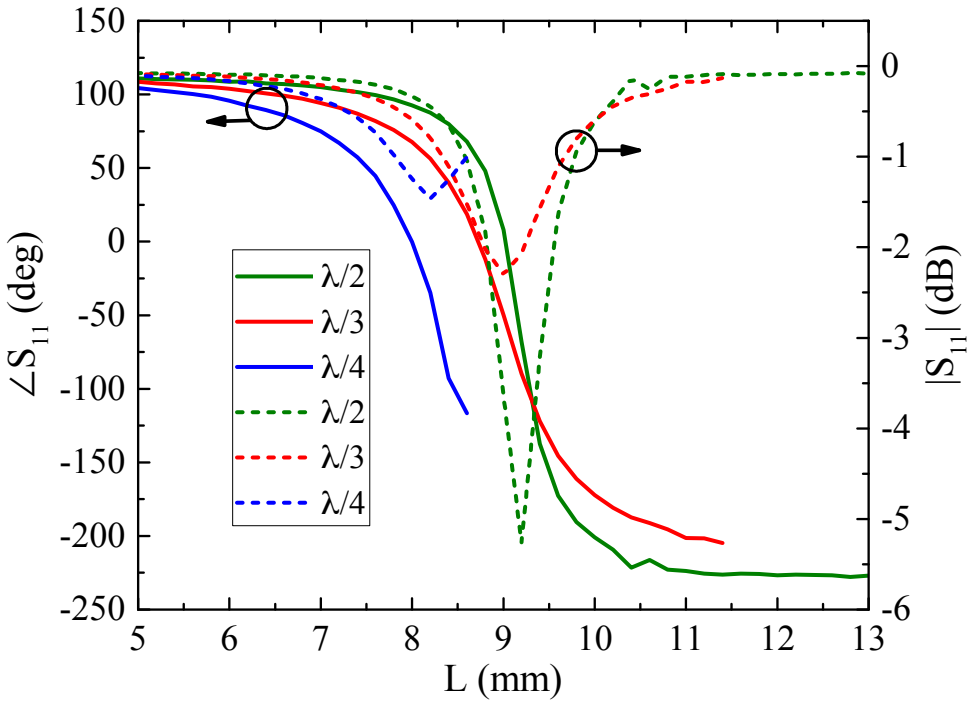

Fig. 5.4: Reflection phase and magnitude of cross dipole element for different lattice sizes.

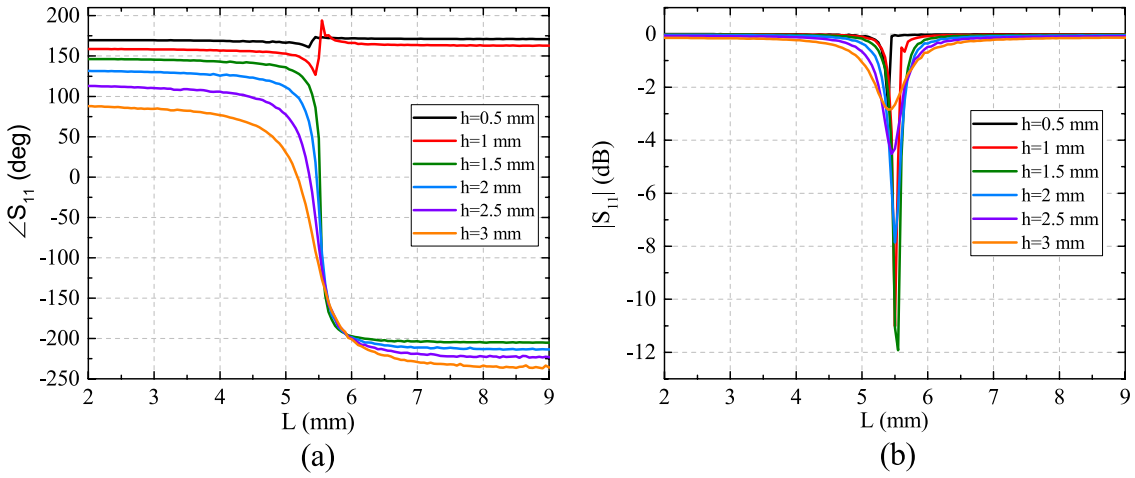

Fig. 5.5: Loop element: (a) Reflection phase. (b) $|S_{11}|$.

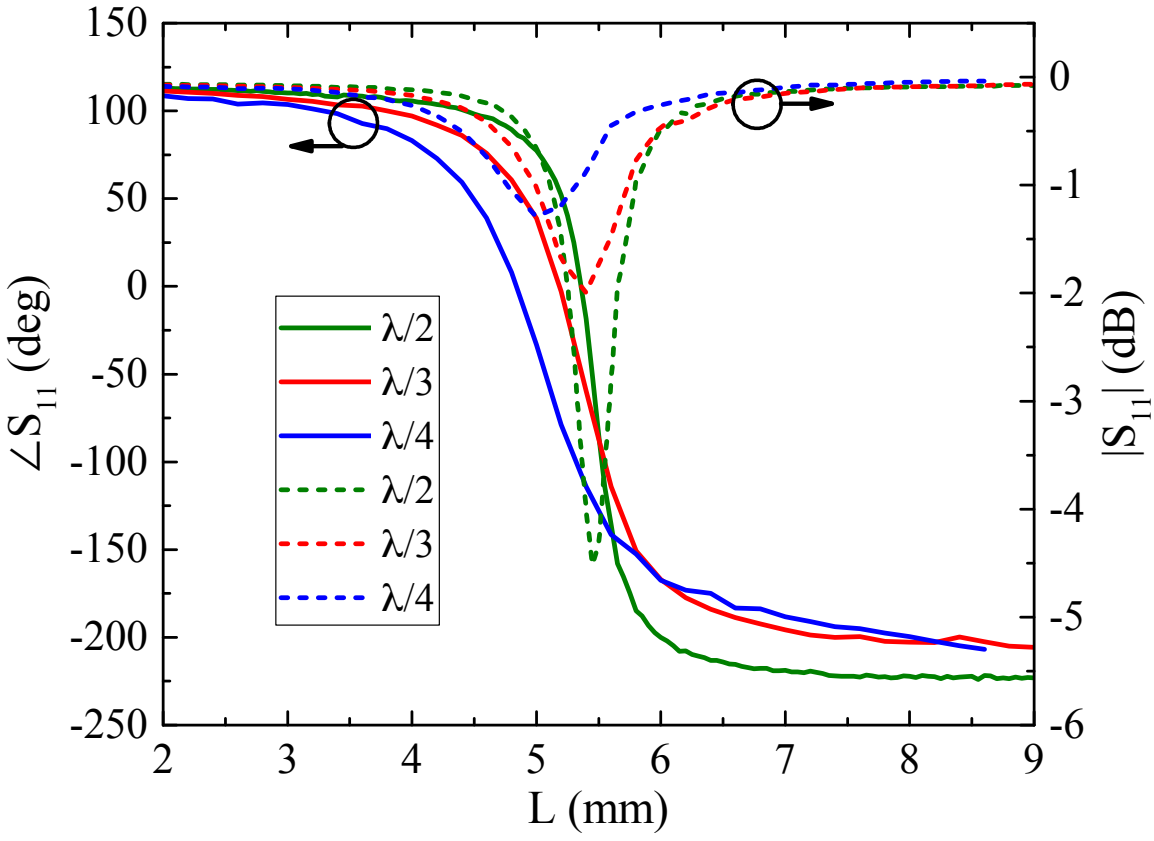

Fig. 5.6: Reflection phase and magnitude of loop element for different lattice sizes.

Comparison of Elements

Fig. 5.7 shows phase responses of the two elements for different lattice sizes. It is seen that both elements are suitable for array design when the lattice size is $\lambda/2$ or $\lambda/3$. When the lattice size is reduced to $\lambda/4$, the phase range of cross dipole is limited (less than 270 degree) and cannot provide sufficient phase range required for array design. Loop unit cell, however, still works well for a $\lambda/4$ lattice. It is also observed that the loss levels for both elements are approximately the same for the same lattice size.

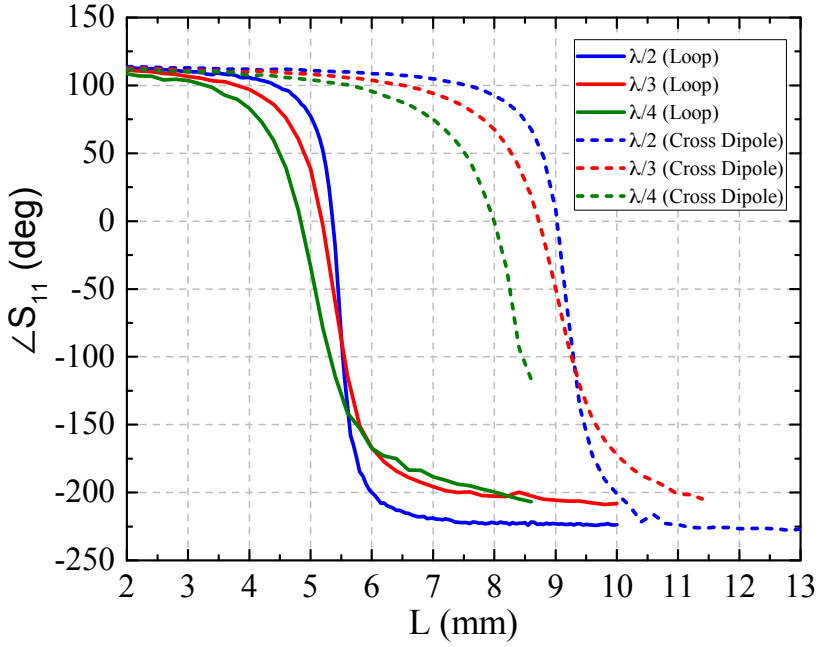

Fig. 5.7: Reflection phase of cross dipole and loop elements.

5.1.3 Conclusion

The paper reported two types of transparent and low profile array elements. The effect of the substrate height was discussed at the 8.475 GHz (NEN radio band). Reflection phase and magnitude of each element for different lattice sizes were studied and compared. It has been shown sub–wavelength loop element ($\lambda/4$) shows superior performance compared to the cross dipole.

5.2 Design of Two Transparent X Band Reflectarray Antennas Integrated on a Satellite Panel

Abstract

This paper presents an integration of highly transparent X band reflectarrays on the cover glass of solar panels. Optimal unit cell element, effect of the solar cell on the antenna, feed consideration, and final design data are presented. The overall transparency and aperture efficiency of the design are more than 90% and 40% respectively, and measured results of the antenna without solar panel underneath match those design data well. When the antenna is integrated on the solar panel, it is seen that there is slightly more than 1 dB gain reduction, which is reasonable, and factors that lead to gain reduction were analyzed in detail.

5.2.1 Introduction

Integrating high gain conformal array antennas with solar panels of small satellites, in particular Cube Satellites (CubeSats) has enormous advantages, especially in expanding mission capacities of CubeSats. NASA's ISARA is one of such successful integrations, where a Ka band antenna array was integrated with the backside of the solar panel [1]. Transparent array antenna integrated directly on solar cells, is not only an alternative to ISARA, but also a novel extension as it promises a more flexible solution. Two types of direct integration of reflectarrays with solar cells have been presented to date [9, 10]. Moharram et al.'s design is to create holes in the acrylic cover glass of solar cells to achieve required phase shift, and the reported aperture efficiency is 25.18% [9]. As the acrylic cover glass is relatively thick, together with the holes, it blocks about 15% of the light. The design in [10] is printing a Ka band reflectarray on the solar cell cover glass. While [10] is a plausible approach that does not require custom designed cover glass, the reported aperture efficiency of 29.8% and optical transparency of 85% need to be further improved. This paper presents an alternative design to [9] and [10] where reflectarrays of transparency higher than 90% are printed on space certified solar cell cover glass at X band for much smaller panels (i.e. 300 mm by 300

mm maximum to fit on a 3U or 6U CubeSat) with improved aperture efficiency.

5.2.2 Reflectarray Geometry and Transparent Element Design

Fig. 5.8 is an illustration of the proposed reflectarray (Fig. 5.8.a) and assembly information (Fig. 5.8.b), where the reflectarray elements (copper) are printed on a commercial space certified glass AF32 that has very high optical transmittance ($\geq 90\%$) and temperature tolerance. The solar cells are sandwiched between AF32 and a copper ground plane. As seen, each solar cell has its own cover glass that hosts array element or elements, facilitating a very low–cost modular design and fabrication process. The AF32 glass has a measured permittivity of 4.5 and loss tangent of 0.015 at X band. Two candidates (Fig. 5.8.c), a cross dipole and a square loop, were examined in terms of reflection magnitude and phase for unit cell size of $\lambda/2$ and $\lambda/4$, where λ is the free space wavelength at 8.475 GHz (Near Earth Network frequency). Both candidates are of low profile that will only block minimal percentage of light, and symmetric to enable both linear and circular polarizations.

Optimal Element Design

In this study (full-wave simulation using HFSS), the width (w in Fig. 5.8.c) of the

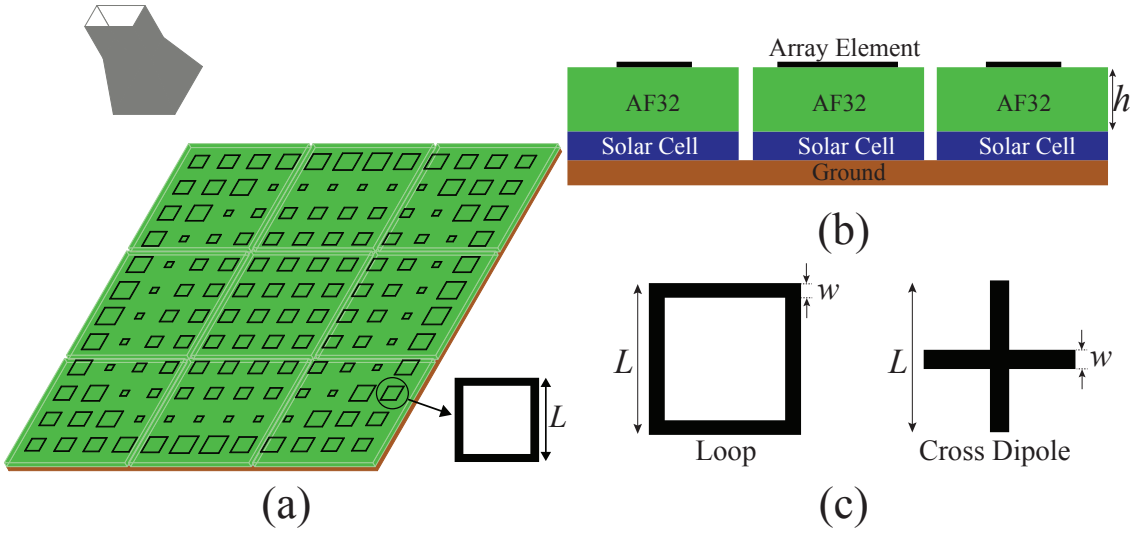

Fig. 5.8: Proposed integration: (a) Reflectarray. (b) Layer information. (c) Array Elements.

cross dipole and loop was chosen to be 0.25 mm, and the reflection phase of the element can be changed by adjusting its length (L in Fig. 5.8.c). The height (h) of the cover glass was chosen to be 2.5 mm by considering the trade–offs between the phase range and phase variation that can be practically realized. It was found that both elements promise reduced loss at sub-wavelength lattice size compared to $\lambda/2$ one (Fig. 5.9.a), and this is consistent with [11]. The cross dipole, however, cannot provide minimum 270 degree required phase range (Fig. 5.9.b). Therefore, the loop element with $\lambda/4$ unit cell was chosen for the reflectarray design.

The Effect of Solar Cells

The lossy nature of solar cells in reducing the antenna's gain has been studied in [5,8,10]. Using the conductivity of common solar cells extracted by [5] and entering it together with the electrodes in solar cells (i.e. silver lines parallel to the width of solar cells) to the full-wave simulator, we obtained the effect of solar cells on the loop unit cell. Fig. 5.10.a and Fig. 5.10.b show the effect of solar cells on the unit cell under normal incident TE and TM plane waves, where the E field of TM wave being parallel to the electrodes and TE being perpendicular. It is seen from Fig. 5.10.a that the solar cell has little effect on the phase response, but it introduces loss (Fig. 5.10.b), which is expected. The phase response is further examined for oblique incidences (Fig. 5.10.c and Fig. 5.10.d), and we see no significant effect from the solar cell.

5.2.3 Reflectarray Design

We designed reflectarray at 8.475 GHz for two panels to beam at 22.7°. Panel I is for a 6U CubeSat and has a size of 200 mm by 300 mm. Panel II is 300 mm by 300 mm, and can be either for a 9U CubeSat or a 3U CubeSat with folded deployable panel. The solar cells are not included in this design because the solar cells are very thin and the computation grids have to be small enough to capture the fine geometry of many solar cells on the panel. Consequently, the simulator generates an extremely large number of grids and results in a very expensive computation costs. As we can assess the effect of solar cells analytically, we

did not include solar cells at this stage. The feed beam is tilted at 22.7° to avoid blockage from the feed horn (Fig. 5.8). The focal distance F (Fig. 5.1) is one of the important design parameters that directly affects array's aperture efficiency. As shown in Fig. 5.11 for Panel I and Figure 5.12 for Panel II , there is an optimum F that maximizes aperture efficiency, which is a multiplication of the illumination and spillover efficiencies [12]. Considering the optimal aperture efficiency and having an edge taper of -10 dB [13], gain of the feed horn and the focal distance (F) were determined to be: 12 dB, 135 mm for Panel I and 165 mm for Panel II. Fig. 5.13 and Fig. 5.14 show the required phase distribution of the loop elements that have been truncated to the accuracy of 0.01 mm for the ease of fabrication. Fig. 5.15 and Fig. 5.16 present normalized gain patterns of the two reflectarrays, and it is seen that both side lobe and cross polarization levels are well below 20 dB.

5.2.4 Discussions and Results

Effect of Solar Cell

Based on the unit cell response, the array radiation efficiency can be calculated from (5.2) [11], where $|\Gamma_i|$ and $|I_i|$ are reflection and illumination magnitude of the i^{th} element. We validated this formula by computing η_r (it is -0.64 dB from computation) for Panel II

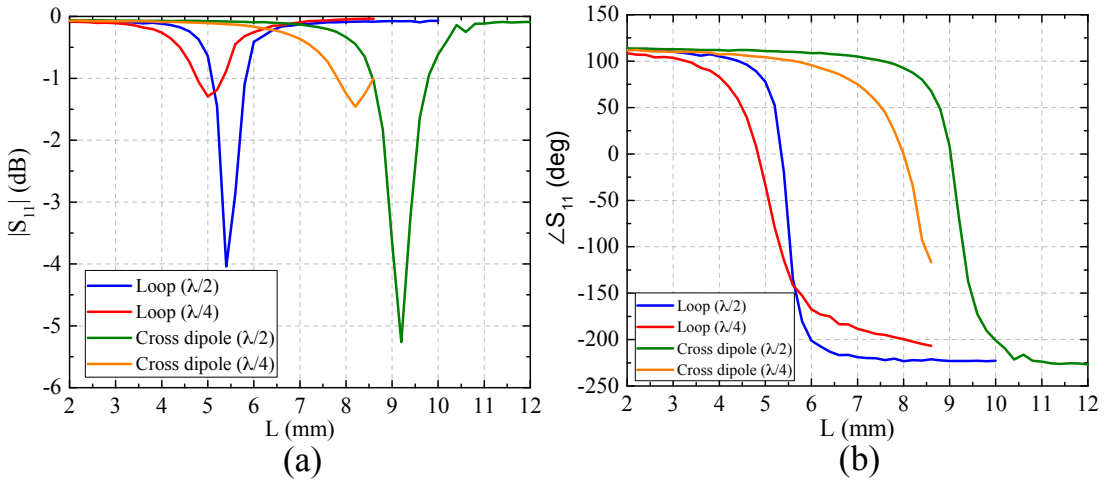

Fig. 5.9: Unit cell response: (a) $|S_{11}|$. (b) Reflection phase.

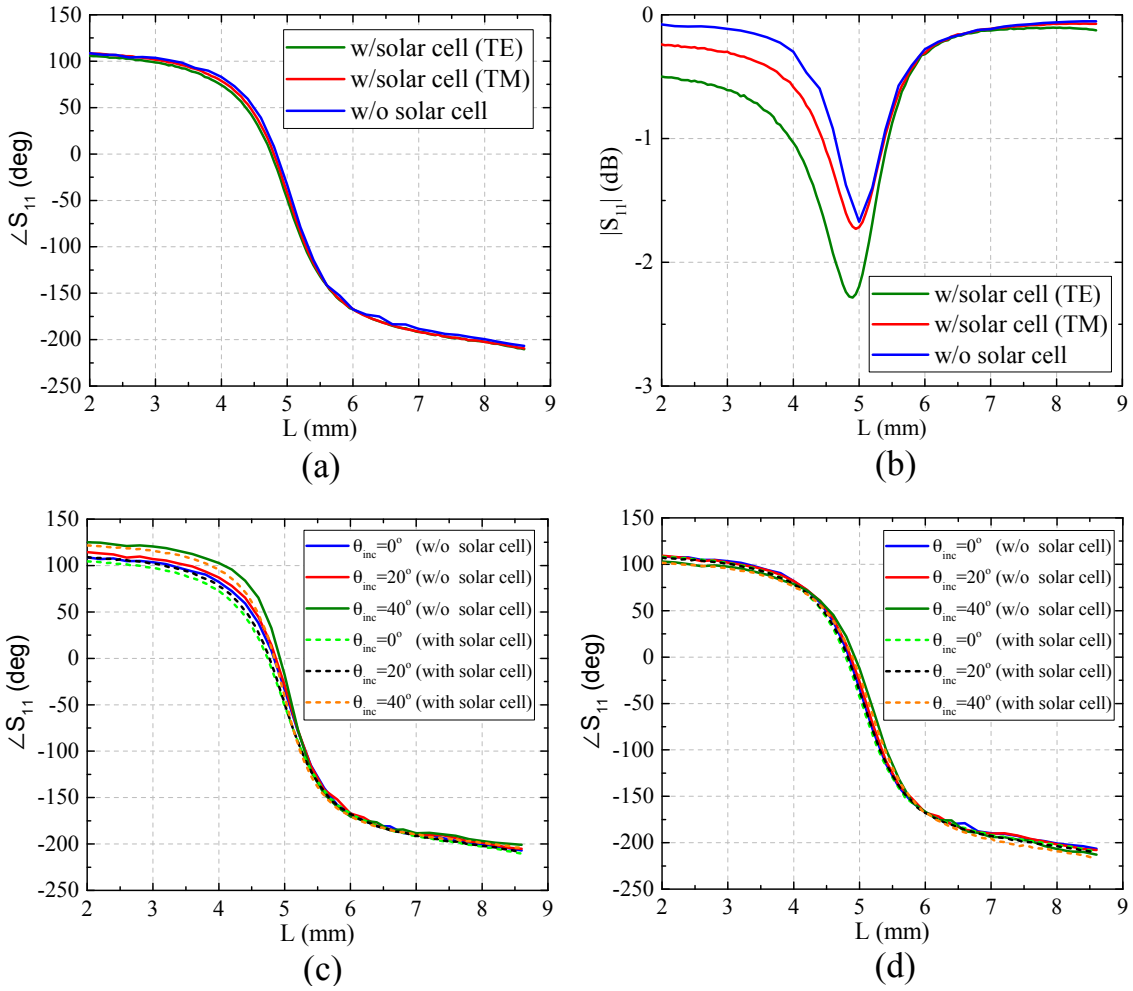

Fig. 5.10: Solar cell effect: (a) Reflection phase (Normal). (b) Reflection magnitude (Normal). (c) Reflection phase (TE oblique). (d) Reflection phase (TM oblique).

without solar cells and compared it with the full–wave simulation result of -0.51 dB. As the agreement is very good, we used the formula and the unit cell response in the presence of solar cell (Fig. 5.10), where $|\Gamma_i|$ can be extracted, to compute the array gain and aperture efficiency (η_{ap}), which is the final measure of the effectiveness of the designed array antenna.

$$\eta_r = \frac{\sum_i (|\Gamma_i|^2 |I_i|^2)}{\sum_i |I_i|^2} \tag{5.2}$$

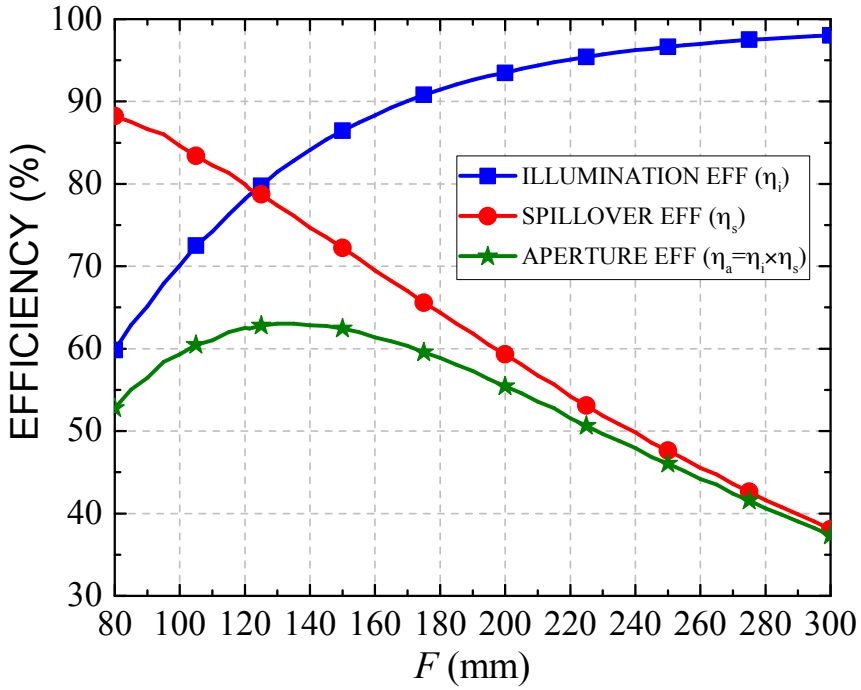

Fig. 5.11: Aperture efficiency versus focal distance (F) for Panel I.

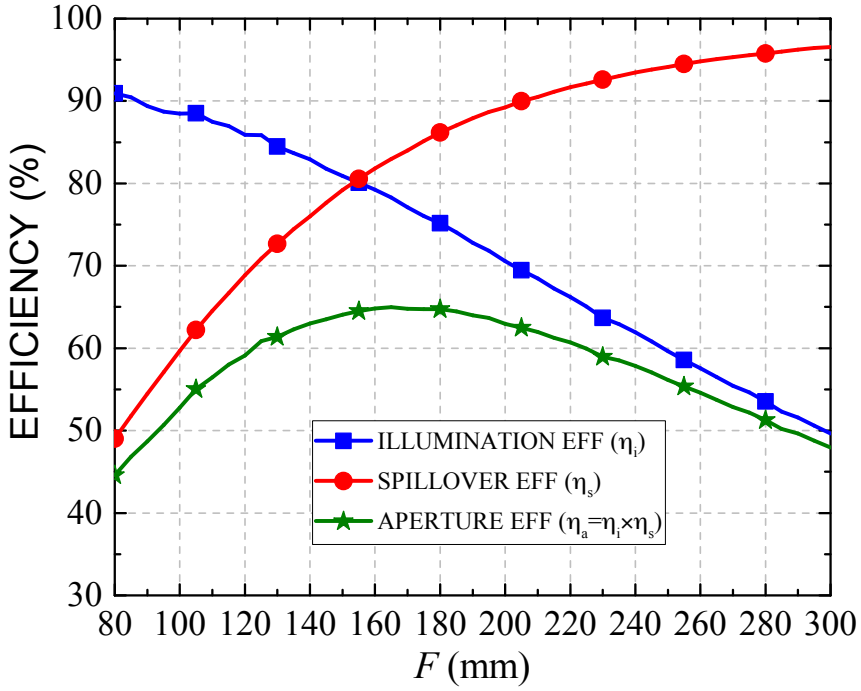

Fig. 5.12: Aperture efficiency versus focal distance (F) for Panel II.

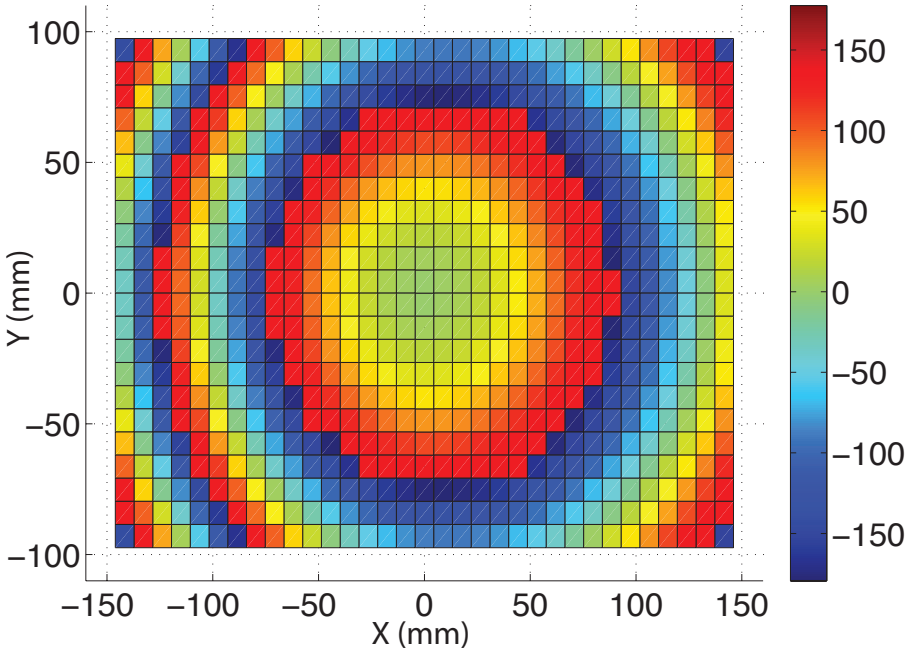

Fig. 5.13: Phase distribution on the aperture of Panel I.

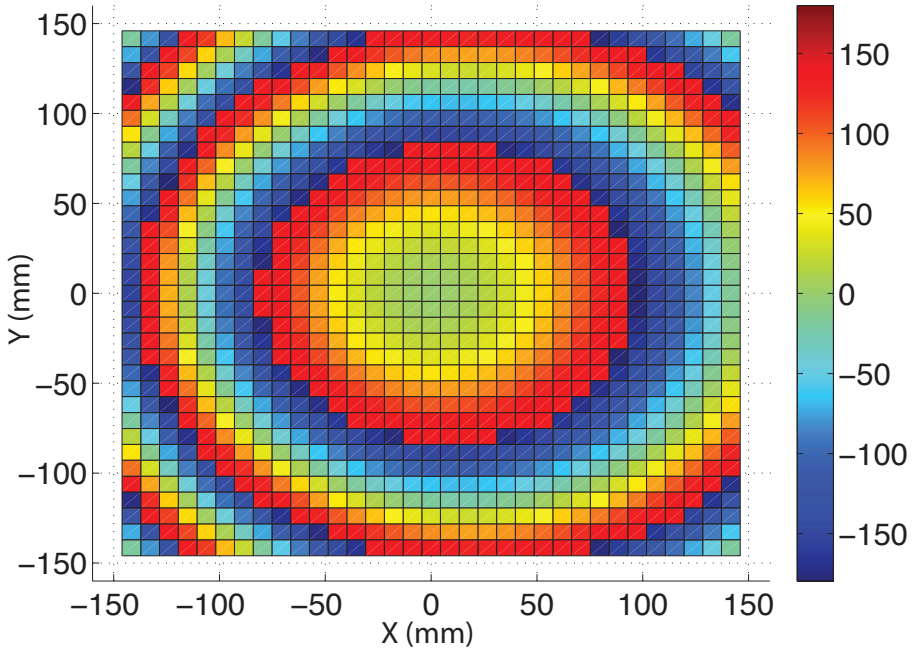

Fig. 5.14: Phase distribution on the aperture of Panel II.

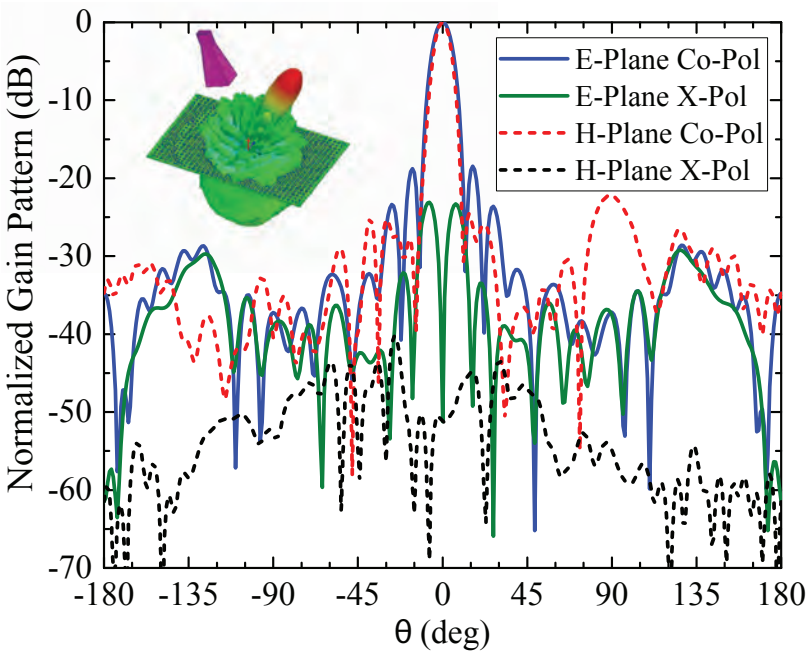

Fig. 5.15: Normalized gain pattern at E and H planes for Panel I.

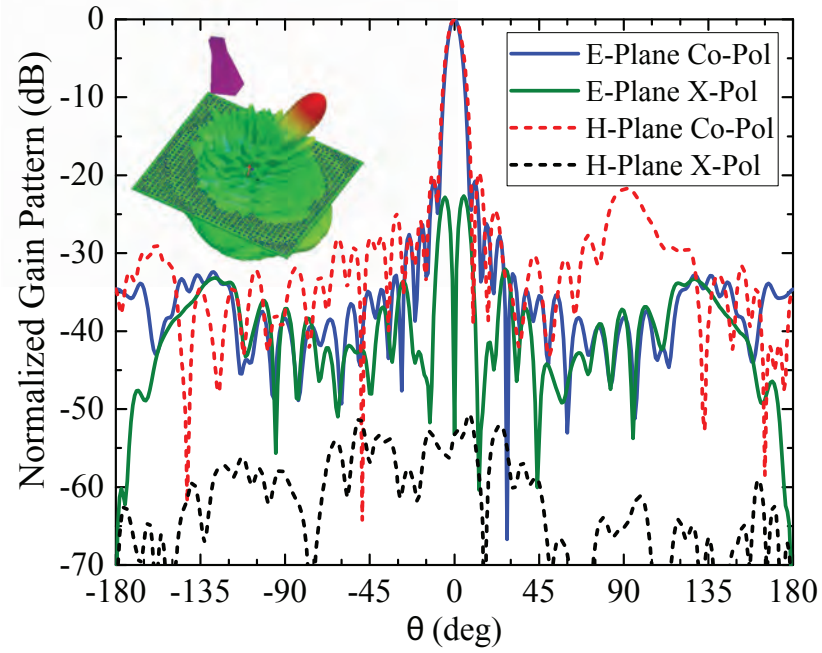

Fig. 5.16: Normalized gain pattern at E and H planes for Panel II.

Optical Transparency

The optical transparency due to the reflectarray is computed from (5.3), where A_{metal} and A_{panel} are the area covered by the printed metal and the area of the solar panel, respectively.

$$T_{ant} = (1 - \frac{A_{metal}}{A_{panel}}) \times 100 \tag{5.3}$$

In the case of presented loop antenna elements, the area covered by the metal is:

$$A_{metal} = \sum_{i} 4(L_i - w)w. \tag{5.4}$$

The overall transparency is determined by the transparency of the AF32 cover glass and the transparency of the antenna. The estimation is straightforward.

Simulation Results

The performance of the designed reflectarray is summarized in Table 5.1, where the effect of solar cells has been taken into account. It is seen that the transparency of the antenna is close to 95%. As the cover glass is highly transparent, we can estimate that the overall transparency is above 90%. It is also seen that the aperture efficiency of the antenna is more than 40%, which is higher than most reported antenna arrays integrated with solar cells.

Table 5.1: Reflectarray performance for both panels.

Panel	Orientation	Gain (dB)	η_{ap} (%)	T_{ant} (%)
I	TE	23.83	40.2	94.54
I	TM	24.24	44.2	94.54
II	TE	25.67	40.9	94.62
II	TM	26.06	44.8	94.62

5.2.5 Measurement and Results

This section covers the design prototyping process, measurement setup, measurement procedure, results, and discussions.

Prototyping Process

To validate the design, the reflectarray for Panel I was implemented on FR4 substrate, which is lossier substrate compared to Rogers' high frequency laminate and has the similar electrical properties to AF32 glass. Such a choice was made because validating the initial design on a FR4 is a much faster and cheaper method than directly on glass. As the chosen FR4 has almost the same properties as glass, the design printed on glass is expected to be similar to the one on FR4. The FR4 substrate has dielectric constant of 4.2, loss tangent of 0.015, and height of 2.36 mm. The protoyped reflectarray has dimensions of 300 mm $\times$ 200 mm as shown in Fig. 5.17.

A horn antenna is used to illuminate the reflectarray as shown in Fig. 5.1. The feed horn (Fig. 5.18) was fabricated by using 3D–printing technique. The inner side of it was sprayed by conductive ink. To launch the feed, a standard WR90 coax to waveguide transition was used. The measured S_{11} of the designed horn antenna is shown in Fig. 5.19. It is clear that the prototyped feed is matched well in the entire of X band.

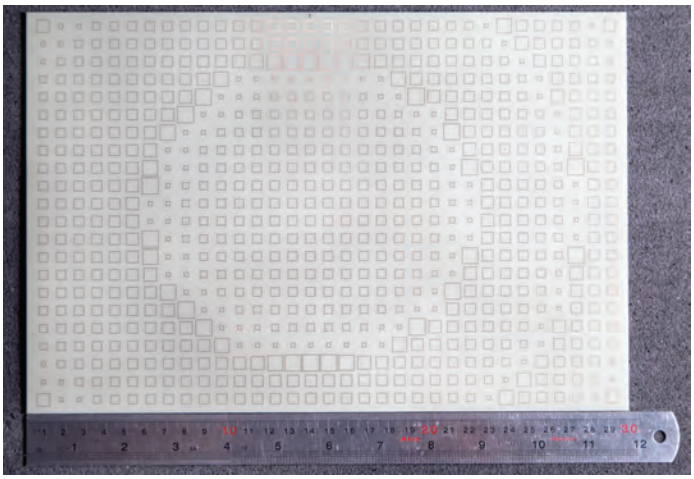

Fig. 5.17: Prototyped reflectarray on FR4.

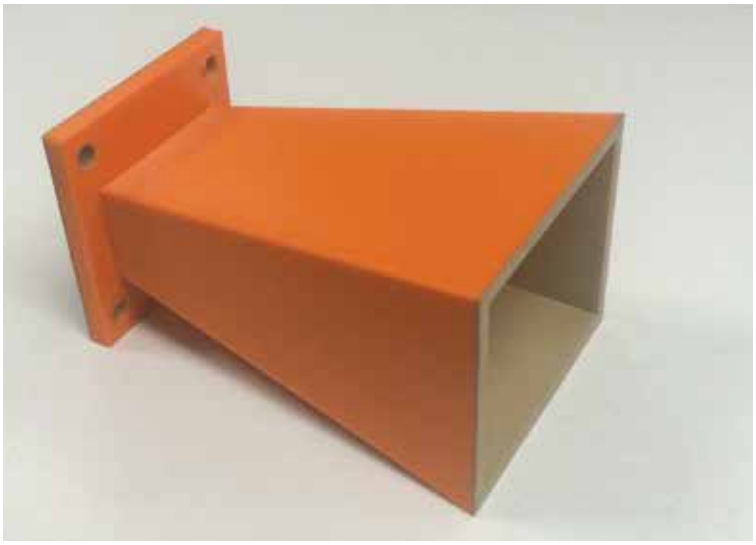

Fig. 5.18: Prototyped horn antenna.

Measurement Setup

To measure the reflectarray, a fixture (Fig. 5.20) made of plastic was fabricated to hold the reflectarray and horn antenna. The position of the horn with respect to the array was adjusted and fixed on the fixture, and the reflectarray was fastened to the fixture by using four plastic screws. The fixture has four legs that make it stable and robust during the measurement.

A near–field NSI planar scanner was used to measure the reflectarray. Fig 5.21 shows the measurement setup. First, the horn antenna was connected to the VNA port so that reflectarray acts as transmitter, and a WR90 waveguide probe on the near–field scanner samples the field radiated by the array. To have accurate results, the array should be placed close to the probe so that it can capture the array near–filed data well. After fixing the reflectarray in front of the probe, the planar scanner will sweep along x–y plane (e.g. the plane parallel to the array surface). Then, the NSI software will do near–field to far–filed transformation to produce far field patterns of the reflectarray.

As the aim of work is to integrate the reflectarray on the solar panel, we need to know

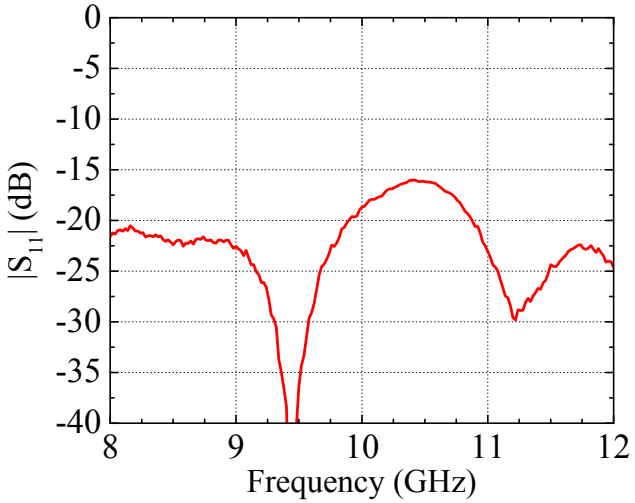

Fig. 5.19: Measured S_{11} of fabricated horn antenna.

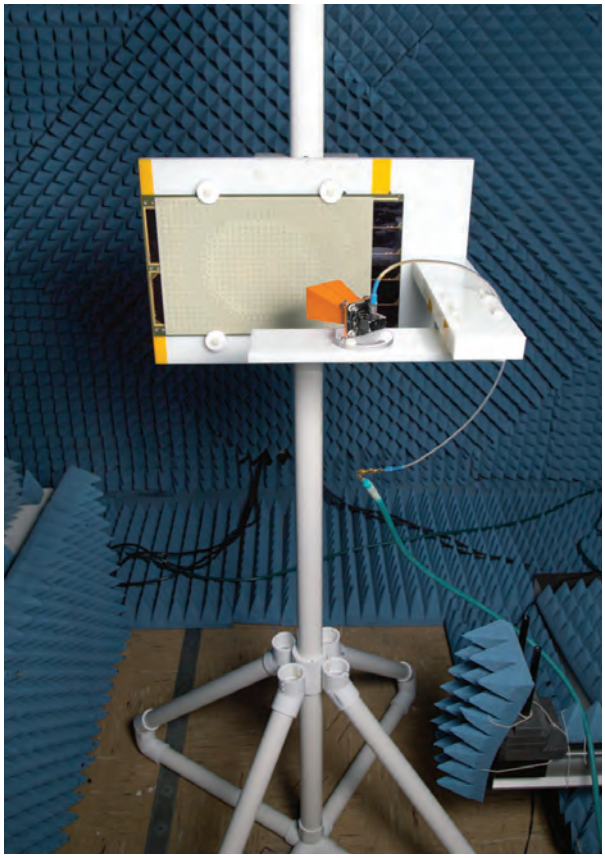

Fig. 5.20: Fabricated fixture.

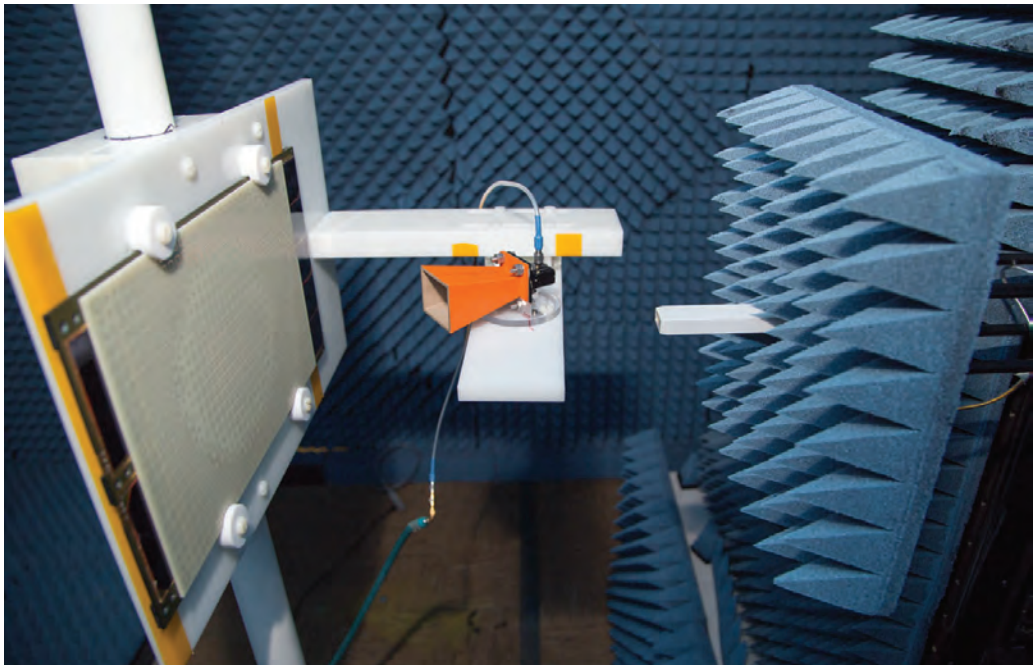

Fig. 5.21: Measurement setup.

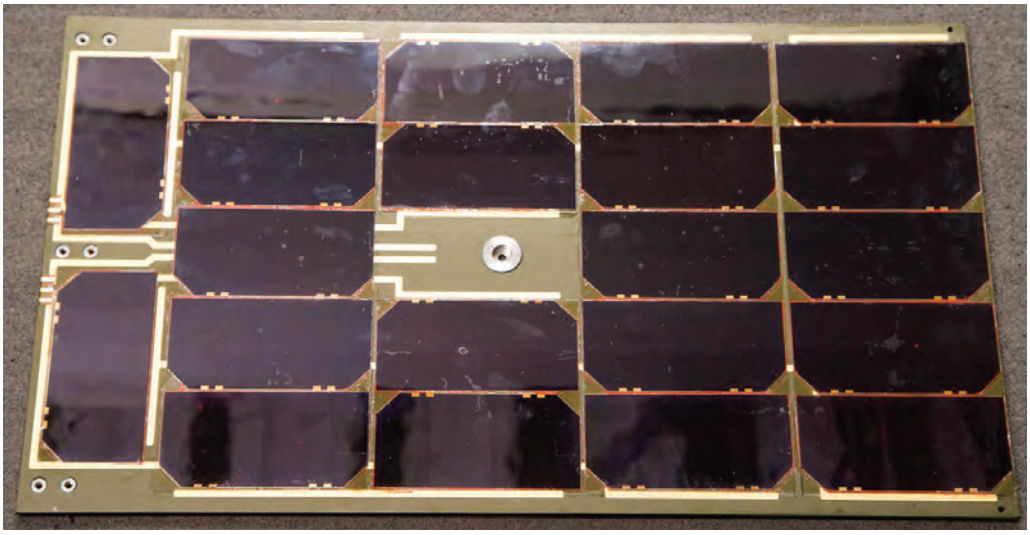

Fig. 5.22: Multi-functional solar panel.

the solar panel well. Fig. 5.22 shows the used solar panel in our experiments which is multi–functional solar panel used in space applications. It measures 355 mm $\times$ 203 mm, which is bigger than the designed array, and includes 21 space–certified solar cells. Each

solar cell has its own cover glass and a transparent adhesive (glue) was used to stick the solar cell to the cover glass of the solar cell. The thickness of the solar panel is 6 mm and the center of this particular panel is empty without any solar cell.

Measurement Procedure

Different experiments were carried out to examine the integrated reflectarray performance. All of the experiments used the designed array (Fig. 5.23.a) and the measurement setup (Fig. 5.21). Three measurements were performed:

- Measurement I: The first experiment was to mount the reflectarray prototyped on a FR4 (top side of the FR4 is the array element, and bottom is metal cladding that acts as ground (Fig. 5.23.a)) on the fixture and do the measurement.

  The focal distance was set to 135 mm and the angle between horn antenna and the array center was fixed to be 22.7^o. This setup was also used for the following experiments.

- Measurement II: To do the second experiment, the metal cladding of the reflectarray in Fig. 5.23.a was removed and the surface of the panel was covered by aluminum sheet. Then, the reflectarray (without cladding on the back) was placed on the panel as shown in Fig. 5.23.b. It is clear that the aluminum sheet acts as the ground. The thickness of the solar panel is 6 mm which would lead to a reduced focal distance and consequently reduce the gain of the reflectarray.

- Measurement III: The setup for this experiment is same as the second one except for at this time the aluminum sheet in between the FR4 and the solar panel was removed. In this case, the ground of the solar panel would be the ground for the reflectarray. To avoid damaging the solar panel, the screws were not tightened and it would result in air bubble between array and the panel. Also, the copper tape was placed at the panel center to fill out the center and be part of the ground plane. Like the second

experiment, the focal distance decreased because of the panel thickness. Fig. 5.23.c shows the integrated reflectarray on the solar panel.

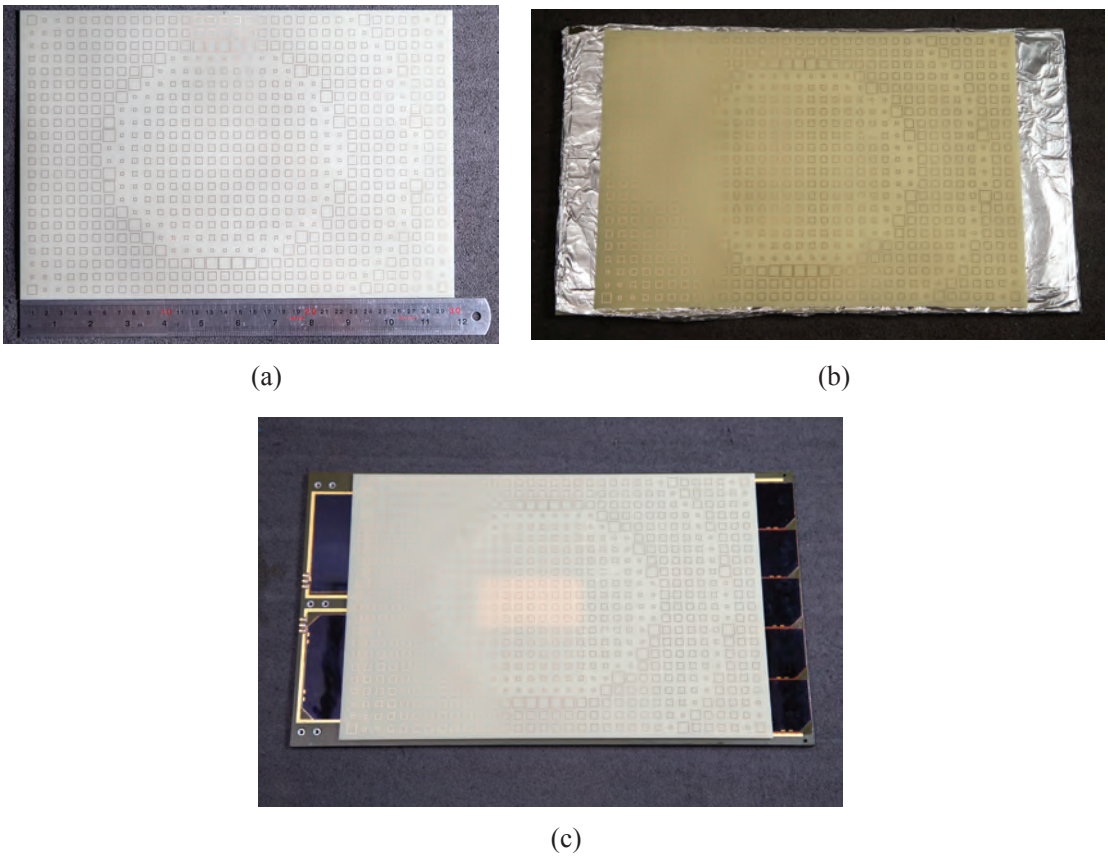

(a) (b)

(c)

Fig. 5.23: Reflectarray in different measurement set—ups: (a) I. (b) II. (c) III.

Measurement Results

Fig. 5.24 shows the measured reflection coefficient of the reflectarray. It confirms that the reflectarray is matched well. Fig. 5.25 shows the normalized radiation pattern for measurement I. It is clear that the simulated pattern is in good agreement with the measured one. The measured radiation patterns for measurements II and III are shown in Fig. 5.26 and Fig. 5.27, respectively. Table 5.2 shows the measured gain and aperture efficiency for the reflectarray in the three measurement set-ups. The gain and aperture

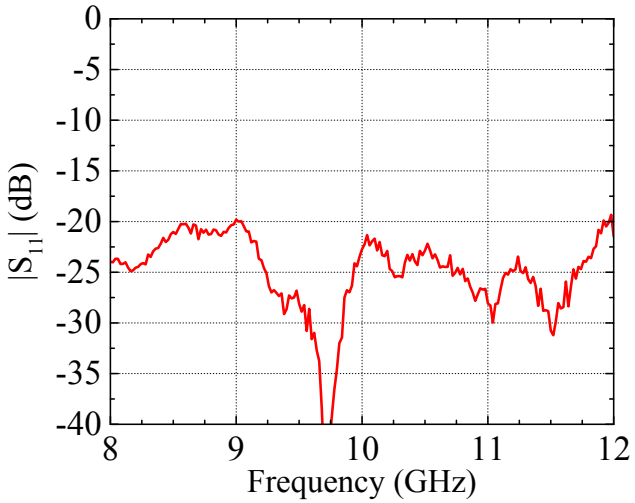

Fig. 5.24: Measured reflection coefficient of the reflectarray.

efficiency from the measurements II and III are lower compared to the measurement I. The reasons for this reduction are discussed in the next section. Despite of the expected gain loss, the measured aperture efficiency of integrated reflectarray (measurement set-up III) is highest to date when considering all the components used were commercial space–certified material, rather than special lab–made ones.

Table 5.2: Measured gain and aperture efficiency for three measurement set-ups.

Name	Gain (dB)	Aperture Efficiency (%)
I	24.35	45.3
II	23.64	38.5
III	22.46	29.3

Discussions

It is seen that the measurement set-ups II and III yield lower gain and aperture efficiency for the reflectarray, and the reasons for this are the reduced focal distance, non–uniformity, and solar cells. As discussed, the focal distance in set-ups II and III were decreased by 6 mm. When the reflectarray is closer to the feed horn by 6 mm, the simula-

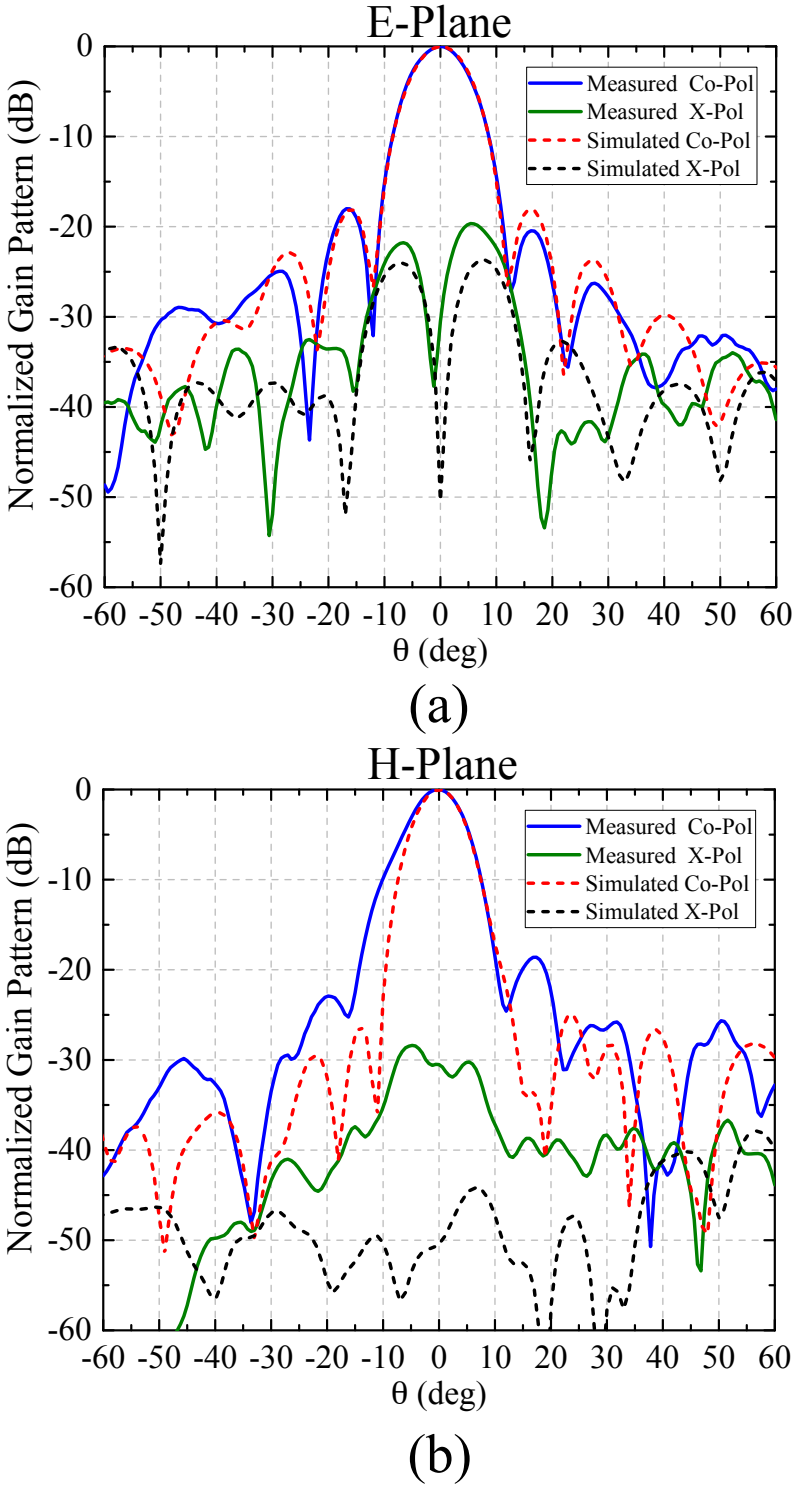

Fig. 5.25: Normalized radiation pattern of measurement I: (a) E–Plane. (b) H–Plane.

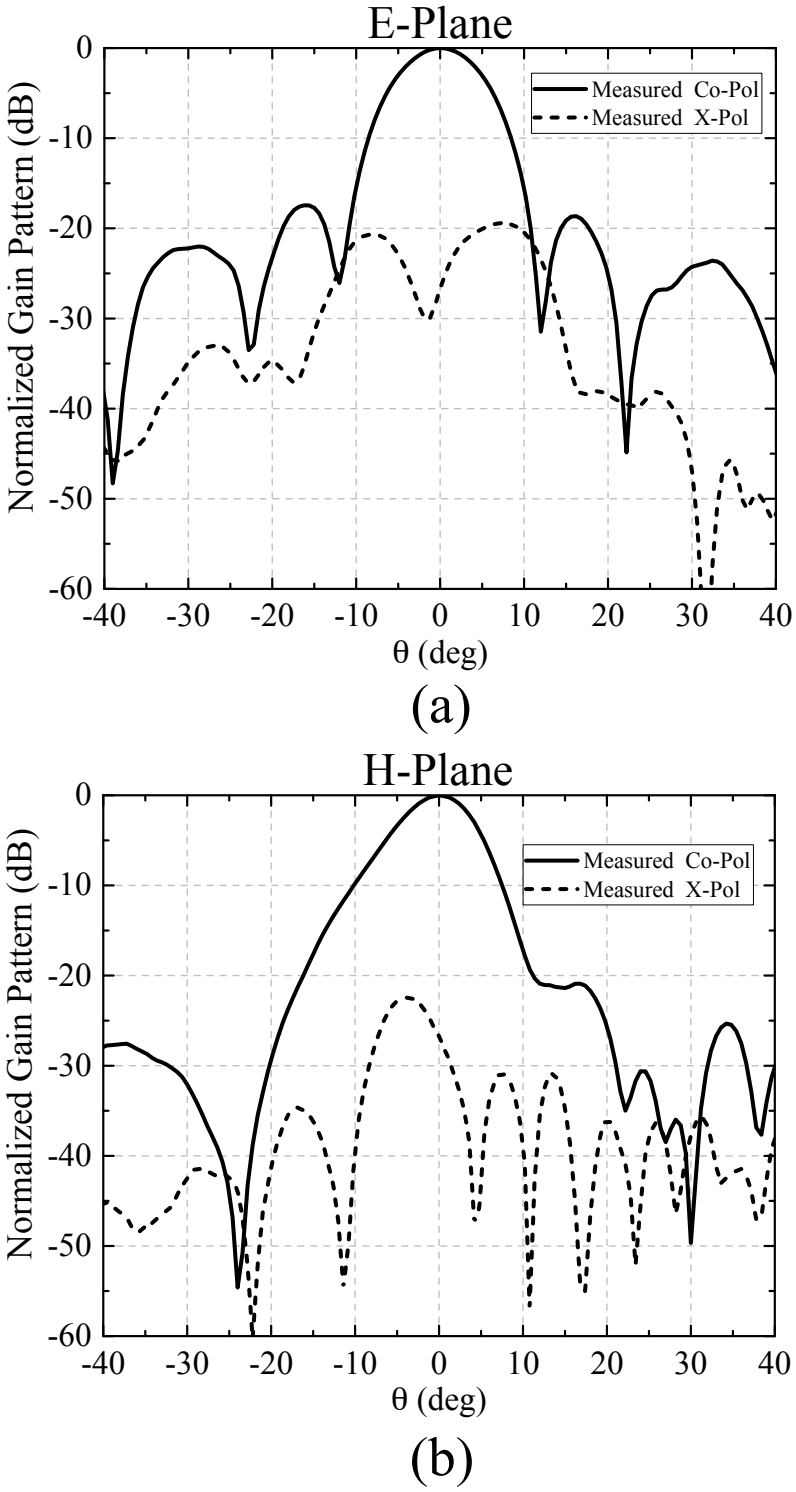

Fig. 5.26: Measured radiation pattern of measurement II: (a) E–Plane. (b) H–Plane.

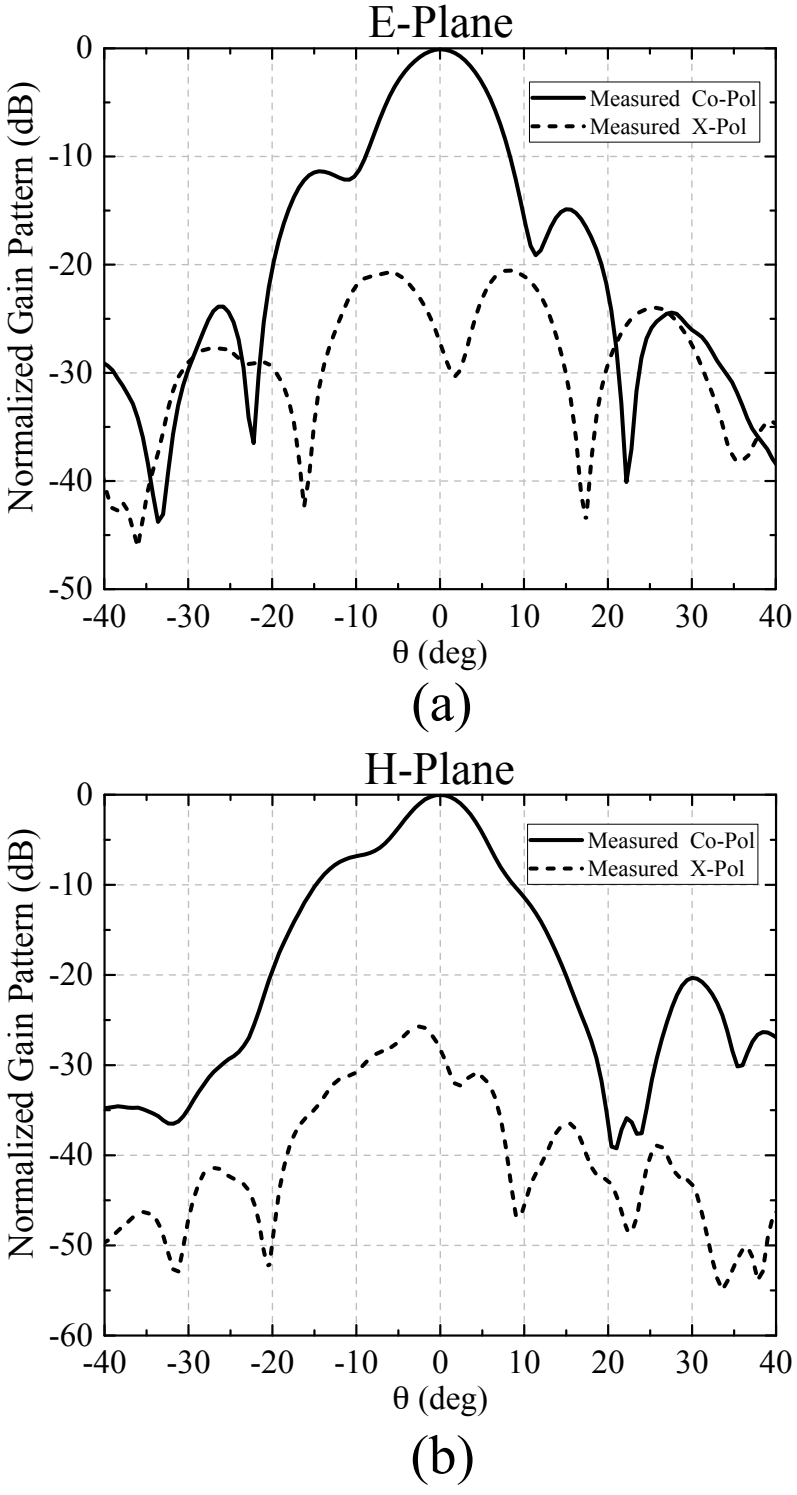

Fig. 5.27: Measured radiation pattern of measurement III: (a) E–Plane. (b) H–Plane.

tion results show that we should expect about 0.46 dB gain reduction. On the other hand, the aluminum ground in the set-up II as shown in Fig. 5.23.b, is not uniform and there is a possibility of having non–uniform air layer between the FR4 substrate and the ground that can contribute to the gain reduction.

The gain in the set-up III is reduced by 1 dB compared to the set-up II. This is mainly because of the solar cells as discussed in section 5.2.4 . Other factors that have possibly contributed to the gain reduction are studied as follows. First of all, the solar panel used in the measurement was a commercial product and was slightly different from the one that we performed the design simulations (section 5.2.4). The main difference is that this solar panel has solar cells with its own cover glass (very thin though) glued on each cell. We had not considered the adhesive that can be lossy in our previous studies. Second of all, when the FR4 was placed on the solar panel (Fig. 5.23.c), there is a high possibility of air layer between two as we could not tight them to each other. To understand the effect of these factors well, we did full–wave simulation for unit cell and reflectarray. The simulated structure's layer information is shown in Fig. 5.28. In the studied structure, the glue layer was modeled as lossy layer with ϵ_r=2.6, $tan\delta$=0.015, and height of 0.15 mm. The cover glass was modeled with ϵ_r=4.5, $tan\delta$=0.015, and height of 0.15 mm. The air layer was considered with height of h_{air}. It should be noticed that the same reflectarray (Fig. 5.23.a) was used in this analysis and the focal distance was set to be 135 mm like the set-up I. It is

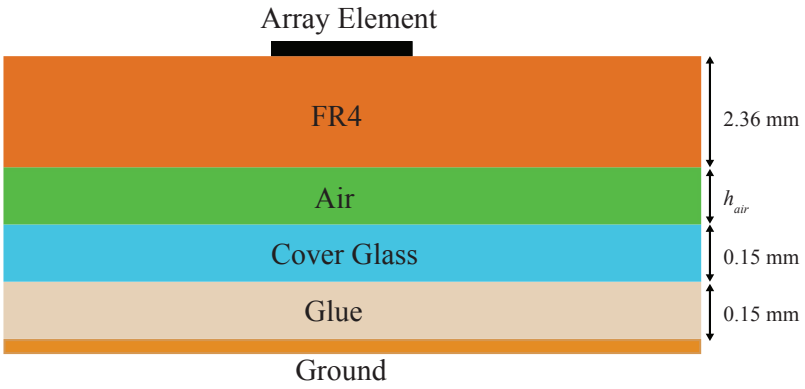

Fig. 5.28: The layer information of integrated solar panel reflectarray.

worth to mention that the mentioned values above for the glue and the cover glass are only estimated ones as we do not have access to the original data sheet of the panel. Table 5.3 shows the simulation results for different values of h_{air}. The phase range was obtained by the unit–cell simulation and gain was obtained by full–wave simulation of the array. The set-up I (Only FR4 substrate) gives the simulated gain of 24.5 dB and phase range of 322.8^o. The simulation results confirm that air bubble can be a big factor in gain reduction. For example, air layer with height of 0.4 mm can reduce the gain of the reflectarray by 0.5 dB. The transparent adhesive (glue) may contribute to some loss, but not as much compared to the air layer. Then, the rest of the gain reduction is from the lossy nature of solar cells as discussed in previous sections.

Table 5.3: Simulated phase range and gain for different h_{air}.

h_{air} (mm)	0.1	0.4	0.8	1.2
Phase Range (deg)	309.2	294.3	279	253.6
Gain (dB)	24.43	24	23.4	22.4

5.2.6 Conclusion

Two transparent reflectarray antennas with transparency and aperture efficiency higher than previous publications are presented. Detailed design method and data are presented. To validate the design, one of the reflectarrays, which is suitable for integration on a 6U CubeSat, was prototyped and measured with and without a multi–functional solar panel for space use underneath the antenna. The measurements agree the design data and analysis. It is seen that the achieved reflectarray antennas are effective and highly transparent, promising an application as high gain antennas for CubeSats.

References

[1] Integrated solar array and reflectarray antenna (ISARA) for high bandwidth cubesats,

NASA document. [Online]. Available: https://www.nasa.gov/sites/default/files/files/ISARA_Fact_Sheet-15Oct14.pdf

[2] J. Huang and J. A. Encinar, *Reflectarray Antennas*. Wiley-IEEE, 2007.

[3] S. Vaccaro, J. R. Mosig, and P. de Maagt, "Two advanced solar antenna "SOLANT" designs for satellite and terrestrial communications," *IEEE Trans. Antennas Propag.*, vol. 51, no. 8, pp. 2028–2034, 2003.

[4] T. W. Turpin and R. Baktur, "Meshed patch antennas integrated on solar cells," *IEEE Antennas Wireless Propag. Lett.*, vol. 52, pp. 693–696, 2009.

[5] T. Shahvirdi and R. Baktur, "Analysis of the effect of solar cells on the antenna integrated on top of their cover glass," in *IEEE Antennas and Propagation Society International Symposium*, Vancouver, BC, 2015, pp. 1522–3965.

[6] K. K. Karnati, Y. Yusuf, S. Ebadi, , and X. Gong, "Theoretical analysis on reflection properties of reflectarray unit cells using quality factors," *IEEE Trans. Antennas Propag.*, vol. 61, no. 1, pp. 201–210, 2012.

[7] J. Ethier, M. Chaharmir, and J. Shaker, "Loss reduction in reflectarray designs using sub–wavelength coupled–resonant elements," *IEEE Trans. Antennas Propag.*, vol. 60, no. 11, pp. 5456–5459, 2012.

[8] T. Shahvirdi and R. Baktur, "Effect of Ag electrode lattice in a commercial space solar cell on a patch antenna integrated on top of it," in *IEEE Antennas and Propagation Society International Symposium*, Vancouver, BC, 2015, pp. 2431–2432.

[9] M. A.Moharram and A. A. Kishk, "A Ka band optically transparent reflectarray design integrated with solar cells," in *IEEE International Conference on Ubiquitous Wireless Broadband (ICUWB)*, Montreal, QC, 2015, pp. 1–4.

[10] W. An, S. Xu, F. Yang, , and J. Gao, "A Ka-Band reflectarray antenna integrated with solar cells," *IEEE Trans. Antennas Propag.*, vol. 62, no. 11, pp. 5539–5546, 2014.

[11] J. Shaker, M. Chaharmir, and J. Ethier, *Reflectarray Antennas: Analysis, Design, Fabrication and Measurement*. Artech House, 2013.

[12] A. Yu, F. Yang, A. Z. Elsherbeni, J. Huang, and Y. Rahmat-Samii, "Aperture efficiency analysis of reflectarray antennas," *Microw. Opt. Tech. Lett.*, vol. 52, no. 2, pp. 364–372, 2010.

[13] D. M. Pozar, S. D. Targonski, and H. D. Syrigos, "Design of millimeter wave microstrip reflectarrays," *IEEE Trans. Antennas Propag.*, vol. 45, no. 2, pp. 287–296, 1997.

CHAPTER 6
POLARIZATION RECONFIGURABLE ANTENNA FOR SMALL SATELLITE APPLICATION

Abstract

A polarization reconfigurable antenna design that enables integration with CubeSat solar panels is presented. The antenna reconfigures between two polarizations by switching pin diodes. The design method and results are presented.

6.1 Introduction

Increasing communication needs demand antennas with diversity [1], and accordingly antennas with polarization reconfigurability through switching have been sought after. Although the main application of antennas with polarization diversity has been in wireless local area networks (WLAN), mobile satellite service and microwave tagging, such class of antenna may be valuable in future space missions, in particular, Cube Satellites (CubeSat) . A basic CubeSat is usually called 1U CubeSat (Fig. 6.1.a), and it is common to fly 1.5U CubeSat such as the DICE spacecraft (Fig. 6.1.b) for enhanced mission capacity. Although CubeSat often uses only one type of circular polarization (CP), having a polarization reconfigurable antenna will be an enhancement and consistent with CubeSat philosophy where smaller, cheaper and better are the basis principles.

It is straightforward to understand how a CubeSat's mission capacity can be enhanced by having multiple polarizations. As the size of a CubeSat is the biggest limiting factor, being able to integrate a single antenna with polarization diversity with the solar panel will be extremely valuable because one can solve two problems (1. a polarization reconfigurable antenna, and 2. integration of antenna with the solar panel to save surface real estate) at the same time. This paper presents an antenna topology that allows switching between two

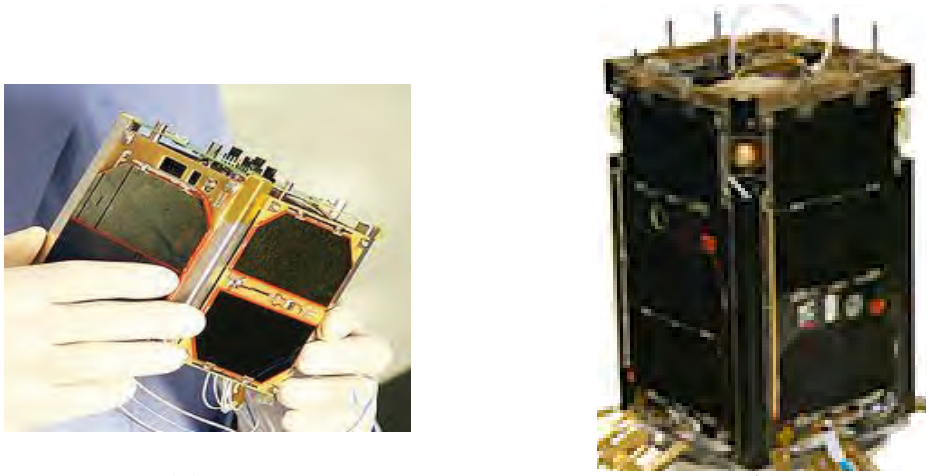

(a) (b)

Fig. 6.1: CubeSats: (a) 1U. (b) USU's DICE.

circular polarizations and can be integrated with the solar panel of a 1U or 1.5U CubeSat. Although there are various reported methods to integrate antennas with solar panels [2], the antenna design of this work is based on cavity backed slot antenna because of its simplicity and minimal impact on the solar cell, including no needs for custom designing solar cells [3].

6.2 Design

Fig. 6.2.a shows the top view of the antenna geometry. The cavity backed crossed slot antenna is integrated with the solar panel of a 1.5U CubeSat; and therefore, the panel dimensions are 10 cm $\times$ 15 cm. The antenna geometry is based on PCB technology, which is a common base for CubeSat surface mount panel. On a PCB substrate, where top and bottom layers are copper (Fig. 6.2.b), a cross slot (composed of two orthogonal slots) is etched on the top layer to create a CP. The slot antenna is excited by a coaxial probe that is placed on the center line of the cross, and the top and bottom layers need to be connected, common to a cavity backed slot antenna design [4]. In order to suppress unwanted cavity modes excited by the probe, instead of connecting the two layers through the side walls of solar panel, a square walls of vias, a.k.a. substrate integrated waveguide (SIW) were created around the crossed slot, just to be sufficient for the antenna while suppressing higher modes.

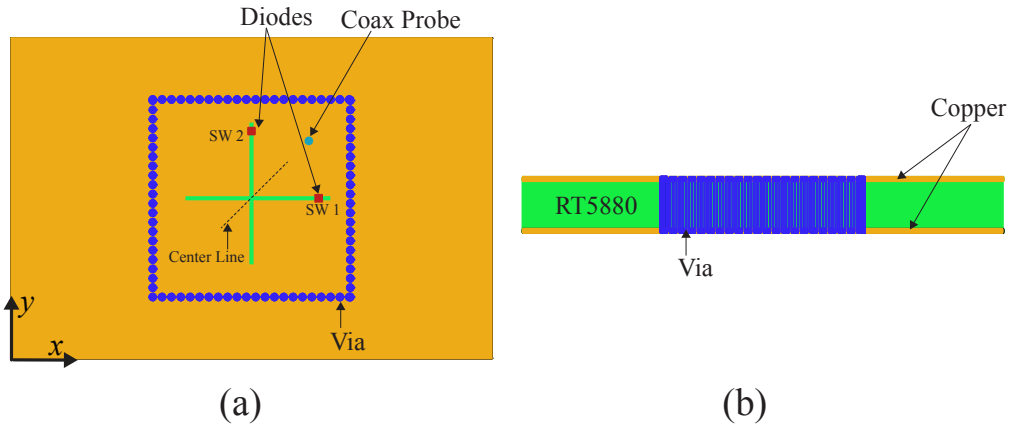

Fig. 6.2: Reconfigurable antenna geometry: (a) Top view. (b) Side view.

The antenna is designed to function at 2.3 GHz. During the simulation using Ansys' HFSS, in order not to consume up computing time, the vias were first modeled as solid conductor, and then converted to SIW using the previously reported method [5].

A CP is produced by the two slots and a 90 degree phase shift. A left handed CP (LHCP) or a right handed CP (RHCP) can be achieved by adjusting the length difference between the two orthogonal slots. When the slot length on y direction is longer, a LHCP is obtained, and a RHCP is produced when the slot on x is longer than the other slot. A Roger's RT5880 (height 1.5 mm, dielectric constant 2.2 and loss tangent 0.009) was chosen to be the PCB substrate. To create the length difference for the slots, two diodes (SW1,SW2) were used as shown in Fig. 6.2.a. The diodes in this project are BAP65LX pin diode manufactured by NXP (www.nxp.com). The on and off stages of the diode change the length of a slot as follows (Fig. 6.3). When the diode is off, then it has appropriately no impact on the slot. When the slot is on, it acts as a short to bridge the top layer conductor across the slot. Such a short truncates the effective length of the slot from l_1 to l_2 or l_4 (when considering the coupling between l_2 and l_3). In simulation, when the diode is on, it was modeled by series resistance $R_s = 0.5\ \Omega$ representing the switch loss and package parasitic inductance $L_p = 0.6$ nH. When the diode is off, it was modeled by series capacitor $C_s = 0.5$ pF and package parasitic inductance. As a summary, a LHCP is achieved by

switching SW1 on and SW2 off, and a RHCP is achieved when SW1 is off and SW2 is on.

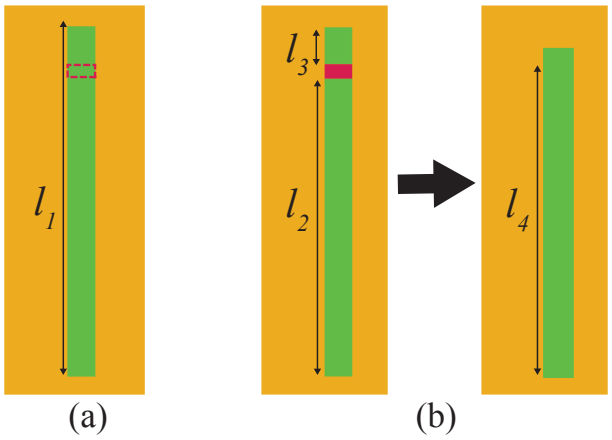

Fig. 6.3: Switch effect on the slot length: (a) Switch is off. (b) Switch is on.

6.3 Results

Fig. 6.4 is simulated S_{11} for the two polarizations. The impedance matching is achieved by tuning the coax feed along the center line. Fig. 6.4 shows good impedance matching has been achieved. The difference between the impedance bandwidth of the two polarizations, is due to the fact that the solar panel is rectangle and does not have diagonal symmetry.

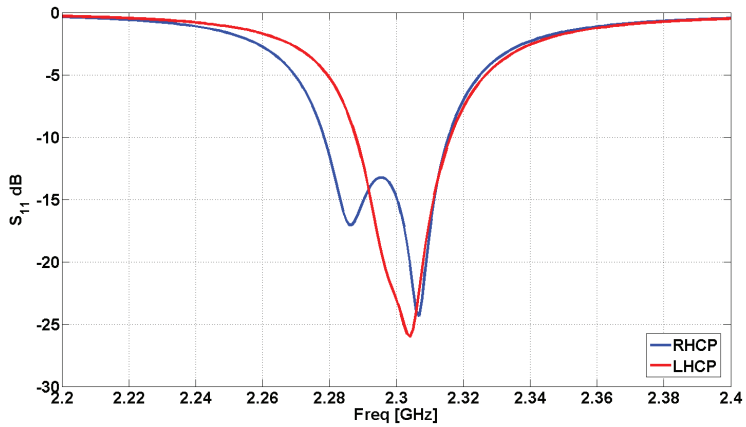

Fig. 6.4: Simulated S_{11} response.

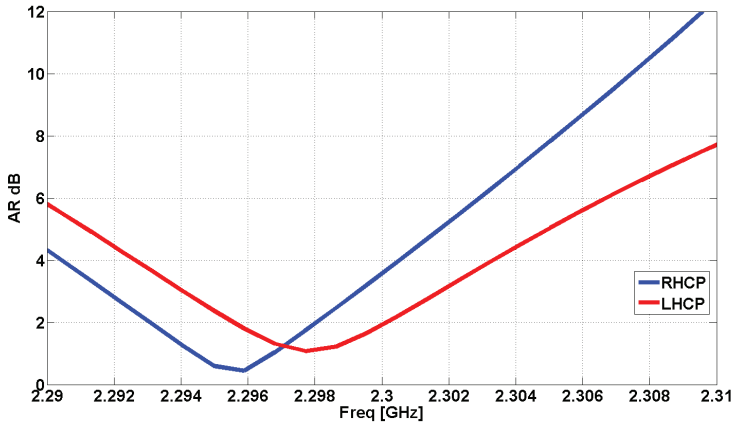

Fig. 6.5: Simulated AR.

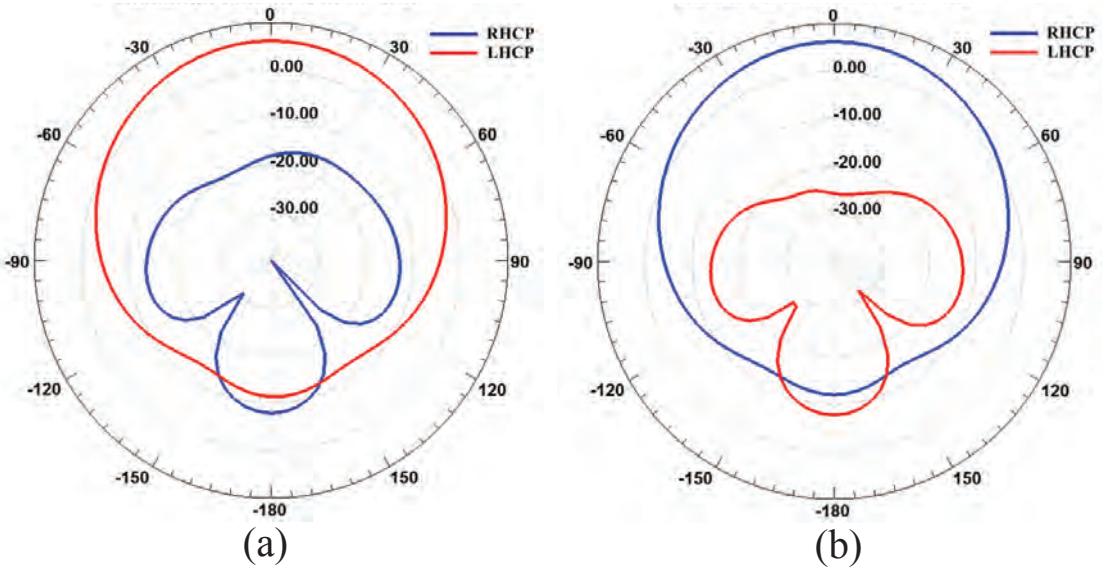

Fig. 6.6: Simulated radiation pattern: (a) when SW 1 is on. (b) when SW 2 is on.

The axial ratio (AR) is plotted in Fig. 6.5 and is below 3 dB for both polarizations. The simulated radiation patterns are presented in Fig. 6.6. Fig. 6.6.a shows that when SW1 is on, a LHCP has been achieved on the boresight as the RHCP is 20 dB below the LHCP. This is consistent with the achieved AR (Fig. 6.5). Fig. 6.6.b shows that switching SW2 on gives rise to a RHCP.

6.4 Conclusion

The paper presents a design that enables an integration of a polarization reconfigurable antenna with the solar panel of a 1.5U CubeSat. The antenna geometry is based on a cavity backed slot, and the polarizations are switched between LHCP and RHCP by using pin diodes. The antenna properties (S_{11}, AR and pattern) confirm that the proposed design is capable of reconfiguring two CPs. Although the simulation is presented for a 2.3 GHz antenna, the design can be easily adjusted to other S band or higher frequencies. Also, the antenna design is not limited to 1.5 U, and can be adjusted to suit 1U to multi–U CubeSats.

References

[1] A. P. Saghati and K. Entesari, "A reconfigurable "SIW" cavity-backed slot antenna with one octave tuning range," *IEEE Trans. Antennas Propag.*, vol. 61, no. 8, pp. 3937–3945, 2013.

[2] T. Shahvirdi and R. Baktur, "A study on the effect of space solar cells on the antennas integrated on top of their cover glass," in *Antennas and Propagation Society International Symposium*, Memphis, TN, 2014, pp. 215–216.

[3] M. Mahmoud, R. Baktur, and R. Burt, "Fully integrated solar panel slot antennas for small satellites," in *Proc. 15th Annual AIAA/USU Conf. on Small Satellites*, Logan, UT, Aug. 2010.

[4] H. P. H. D. Sievenpiper and R. M. Riley, "Low-profile cavity-backed crossed-slot antenna with a single-probe feed designed for 2.34-"GHz" satellite radio applications," *IEEE Trans. Antennas Propag.*, vol. 52, no. 3, pp. 873–879, 2004.

[5] T. Shahvirdi and A. Banai, "Applying contour integral method for analysis of substrate integrated waveguide filters," in *Mediterranean Microwave Symposium (MMS)*, 2010, pp. 418–421.

CHAPTER 7

CONCLUSION AND FUTURE WORK

The dissertation reports comprehensive studies on effective integration antennas and solar cells. It presents detailed design philosophy, prototyping method, measurements, and assessments of interaction between the antenna and solar cells. The shadow of the antenna casts on solar cells, however, it has been found that it is not significant (less than 2%). The solar cell, as a lossy layer under the antenna, reduces the antenna's gain to 2–3 dB from C to X bands, but the gain reduction is expected to be less severe for higher frequencies. This research also presents an analytical model of the most common commercial space solar cell. The integration of the antenna with solar cells can be furthered at higher frequencies by using the proposed model.

On the array level, the dissertation presents discussions and design philosophy of an optically transparent reflectarray for solar panel integration. The design can be easily adapted to 6U or larger CubeSats. As a sample design, a sub–wavelength (quarter wavelength) reflectarray with square loops as elements, which has been found to exhibit the most overall superior properties both in terms of gain and optical transparency, is presented. The effect of solar cells on the reflectarray has been considered, and the antenna promises high aperture efficiency and optical transparency. The reflectarray design has been validated and can be easily tuned to be compatible with Space Network (SN), and Deep Space Network (DSN) communication needs.

For future studies, the proposed reflectarray can be directly printed on the cover glass of solar panel. The current initial prototype is done by using circuit board material to save time. Looking further ahead, the reflectarray can be redesigned at Ka band with planar feed so that the entire system can be integrated onto solar panels of a CubeSat. When needed higher gain, the discussed array can be designed for DSN at higher frequencies such as Ka band. Designing dual band integrated transparent array for X and Ka bands would

be another method to take advantage of both NEN and DSN simultaneously.

CURRICULUM VITAE

Taha Shahvirdi Dizaj Yekan

Education

Ph.D. in Electrical Engineering, Utah State University, Logan, Utah (2012 $\sim$ 2016)

M.Sc. in Microwave Engineering, Sharif University of Technology, Tehran, Iran (2008 $\sim$ 2010)

B.Sc. in Telecommunication Engineering, Iran University of Science and Technology, Tehran, Iran (2003 $\sim$ 2008)

Journal Papers

- An Experimental Study on the Effect of Commercial Triple Junction Solar Cells on Patch Antennas Integrated on Their Cover Glass, T. Yekan and R. Baktur, *Progress In Electromagnetics Research C*, Vol. 63, 131–142, 2016.
- Two Types of Optically Transparent Antennas, R. Baktur, T. Yasin, T. Yekan, *to be submitted*.
- Conformal Integrated Solar Panel Antennas, T. Yekan and R. Baktur, *to be submitted*.
- An X Band Patch Antenna Integrated with Commercial Triple Junction Solar Cells, T. Yekan and R. Baktur, *to be submitted*.
- Analysis of Soalr Cells' Effect on the Integrated Antenna, T. Yekan and R. Baktur, *to be submitted*.
- Reflectarray Antenna Integrated on Top of a Solar Panel, T. Yekan and R. Baktur, *to be submitted*.

Conference Papers

- Integrated Solar–Panel Antenna Array for CubeSats (ISAAC), T. Yekan, R. Baktur, H. Shaw, and O. Kegege, in *Proc. 30th Annual AIAA/USU Conf. on Small Satellites*, Logan, 2016.
- Design of Two Transparent X Band Reflectarray Antennas Integrated on a Satellite Panel, T. Yekan and R. Baktur, in *IEEE International Symposium on Antennas and Propagation*, Fajardo, 2016.
- A Study of Meshed Patch Reflectarray Unit Cell, T. Yekan and R. Baktur, in *IEEE International Symposium on Antennas and Propagation* , Fajardo 2016.
- Examination of Two Types of Quasi Transparent Reflectarray Elements, T. Yekan, R. Baktur, and C. Swenson, in *IEEE International Symposium on Antennas and Propagation* , Fajardo 2016.
- Transparent Reflectarray Antenna Printed on Solar Cells, T. Yekan, R. Baktur, C. Swenson, O. Kegege, S. Altunc, H. Shaw, J. Lyons, and M. Deshpande, in *IEEE Photovoltaic Specialties Conference*, Oregon, 2016.
- Polarization Reconfigurable Antenna for Small Satellite Application, T. Yekan and R. Baktur, in *National Radio Science Meeting*, Boulder, Jan. 2016.
- Analysis of the Effect of Solar Cells on the Antenna Integrated on Top of Their Cover Glass, T. Shahvirdi and R. Baktur, in *IEEE International Symposium on Antennas and Propagation*, Vancouver, July. 2015.
- Effect of Ag Electrode Lattice in a Commercial Space Solar Cell on a Patch Antenna integrated on Top of It, T. Shahvirdi and R. Baktur, in *IEEE International Symposium on Antennas and Propagation*, Vancouver, July. 2015.
- A Study on the Effect of Space Solar Cells on the Antennas Integrated on Top of their Cover Glass, T. Shahvirdi and R. Baktur, in *IEEE International Symposium on Antennas and Propagation*, Memphis, July. 2014.

- Applying Contour Integral Method for Analysis of Substrate Integrated Waveguide Filters, T. Shahvirdi and A. Banai, in *10th Mediterranean Microwave Symposium*, Northern Cyprus, Aug. 2010.